IN SILICO AND *IN VITRO* SCREENING OF MARRUBIIN AND MARRUBIIN DERIVATIVES FOR ANTIDIABETIC ACTIVITY ON PTP1*β*, C2C12 MYOCYTES, CHANG LIVER HEPATOCYTES AND 3T3-L1 ADIPOCYTES

By

Rudi Berto Nicholas

Submitted in fulfillment/partial fulfillment of the requirements for the degree *Magister Scientiae* qualification to be awarded at the Nelson Mandela Metropolitan University

JANUARY 2013

Supervisor: Prof. C.L Frost

Co-Supervisor: Mrs. R.A. Levendal

TABLE OF CONTENTS **PAGE**

DECLARATION

I, *Rudi Berto Nicholas 206015470*, hereby declare that the *dissertation* for *Students qualification to be awarded* is my own work and that it has not previously been submitted for assessment or completion of any postgraduate qualification to another University or for another qualification.

Rudi Berto Nicholas

Official use:

In accordance with Rule G4.6.3,

4.6.3 A treatise/dissertation/thesis must be accompanied by a written declaration on the part of the candidate to the effect that it is his/her own work and that it has not previously been submitted for assessment to another University or for another qualification. However, material from publications by the candidate may be embodied in a treatise/dissertation/thesis.

ABSTRACT

Diabetes mellitus (DM) is a life changing disease which affects a large portion of the population and the economy through high medical costs and loss of productivity. Marrubiin (MAR), a diterpenoid isolated from *Leonotis leonurus*, a plant indigenous to Southern Africa, is used by traditional healers to alleviate DM symptoms. This study aims to screen the inhibitory potential of MAR and MAR derivatives on PTP1*β* and glucose uptake properties of Chang liver, C2C12 and 3T3-L1 cells.

Marrubiin and 19 of its derivatives were tested to determine the inhibition constants for PTP1*β*. A K_i of 21 µM and 0.047 µM was detected for oleanolic acid *in silico* and *in vitro*, respectively. All other diterpene derivatives did not display substantial levels of inhibition of PTP1*β*.

Treatment of Chang liver cells with the various MAR derivatives (10 µM) did not significantly increase glucose uptake beyond metformin, a known antidiabetic drug. The various treatments showed a protective/proliferative effect on the C2C12 muscle cells with two MAR treatments (DC16 and DC18) significantly increasing glucose uptake as compared to metformin in C2C12 muscle cells. It was noted that DC17, DC18 and MAR significantly increased glucose uptake in 3T3-L1 adipocytes, relative to the control. Contrary to cytotoxicity studies with Chang liver and C2C12 muscle cells, adipocytes displayed no cytotoxicity to treatments while a significant increase in cell viability was seen for DC9 and DC15. To unravel the mechanism of action, Western blotting analysis was completed and an increased expression of PTP1*β* was observed for treatments with DC17 and DC6 was seen in adipocytes, while DC18 and metformin decreased expression significantly. This correlated with a significant decrease of Ser 612 phosphorylation of insulin receptor substrate (IRS1) for DC17. Real time qPCR of IRS1 and GLUT4 highlighted that DC17 and MAR were able to significantly increase expression of IRS1 and GLUT4, respectively.

The results show that MAR and the selected derivatives (DC6, DC17, DC18) have been found to increase glucose uptake in peripheral tissue types with IRS1, GLUT4 and PTP1*β* being associated with the mechanism of action. However, a complete understanding of the mechanisms is yet to be established.

Keywords: Marrubiin, *L. leonurus*, PTP1*β*, 3T3-L1, Autodock, diabetes mellitus

ACKNOWLEDGEMENTS

Firstly I'd like to thank my parents for all their support and encouragement. If it were not for their flawless example, I would never have been able to continue my journey. To my friends and extended family that supported me throughout my entire university career, thank you for the great times and for sticking with me through the tough times where more than just midnight oil was burnt.

To my supervisors, Prof. C.L Frost and Mrs. R.A. Levendal, thank you for all the patience, guidance and dedication which you showed daily to the entire research group and including me. You give us the fuel to continue through the worst of times.

To our research group, you know who you are, thank you for all the guidance, and all the laughs that we shared on a daily basis. I could only hope that my influence on your lives was as pleasant.

The entire BIOTECH society and Hons '09, have initiated a new breed of microbiologists and biochemists. Kyle, Dwain and Reza, thank you for the friendship. A special mention has to be made to Marc Chong-Seng who patiently assisted me with the presentation of the 3D chemical structures.

Thank you to Dr. Kevin Lobb for his hospitality during my two week stay and for his knowledge which he so unselfishly instilled in me with regards to computational modelling. To Prof. Mike Davis-Coleman and Dr. Zeni Tshentu who provided the marrubiin derivatives for this investigation.

Last but not least I'd like to thank the NMMU academic and technical staff of the biochemistry and microbiology who contributed to my education along this long yet fruitful journey during my undergraduate and postgraduate studies.

DECLARATION

LIST OF FIGURES

LIST OF TABLES

LIST OF ABBREVIATIONS

2D	Two dimensional
3D	Three dimensional
3T3-L1	Mouse preadipocyte cell line
ACC	Acetyl-CoA carboxylase
ACD	Advanced chemistry development inc.
ADP	Adenosine diphosphate
ADT	AutoDockTools 4.2
AKT	Protein kinase B
Ala 217	Alanine 217
ALP	Alkaline phosphatase
AMP	Adenosine monophosphate
AMPK	Adenosine monophosphate-activated protein kinase
AP	Alkaline phosphatase (detection antibody)
APS	Adaptor protein containing PH and SH2 domains
Arg 221	Arginine 221
AS160	Akt substrate of 160 kDa
Asp	Aspartate
ATP	Adenosine triphosphate
B2M	Beta-2-microglobulin
BCA	Bicinchoninic acid
BCIP/NBT	5-bromo-4-chloro-3'-indolyphosphate p-toluidine salt/Nitro-blue tetrazolium chloride
BSA	Bovine serum albumin
C2C12	Mouse myoblast cell line
C3G	Guanine nucleotide-exchange factor 2
^{o}C	Degrees Celsius
Ca^{2+}	Calcium ion
CAP	Cbl-associated protein
Cbl	Casitas B-lineage lymphoma
c-Cbl	Mouse casitas B-lineage lymphoma
cDNA	Complimentary deoxyribose nucleic acid
C/EBPα	CCAAT-enhancer binding protein alpha
CHARMM	Chemistry at Harvard Molecular Mechanics

CIP4	Cdc42 interacting protein 4
CO_2	Carbon dioxide
CON	Vehicle control
CREB	cAMP response element binding protein
CrkI	Crk-like protein
Cys	Cysteine
DD	Double Dixon plot
DM	Diabetes mellitus
DMEM	Dulbecco's modified eagle medium
DMSO	Dimethyl sulfoxide
DNA	Deoxyribose nucleic acid
Doc2*β*	Double C2-like domain containing protein beta
DSV	Discovery Studio Visualizer 2.5
DTT	Dithiotheitol
EDTA	Ethylenediaminetetraacetate
Epac2	Exchange protein directly affected by cAMP 2
ER	Endoplasmic reticulum
ERK	Extracellular-signal-regulated kinase
F-1,6-Pase	Fructose-1,6-bisphosphatase
FAS	Fatty acid synthase
FCS	Foetal calf serum
FDA	U.S. Food and Drug Administration
FOX	Forkhead box protein
FOXO1	Forkhead box protein O1
FOXO1/A_2	Forkhead box protein O1/A_2
FRET	Fluorescence resonance energy transfer
gDNA	Genomic deoxyribose nucleic acid
G-6-Pase	Glucose-6-phosphatase
Gab-1	GRB2-associated-binding protein1
GAP	GTP-activating protein
GATA2/3	GATA binging protein 2/3
gDNA	Genomic DNA
GK	Glucokinase
GLUT2	Glucose transporter 2

GLUT4	Glucose transporter 4
Gly 220	Glycine 220
Grb2	Growth factor receptor-bound protein 2
GSK3	Glycogen synthase kinase-3
GSV	GLUT4 storage vesicles
GTP	Guanosine-5'-triphosphate
GTPase	Guanosine triphosphatase
HEPES	4-(2-hydroxyethyl)-1-piperazineethanesulfonic acid
His	Histidine
HIV/AIDS	Human immunodeficiency virus or Acquired immunodeficiency syndrome
HNF/FoxA	Hepatocyte nuclear factor/Forkhead box protein A
IDF	International Diabetes Federation
IDDM	Insulin dependent diabetes mellitus
IDV	Integrated density value
Ig-G	Immunoglobulin G
IGF1R	Insulin-growth factor 1 receptor
IL-6	Interleukin 6
Ile	Isoleucine
INSR	Insulin receptor alleles
IR	Insulin receptor
IRS (1/2/3/4)	Insulin receptor substrate (1/2/3/4)
JAK	Janus kinase
K_{ATP}	ATP-regulated potassium ion channel
K^+	Potassium ion
K_i	Inhibition constant
LB	Lineweaver-Burk
MAPK	Mitogen-activated protein kinase
MAR	Marrubiin
MCE	Mitotic Clonal Expansion
MET	Metformin
MeV	1 million electron volts
mM	Millimolar
mTOR	Mammalian target of rapamycin

MTT	3-(4,5-dimethylthiazol-2-yl)-2,5-diphenyltetrazolium bromide
mU	Milliunits
Munc18c	Mammalian uncoordinated-18
mV	Millivolt
Mw	Molecular weight
NCD	Noncommunicable diseases
NIDDM	Non-insulin dependent diabetes mellitus
nM	Nanomolar
nm	nanometer
NSF	N-ethyl-maleimide-sensitive protein
p85	Phosphatidylinositol 3-kinase 85 kDa regulatory subunit
p110	Phosphatidylinositol 3-kinase 110 kDa catalytic subunit
p-IRS1	Phosphorylated IRS-1
PBSA	Phosphate buffered saline containing EDTA
PDB	Protein databank
PDK-1	3-phosphoinositide-dependent protein kinase 1
PEPCK	Phosphoenolpyruvate carboxykinase
PFK	Phosphofructokinase
PGC1	Peroxisome proliferator-activated receptor-γ coactivator
PH	Pleckstrin-homology
pH	Potential of hydrogen
PI3K	Phosphatidylinositol 3-kinase
PIP_2	Phosphatidylinositol 4,5-bisphosphate
PIP_3	Phosphatidylinositol 3,4,5-triphosphate
p-IRS1	Phospho-IRS1
PK	Pyruvate kinase
PKB	Protein kinase B
*p*NPP	para-Nitrophenylphosphate
PPARγ	Peroxisome proliferator-activated receptor gamma
Pro	Proline
PTB	Phosphotyrosine-binding
PTEN	Phosphatase and tensin homolog
PTP (1*β*)	Protein tyrosine phosphatase (1 beta)
pTyr	Phosphotyrosine

PVDF	Polyvinylidene difluoride
qPCR	Quantitative polymerase chain reaction
RalA	Ras-related protein A
Rap	Receptor associated protein
Ras	Monomeric GTP-binding protein
rDNase	RNase free DNase
RIN	Relative integrity number
Rip11	Rab11 interacting protein
RMSD	Root-mean-squared deviation
RNA	Ribose nucleic acid
RPMI	Roswell Park Memorial Institute medium
RT	Reverse transcriptase
SAP97	Synapse-associated protein 97
SD	Standard deviation
SDS-PAGE	Sodium dodecyl sulphate polyacrylamide gel electrophoresis
Ser	Serine
SH2	Scr-homology-2
Shc	Src homology and collagen protein
SHP2	Protein tyrosine phosphatase, nonreceptor-type 11
SHIP	SH2-containing Inositol 5'-phosphatase
SNAP23	Synaptosomal-Associated protein 23
SNARE/SNAP	Soluble NSF attachment protein receptor
SOCS	Suppressor of cytokine signalling
SOS	Son of sevenless protein
SREBP-1	Sterol regulatory element-binding protein 1
STAT	Signal transducer and activator of transcription
STZ	Streptozotocin
SU	Sulfonylurea
SUR1	Sulfonylurea receptor 1
T1DM	Type 1 Diabetes mellitus
T2DM	Type 2 Diabetes mellitus
TBS	Tris Buffered Saline
TC10	Ras-related GTP binding protein
TCF/LEF	T-cell factor/Lymphoid enhancer factor

TCPTP	T-cell protein tyrosine phosphatase
TEMED	Tetramethylethylenediamine
Thr	Threonine
TK	Temperature in Kelvin
TNFα	Tumour necrosis factor-alpha
TORC2	Transducer of CREB protein 2
Trp	Tryptophan
Tyr	Tyrosine
TZD	thiazolidinedione
U	Units
VAMP	Vesicle associated membrane protein
V_{max}	Maximum velocity
V_o	Initial velocity
WPD	Tryptophan-Proline-Aspartate
Ywhaz	Tyrosine-3-monooxygenase/tryptophan-5-monooxygenase-activation protein, zeta polypeptide

PART I: LITERATURE SURVEY

CHAPTER 1: INTRODUCTION AND LITERATURE REVIEW

1.1. GLOBAL DISTRIBUTION OF DIABETES MELLITUS

Noncommunicable diseases (NCD) such as Diabetes mellitus (DM) pose a phenomenal threat to the world's population. DM is a condition whereby glucose is not efficiently absorbed into relevant tissues such as fat, muscle and liver. DM directly translated means sweet urine, due to high amounts of the blood glucose being excreted in the urine (Sowattanangoon *et al.,* 2009). It is associated predominantly with the hormone insulin, secreted by the pancreas, to control glucose homeostasis in the body. There are two main types of DM, type 1 DM (T1DM) and type 2 DM (T2DM) (http://www.idf.org/types-diabetes). T1DM, or insulin dependent DM (IDDM), is found chiefly in younger individuals and is caused by insufficient amounts of insulin being secreted by the pancreas. T2DM, or non-insulin dependent DM (NIDDM), is found mainly in older individuals and has been linked to obesity (Boura-Halfon and Zick, 2009). T2DM is characterized by the inefficiency of target tissues in the body to recognize the insulin signal which is present after a meal (i.e. a high blood glucose concentration) (Boura-Halfon and Zick, 2009).

Figure 1.1: A global atlas illustrating the prevalence of DM for 2011. The intensity of green coloration illustrates the approximate population of DM sufferers in a specific country (http://www.idf.org/atlasmap/atlasmap).

The 5th edition of the International Diabetes Federation's (IDF) diabetes atlas was released in 2011 with figures which suggest that immediate action is imperative as the incidence rate of DM is on the increase globally (figure 1.1). The article states that the population of DM sufferers will increase from 366 million in 2011 to 552 million in 2030 and that currently 183 million people are not even aware that they are living with DM (IDF, 2011). Although 78 000 children are diagnosed with DM annually, the age group between 40 and 59 years of age hold the highest percentage of diagnosed diabetics (IDF, 2011). Unfortunately the leaders of many countries still underestimate the prevalence of DM as well as the importance of DM research, treatment and detection. This essentially leads to an ever increasing prevalence, and this is most relevant in developing countries which place most of their attention on the issue of infectious diseases (e.g. HIV/AIDS and malaria). However diabetes is expected to increase by 90% in the next 18 years (IDF, 2011). Currently there are an estimated 78% of people in Africa which have not been diagnosed (IDF, 2011). The IDF has declared the 17th November as 'international diabetes day' and have addressed many heads of state about the ongoing concern of DM. Through this act, the IDF has brought to light the severity of the disease allowing for world leaders to recognize the impact of DM on the world (IDF, 2011).

Prevalence of DM and associated diseases like cardiovascular diseases, thrombosis, tuberculosis, immunodeficiency and several others affects the economy negatively (Amin *et al*., 2012; Bitzur, 2011). The cost of DM treatment, indirect medical treatment and work loss due to illness and/or disability results in the inability of diagnosed workers to care for themselves financially in the form of medical treatment while loss in working days also dramatically affects the economy. Developing countries, including South Africa, are expected to be affected more by the expected increase in DM due to the rapid lifestyle change of rural individuals (www.diabetessa.co.za). Global costs were estimated to be approximately $1 274 per person and $499 billion in total in 2011 (http://www.idf.org/diabetesatlas/5e/healthcare-expenditures). In 2010 South

Africa had spent $674.06 per diabetic patient and $1.5 million for direct DM care which represents 7% of the annual heath care expenditure (Zhang *et al*., 2010). Over and above the high cost of conventional therapy, the marketed treatment has harsh side-effects and potential mortality. The global statistics for DM portrays a disturbing picture and presents a need to educate global citizens regardless of geographic or economic status. On-going research into potential treatments should be encouraged to determine why certain areas are more affected than others and allow for strategies to be implemented, counteracting the onset of DM.

1.2. DM METABOLIC CHARACTERISTICS

The relevant tissues associated with DM include those directly affected by insulin as well as those indirectly affected due to the increase in blood glucose. Tissues which play a part in T2DM are those known to store glucose as fat or glycogen or use the glucose rapidly (thereby regulating blood glucose homeostasis). Tissues having a high demand for energy include adipocytes, myocytes and hepatocytes (Novack, 2010). Pancreatic tissue contains α- and β-cells situated in the islets of Langerhans from which the hormones glucagon and insulin are secreted, respectively. In T1DM, the pancreatic β-cells malfunction, causing decreased insulin secretion (Rorsman *et al.,* 2000). In T2DM, insulin secretion is also impaired as a result of decreased β-cell mass; however the target peripheral tissues fail to recognise the insulin secreted and therefore do not elicit a response to the high extracellular glucose (Ahren, 2005).

Some tissues and systems in the body are indirectly and adversely affected by DM such as blood coagulation and the immune system. Thrombocytes are involved in blood coagulation in response to injury. Individuals with DM are known to be in a “hypercoagulable state”. These individuals lack the ability to breakdown the clots which are formed, and thus suffer from thrombosis (Carr, 2001). As a result of thrombosis, blood circulation may be affected resulting in

many DM patients often requiring amputation of certain body parts (Meltzer *et al.,* 2002). People suffering from DM have a weakened immune system and thus offers little resistance to bacterial infection as well as defective gingival epithelial cells which together increases the risk and progression of periodontal disease (Silva *et al.,* 2008). Due to the suppressive effect of DM on the immune system, tuberculosis was shown to be related to DM acquisition as there is a proportional increase in the risk of acquiring tuberculosis with DM progress (Baker *et al*., 2012).

Understanding the insulin signalling cascades, which differ in the pancreatic, adipocyte, myocyte and hepatocyte cell types, allows investigators to identify possible causes of DM and targets for DM therapy. These are discussed in the section 1.3.

1.3. INSULIN SIGNALLING CASCADES

1.3.1. PANCREATIC β-CELLS

Insulin secretory cells or β-cells are found in the Islets of Langerhans in the pancreas and function based on an electrochemical potential which exists between the extracellular and intracellular environment (Saltiel and Kahn, 2001). Human basal glucose concentration ranges from 4 to 7 mM and after a meal can reach 10 mM which triggers insulin secretion. Glucose levels are governed by the tight regulation between intestinal glucose uptake and secretion by liver cells and metabolism in other tissues like fat and muscle (Kulkarni *et al.,* 1999; Saltiel and Kahn, 2001). Hyperglycaemia triggers the β-cells to undergo depolarisation from its normal resting electrical potential which is -70 mV (Rorsman *et al.,* 2000). Ion channels are responsible for the creation of an electrical potential via two ion channels, namely the voltage-gated L-type calcium (Ca^{2+}) ion channel and the ATP-regulated potassium ion channel (K_{ATP}) (Rorsman *et al.,* 2000).

Initially the presence of glucose in the extracellular environment is increased and is then transported into the β-cells by the glucose transporter membrane proteins 2 (GLUT2) (figure 1.2). Influx of glucose causes an increase in glucose metabolism resulting in an increase in the ATP/ADP ratio which directly closes the K_{ATP} channels resulting in depolarisation of the cell (Henquin, 2000). At basal levels of glucose concentration, the K_{ATP} channels are open and cause the continuous outflow of K^+, resulting in the negatively charged intracellular environment. As depolarisation is accomplished, the Ca^{2+} ion channels are activated and opened, allowing an influx of Ca^{2+} in an oscillatory manner continually changing the concentration of Ca^{2+} in the β-cells (Henquin, 2000). The means to which Ca^{2+} causes insulin release is still vague though Ca^{2+} is known to be the key regulator if insulin secretion (Gustavsson *et al*., 2010).

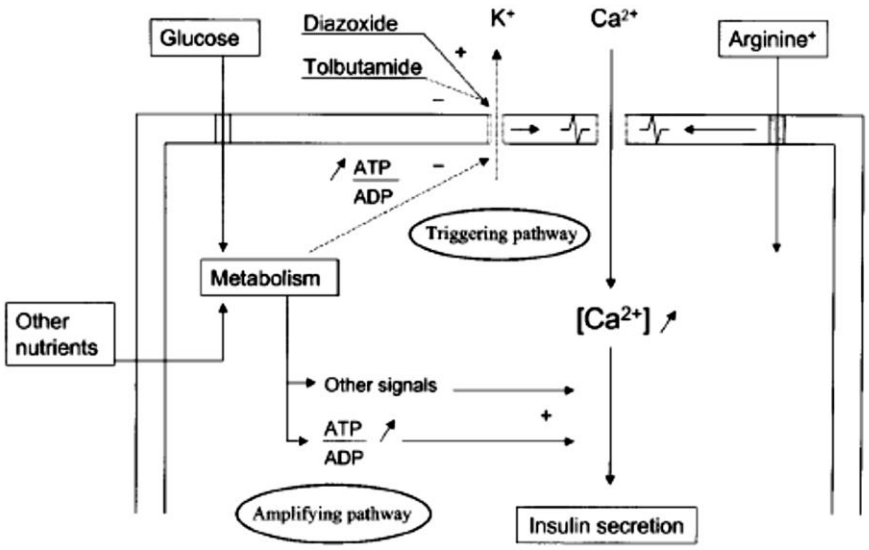

Figure 1.2: A schematic diagram illustrating the mechanism of insulin release from β-cells due to glucose metabolism (Henquin, 2000). (ATP=adenosine triphosphate, ADP=adenosine diphosphate)

Insulin secretion follows a biphasic pattern, where the first phase of secretion is disrupted in T2DM while the second phase is functional. This is an early and detectable sign of T2DM onset. β-cell insulin receptor (IR) knockout mice illustrate phenotypic changes similar to that of an individual who has an early

onset of T2DM as there is a loss in first phase insulin secretion due to glucose and sustained insulin secretion in the presence of arginine (Kulkarni *et al.,* 1999). These mice also exhibit a delayed onset to T2DM as with people suffering from the early onset of T2DM. This suggests a direct link between β-cell insulin signalling and the onset of T2DM (Kulkarni *et al.,* 1999).

Within the β-cells, vesicles containing insulin are found in two pools, the readily releasable pool which is ready to be excreted from the cell and granules which are yet to be modified and mobilised to the readily releasable pool. Approximately 13 000 of these granules are found in each cell but only 5% are readily available for excretion at the initiation of insulin secretion. Straub and Sharp (2002) refers to the two stages of insulin secretion as the K_{ATP}-channel dependent and independent pathways. Pancreatic malfunction in T2DM is characterised by the fact that glucose is not metabolised fully and ends at the first enzymatic conversion of glucose to glucose-6-phosphate which is ATP dependant causing a decrease in the ATP/ADP ratio. K_{ATP} channels remain open due to the lowering in ATP concentration and depolarisation does not continue as it should. Treatment is available in the form of sulfonylurea, for example, which is able to keep the ion channel closed even in the absence of glucose (Renstrom *et al.,* 2002; Rorsman *et al.,* 2000).

1.3.2. ADIPOCYTES AND MYOCYTES

Myocytes are the major glucose assimilating tissues in the human body and display IR's on their cell surface for extracellular insulin recognition. Seventy five percent of glucose is utilized by muscle cells under the influence of insulin (Saltiel and Kahn, 2001). Insulin signals myocytes to enhance glucose uptake from the blood either for immediate use or to be converted to glycogen which is stored for later use when glucose levels are low. Cross talk between myocytes and adipocytes has been found to be of importance in the development of T2DM in the obese state. Free fatty acids (saturated fatty acids, i.e. palmate) and

adipokine (hormones secreted by adipose tissue) levels are increased in the obese state which affects muscle cells by interference with insulin signalling and glucose uptake (Taube *et al.,* 2012). In T2DM the cascade shown in figure 1.3 does not function optimally and may be as a result of several enzymes in the signalling cascade.

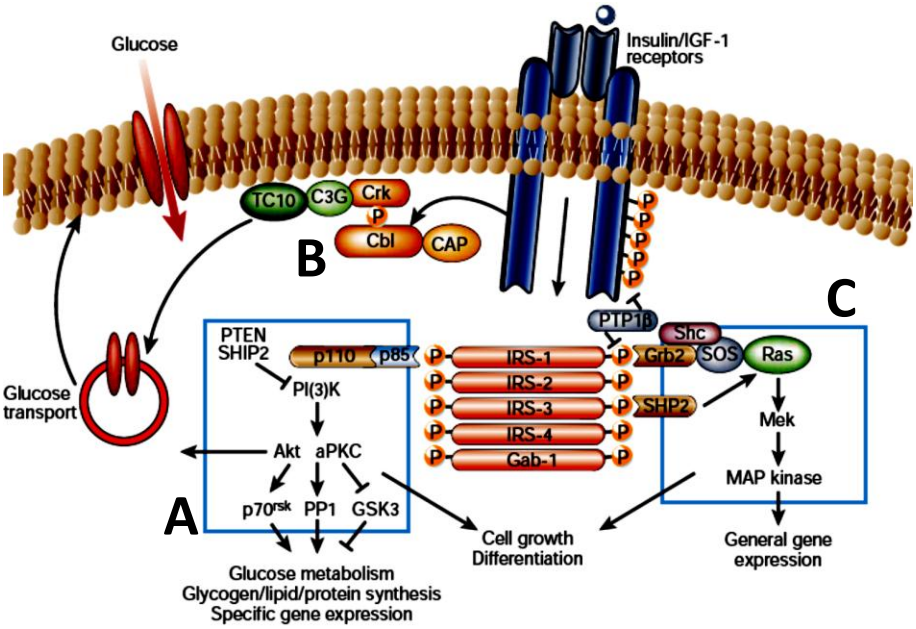

Figure 1.3: A schematic diagram showing the insulin signalling cascade in myocytes which results in the GLUT4 trafficking to the cell membrane. Three nodes are highlighted: A) PI3K-AKT/PKB, B) Cbl/CAP and C) MAPK (Dipl-Pharm and Zierath, 2005). (TC10=Ras related GTP binding protein, C3G=Guanine nucleotide-releasing factor 2, Crk=CT10 regulator of kinase, Cbl=Casitas B-lineage Lymphoma, CAP=Cbl-associated protein, Shc=Src homology and collagen protein, Grb2=Growth factor receptor-bound protein 2, SOS=Son of sevenless protein, Ras=Rat sarcoma protein, SHP2=Protein tyrosine phosphatase nonreceptor-type 11, Gab-1=Grb2-associated-binding protein1).

There are several essential intermediaries of insulin signalling in the cascade which are represented by three criteria:

1] A group of proteins which are related in structure by gene isoforms and have similar biological activity but with unique roles.

2] Proteins are highly regulated.

3] The junction should be an area which acts as a central point for several other signalling systems and thus does not cause only one phenotypic response but several (Taniguchi *et al.,* 2006a).

By analysis of the insulin signalling cascade (figure 1.3), it can be seen that there are three principle pathways in which the insulin signal is transmitted, the Phosphatidylinositol 3-kinase (PI3K)-AKT/protein kinase B (PKB) pathway (figure 1.3A), the Cbl associated protein (Cbl/CAP) (wortmannin insensitive) pathway (figure 1.3B), and the MAPK (mitogen-activated protein kinase) pathway (figure 1.3C). The PI3K-AKT/PKB pathway is mainly responsible for the glucose uptake, cell differentiation and growth (thus metabolic actions of insulin signalling), while the MAPK pathway is involved with the regulation of gene expression (Taniguchi *et al.,* 2006a). The Cbl/CAP pathway is involved in glucose transport through the activation of TC10, a GTP-binding protein, and recruitment of the CIP4/Gappex-5 complex to the cell membrane (Bouran-Halfon and Zick, 2009). When looking at the first stages of the insulin signalling pathway with regards to the IR and insulin-growth factor 1 receptor (IGF1R) (not show in figure 1.3), these interact with about six known substrate proteins (Taniguchi *et al.,* 2006a). These substrates can also interact with approximately eight other proteins, which results in over 1000 combinations further downstream of the receptors. Of these combinations of interactions only three are well defined junctions which have been identified namely, the insulin receptor substrate (IRS), PI3K and AKT/PKB.

Analysis of the insulin signalling cascade allows for the identification of protein targets in the cascade which can be considered since several of these proteins have already been implicated as the cause of insulin resistance, as they become impaired in the obese state associated with diabetes.

1.3.2.1. IR

Insulin signalling begins at the IR which is composed of two extracellular α subunits and two intracellular β subunits which are inhibited by the α subunits (Saltiel and Kahn, 2001). Subunits form a heterotetrameric complex ($\alpha_2\beta_2$). Insulin binds α subunits which causes conformational changes called intramolecular transphosphorylation in the intracellular β subunits. β subunits are altered predominantly on the activation loop (A-loop) which ranges from residues 1149-1170 such that Tyr 1162, Tyr 1163 and Tyr 1158 become autophosphorylated allowing a 30Å displacement of Tyr 1158 (Hubbard, 1997). The end result allows for ATP binding, tyrosine kinase activation of the substrates: IRS, Gab-1, p60, Cbl (Casitas B-lineage Lymphoma), adaptor proteins containing PH and SH2 domains (APS) and other proteins which are isoforms of Shc have full access to the active site (Pessin and Saltiel, 2000; Dipl-Pharm and Zierath, 2005; Saltiel and Kahn, 2001). Phosphorylated versions of these substrates are known to be activators of proteins which contain the Scr-homology-2 (SH2) domains.

In some cases it has been found that it is the IR itself which is impaired due to: 1) low expression levels, 2) loss of kinase activity, and 3) the inability to be phosphorylated. In some cases of T2DM it was found that there tends to be a decrease in IR expression as it is degraded at the protein level or internalised by ligand interaction (Taniguchi *et al.,* 2006a). This elicits severe insulin resistance as the entire cascade is immobilized. Insulin receptor alleles (*INSR*) can be flawed resulting in familial insulin resistance (Pessin and Saltiel, 2000). There is also evidence that IRs may be impaired in people with a T2DM phenotype caused by obesity although not in all cases. A small molecule, L-783,281, was isolated from the fungus *Pseudomassaria* spp. which acts as insulin and thereby activating impaired IR in a mouse model (Zhang *et al.*, 1999). This finding highlighted the potential use of insulin mimetics in diabetic therapy. Recently, a review by Patel *et al*., (2012) had listed a collection of 65 plants which were

tested for antidiabetic activity through their insulin mimetic properties. Compounds have been isolated from some of these plants which and are now used as bioactive drugs.

1.3.2.2. IRS

There are four known IRS isozymes: IRS1, IRS2, IRS3 and IRS4. In rats the IRS3 and IRS4 are more active whereas in humans the IRS1 and IRS2 isozymes function and have been mostly studied. In humans IRS3 and IRS4 have been found to be predominantly expressed in the adipocytes, brain, and embryonic tissues, respectively. IRS proteins have three domains of interest: 1) the pleckstrin-homology (PH) domain which is critical for interaction between the IR and IRS enabled by plasma membrane lipids, the cytoskeleton and several protein elements (Boura-Halfon and Zick, 2009), 2) the phosphotyrosine-binding (PTB) domain which allows for adequate binding to IR while also harbouring approximately 20 tyrosine residues on the COOH-tail which are able to be phosphorylated by IR (Taniguchi *et al.,* 2006a), and 3) the kinase regulatory loop binding which is only found on IRS-2 which is necessary for binding to the IR (Boura-Halfon and Zick, 2009). IRS is activated by the IR via tyrosine kinase phosphorylation which in turn activates PI3K (Dipl-Pharm and Zierath, 2005) which occurs on approximately 70 sites of the IRS proteins. Serine phosphorylation causes IRS not to interact successfully with PI3K and IR, as well as causing an increased rate in IRS degradation (Draznin, 2006). Defects in these proteins have been found in skeletal muscle and fat cells in patients with T2DM. As expected, repetition of the genes in humans should compensate for one of the IRS proteins being inactive (Pessin and Saltiel, 2000; Dipl-Pharm and Zierath, 2005). This has only been seen to be true for adipocytes. Thus IRS proteins can be targeted for antidiabetic treatment in cells when defective or highly down-regulated.

1.3.2.3. PI3K

PI3K has p110 (Phosphatidylinositol 3-kinase 110 kDa catalytic subunit) and p85 (Phosphatidylinositol 3-kinase 85 kDa regulatory subunit) subunits which are the catalytic and regulatory subunits, respectively. There are three types of catalytic subunits denoted by p110α, p110β and p110δ which are almost always bound to the regulatory subunits as they are easily degraded when free. Unlike the IRS proteins, PI3K proteins are all essential for a cell to function and develop properly and thus deletion of one of the genes will be detrimental to the cell (Taniguchi *et al.,* 2006b). Activation of PI3K is accomplished by activated IRS binding to the p85 subunit which up regulates the activity of the p110 catalytic subunit allowing PI3K to catalyse the conversion of phosphatidylinositol 4,5-bisphosphate (PIP_2) to phosphatidylinositol 3,4,5-triphosphate (PIP_3). Studies have shown that when expression of p85 regulatory subunits is increased, the inhibition of p110 occurs at a higher rate thus silencing insulin signalling (Dipl-Pharm and Zierath, 2005). In rat models where the expression of p85 is silenced, a hypoglycaemic phenotype is observed even though PI3K activity is decreased. Considering these results it has been proposed that, discovery of a novel p85 expression or activity inhibitor will allow for people with T2DM to be more sensitive to insulin signalling (Dipl-Pharm and Zierath, 2005).

1.3.2.4. PDK-1, AKT/PKB AND DOWNSTREAM EFFECTORS

PIP_3 lipids are able to recruit proteins which have PH-domains like serine-threonine kinases. PDK-1(3-phosphoinositide-dependent proteins kinase 1) and AKT are two such examples (Dipl-Pharm and Zierath, 2005). Recruitment of these proteins causes activation. The most important of these proteins is PDK-1 which enables activation of AKT/PKB and αPKC's (Taniguchi *et al.,* 2006b). Negative regulation of the insulin signal can be seen at the PIP_3 level as proteins such as Phosphatase and tensin homolog (PTEN) and Protein tyrosine phosphatase, nonreceptor-type II (SHP2) dephosphorylate PIP_3 on the 3'

position and the 5’ position, respectively. PTEN, being a negative regulator of the insulin cascade, has been found to be regulated by the p85 regulatory subunit of PI3K which is also a negative regulator of the insulin cascade (Taniguchi *et al.,* 2006b). PTEN and SHP2 have been investigated as potential targets for anti-diabetic research and have shown that when the expression of these phosphatases is silenced by siRNA, it causes increased insulin sensitivity in 3T3-L1 adipocytes (Tang *et al.,* 2005; Taniguchi *et al.,* 2006b).

PDK-1 and TORC2 (Transducer of CREB protein 2) are able to activate the AKT/PKB by Thr 308 and Ser 473 phosphorylation, respectively (Bayascas and Alessl, 2005). Substrates of AKT are the glycogen synthase kinase-3 (GSK3) as well as AS160 (Akt substrate of 160 kDa) which contains a GTP-activating protein (GAP). In AS160 knockout rats, the GLUT4 protein is unable to be mobilized to the cell membrane in adipocytes and phosphorylation of AS160 in muscle cells allows for an increased response to insulin thus showing a direct link through all the proteins mentioned in the cascade (Dipl-Pharm and Zierath, 2005). GLUT4 trafficking to the cell membrane is dependent on cytoskeletal rearrangement which relies on activation of Rab small GTPases by the AS160 (Taniguchi *et al.,* 2006a). However there are 70 known Rab GTPases. Rab10 has been discovered to be involved in GLUT4 trafficking as seen in results published by Sano *et al.,* (2007). They have illustrated that by upregulating the expression of Rab10 in 3T3-L1 cells, GLUT4 trafficking increased on the surface. Conversely, they have shown that when Rab10 is silenced in cells, that there is a two-fold decrease in GLUT4 trafficking. Other Rabs have also been identified as substrates of AS160 and were found to be associated with the GLUT4-containing vesicles. These are, Rab2A, Rab8A and Rab14 (Miinea *et al.,* 2005). The FOX (forkhead box protein) family of proteins are regulated by AKT/PKB. These are a family of over 100 transcription factors which include FOXO1 (Forkhead box protein O1), known to increase the expression of gluconeogenic genes in hepatocytes while inhibiting adipogenesis. Thus when the insulin signal is transmitted, FOXO1 is inhibited by AKT/PKB by phosphorylation of Ser 256

(Taniguchi *et al.,* 2006a). Regulation of AKT/PKB is by the action of direct dephosphorylation of several enzymes like protein phosphatase-2A and PH-domain leucine-rich repeat protein phosphatase (Bayascas and Alessl, 2005; Taniguchi *et al.,* 2006a). Other proteins like the tribbles-3 binds to the inactive form of AKT/PKB and ensure that the protein remains inactive. Tribbles-3 has also been identified as a means to improve insulin sensitivity by induction of its down regulation (Du *et al.,* 2003).

1.3.2.5. PROTEIN TYROSINE PHOSPHATASE 1 BETA (PTP1*β*)

PTP1*β* is a 435 amino acid base protein (figure 1.4) with a 35 residue C-terminal solely devoted to the translocation of the phosphatase to the endoplasmic reticulum (ER). Residues 214 to 221 are known as the P-loop (phosphotyrosine binding loop/active site). The Tryptophan-Proline-Aspartate (WPD) loop (177 to 185) consisting of Trp, Pro and Asp and R loop (113 to 118) converges with the substrate, allowing for the position of Cys 215 as a nucleophile (Combs, 2010; Kumar *et al.,* 2010). Asp 181 acts as an acid catalyst in the mechanism while His 214 and Asp 221 are also involved (Kumar *et al.,* 2010; Tonks, 2003).

IR and IRS activities are tightly regulated by protein tyrosine phosphatases (PTP's) and serine phosphorylation (Pederson *et al.,* 2001; Taniguchi *et al.,* 2006a). Important proteins which are found at this point are the PTP1*β* and the suppressor of cytokine signalling (SOCS) proteins. PTP1*β* has become the focus of antidiabetic research as it was found that when silenced in diabetic rats, a noticeable increase in insulin sensitivity results (Klaman *et al.,* 2000). SOCS1 has been found to be of interest as well, as it has been concluded that this protein is up regulated in states such as obesity and lipopolysaccharide-induced endotoxemia which are known to be associated with T2DM (Rieusset *et al.,* 2004). SOCS1 and SOCS3 are now known to cause a decrease in tyrosine phosphorylation of IRS proteins as well as initiating IRS degradation via the ubiquitin-proteosome pathway (Gual *et al.,* 2005; Ueki *et al.,* 2004).

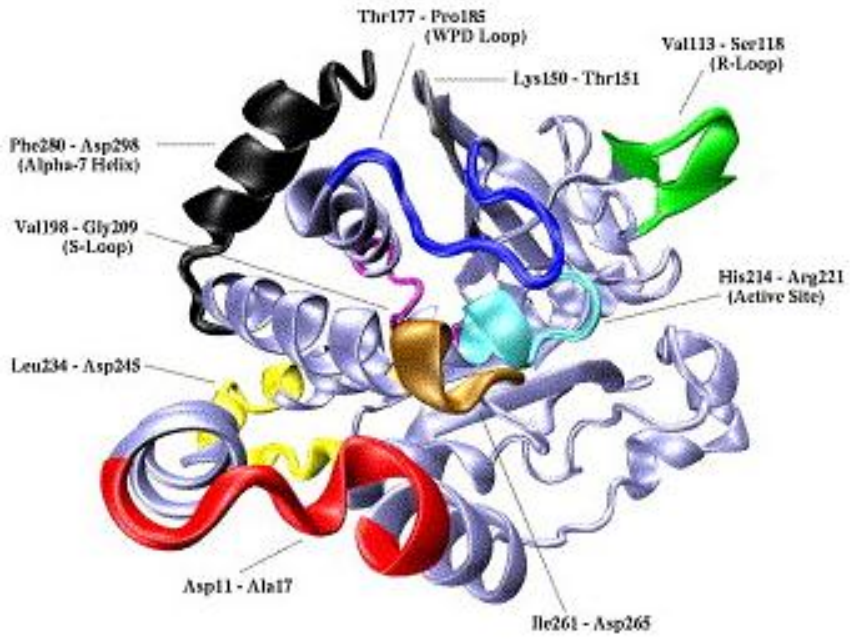

Figure 1.4: The 3-dimentional structure of PTP1*β*. Several domains are highlighted and labelled including the active site (light blue), the WPD loop (dark blue), S- (purple) and R-loop (green) (Kramerlin *et al.,* 2006).

Protein tyrosine phosphatases as well as other kinases play an important role in regulating cell signalling cascades and there are several different types. These can either be activators or inhibitors of certain cellular processes thus highlighting their importance in diabetes research as regulators of the insulin signalling pathway. Knowledge of phosphatases involved in the insulin signalling pathway allows for their manipulation and consequently manipulation and control of the specific cell signalling cascades involved. PTP's are enzymes which catalyse the dephosphorylation of proteins and there are more than a 100 PTP isoforms active in human cells (Zhang and Zhang, 2007).

It was found that PTP1$\beta^{-/-}$ mice became much more sensitive to insulin (Klaman *et al.,* 2000; Gum *et al.,* 2003). It was illustrated that increasing PTP1*β* expression levels decreased insulin activity in cell lines while inhibition of PTP1*β* increased activity of insulin signalling (Zhang and Zhang, 2007). PTP1*β* acts as a negative regulator of insulin signalling and therefore PTP1*β* inhibition allows for the signal to remain active for longer periods in targeted cells (figure 1.5).

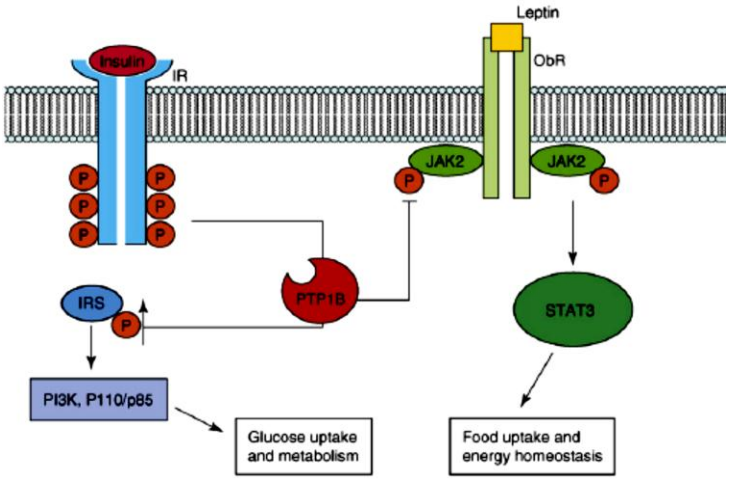

Figure 1.5: Activity of PTP1*β* showing the phosphatase action on JAK2, IRS and IR (Zhang and Zhang, 2007). (IR=Insulin receptor, IRS=Insulin receptor substrate, P=Phosphate, PI3K=Phosphatidylinositol 3-kinase, PTP1*β*=Protein tyrosine phosphatase 1 beta, STAT3=Signal transducer and activator of transcription, JAK2=Janus kinase 2).

PTP1*β* is expressed ubiquitously in humans and is found on the cytoplasmic side of the ER membrane (Zhang and Zhang, 2007). Muscle cells have been implicated in T2DM since these absorb 80% of glucose in response to insulin signalling. PTP1*β* was silenced in C2C12 myoblasts and was found to be resistant to T2DM induced by the introduction of palmate (Bakhtiyari *et al.,* 2010). It was expected that PTP1*β* inhibition should result in weight gain as glucose would be absorbed into adipocytes at a higher rate. However this is not the case as these phosphatases are involved with leptin signalling (figure 1.5) (Koren and Fantus, 2007). Experiments have shown that PTP1$\beta^{-/-}$ mice illustrate their inability to gain weight and increased insulin sensitivity (Koren and Fantus, 2007; Zhang and Zhang, 2007). When active, PTP1*β* is able to dephosphorylate Janus kinase (JAK2) thus inactivating it. When PTP1*β* is inhibited, JAK2 can activate STAT3 which acts as a transcription factor (figure 1.5). Leptin signalling becomes more sensitized as a result, causing increased metabolism of glucose and thus is released as energy promoting cell growth and differentiation (Koren and Fantus, 2007). This double function of PTP1*β* is extremely valuable in the treatment of diabetes as there is a correlation between obesity and T2DM (Montalibet and Kennedy, 2005).

Inhibition studies with small molecule inhibitors and PTP1*β* have been completed extensively over the last decade. Downfalls in attempts to create adequate PTP1*β* inhibitors have been hindered by inadequate pharmacokinetic properties. PTP's are subdivided into two categories; the receptor-like PTP's and intracellular PTP's. PTP1*β* belongs to the intracellular group and is moved to the ER where it conducts its phosphatase activity. Within this group there are many subfamilies with similar biological activity but very different biological functions. TC-PTP (T-cell protein tyrosine phosphatase) has 74% total sequence similarity to PTP1*β* and 94% similarity with the PTP1*β* active site; however they have very different biological functions (Iversen *et al.,* 2002; Montalibet and Kennedy, 2005). This was demonstrated in TC-PTP$^{-/-}$ mice which do not live longer than 3-5 weeks (Iversen *et al.,* 2002), while TC-PTP$^{-/-}$ and PTP1*β*$^{-/-}$ mice die at day 10 of embryonic development (Heinonen *et al.,* 2009). In muscle cells it was found that TC-PTP deficiency does not affect glucose homeostasis or insulin signalling highlighting a non-redundant role in development, macrophage development and insulin signalling (Loh *et al.,* 2012) As a consequence, inhibition of PTP1*β* has to be highly specific (Kramerlin *et al.,* 2006). Essentially, inhibition studies should not be confined to active site interactions only, as the active site of this family of enzymes tends to be highly conserved. Attention needs to be placed on domains like the WPD, R or S-loops which are known to change conformation in accordance with p-tyr (phosphotyrosine) binding.

Many PTP1*β* inhibitors which exhibit potent inhibition as low as nanomolar (nM) range have been discovered. This is partially attributed to the charge difference between positively charged PTP1*β* active sites and the negatively charged small molecule inhibitors (Zhang and Zhang, 2007). This creates an issue through their bioavailability at PTP1*β* within cells as these molecules are repelled by the hydrophobic cell surface. Advancements were made in the form of pro-drug development and generating more lipophilic drugs but have only been partially successful (Montalibet and Kennedy, 2005).

There has been extensive research completed on PTP1*β* since the X-ray structure was determined in 1994 (Combs, 2010). Analysis of this included inhibition assays and *in silico* docking of potential inhibitory compounds. Compounds included biflavonoids, thiophene derivatives, formylchromone derivatives, thiazolidinedione derivatives, and many more. (Kim *et al*., 2007; Lee *et al.,* 2008; Bhattarai *et al.,* 2009; Ye *et al.,* 2010). Inhibition of this protein target has been documented in several investigations with inhibition constant values as low as micromolar and nanomolar range (Combs, 2010). Results are not as favourable when effects of the compounds are completed on cell lines as they may be cytotoxic and have no *in vivo* effect based on their pharmacokinetic properties.

1.3.3. GLUT4 TRAFFICKING

The link between GLUT4 and insulin signalling has been under intense investigation and has been found to be an intricate network of reactions within the cell ultimately organizing subcellular compartments to facilitate GLUT4 trafficking to the cell surface (Watson and Pessin, 2006). GLUT4 is stored within intracellular tubulovesicular structures, vesicles in the cytoplasm and clathrin-coated pits near the plasma membrane. However most GLUT4 is found within a set of biologically distinct vesicles closely related to recycling endosomes and are referred to as GLUT4 storage vesicles (GSV) (Leney and Tavare, 2009). GSV's are recycled between the cell surface and the trans-Golgi apparatus but under insulin-free conditions, 90% of GLUT4 is found in the trans-Golgi network in 3T3-L1 cells (Leney and Tavare, 2009). Besides the PI3K pathway described above, there is another pathway called the wortmannin-insensitive pathway which is stimulated by insulin signalling (figure 1.3 and 1.6). Mouse Casitas B-lineage Lymphoma (c-Cbl) is recruited by APS and CAP to activated IRs' and phosphorylated on tyrosine residues (Leney and Tavare, 2009). Activated c-Cbl recruits Crk-like protein (CrkI) and guanine nucleotide-releasing protein (C3G)

where C3G activates the GTP binding protein, TC10, which has several downstream targets. IR activation via both the wortmannin-insensitive and PI3K pathways results in actin rearrangements and PIP_3 formation at the plasma membrane (Lopez *et al.,* 2009). There has been resounding evidence that the Cbl pathway plays a minimal role in GLUT4 translocation which was found by siRNA silencing of CAP and Cbl as well as APS knockout mice (Leney and Tavare, 2009). This allows for the conclusion that the main player in GLUT4 translocation should be the PI3K pathway.

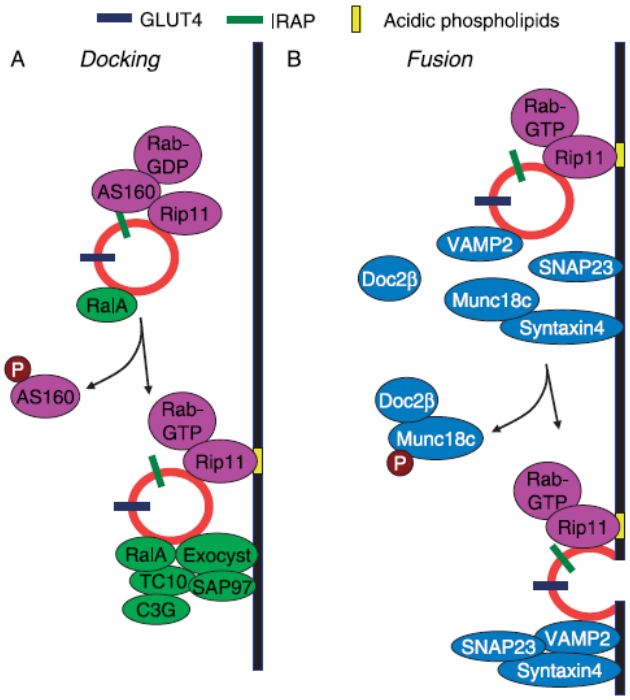

Figure 1.6: GLUT4 fusion to the plasma membrane is facilitated by several proteins which occur in two stages, A) docking and B) fusion (Leney and Tavare, 2009). (AS160=Akt substrate of 160 kDa, Rip11=Rab11 interacting protein, RalA=Ras-related protein A, P=Phosphate, TC10=Ras related GTP binding protein, SAP97=Synapse-associated protein 97, C3G=Guanine nucleotide-releasing factor 2, VAMP2=Vesicle associated membrane protein 2, Doc2β=Double C2-like domain containing protein beta, Munc18c=Mammalian uncoordinated-18, SNAP23=Synaptosomal-Associated protein 23,).

AS160 is phosphorylated by PKB which allows for its dissociation from GSV's allowing activation of Rab-GDP and release of Rab11 interacting protein (Rip11). Rip11 is then able to bind to acidic phospholipids in the plasma membrane while remaining bound to the GSV (Leney and Tavare, 2009). Shown in green in figure 1.6 is the exocyst complex which assembles in a manner which is not fully understood although it is believed that assembly is regulated by TC10 and RalA via the wortmannin-insensitive pathway. After docking with the plasma membrane, fusion takes place with a specific set of proteins called SNARE proteins (VAMP2, SNAP23 and syntaxin4) and Rab-GTPases. As GSVs dock with the plasma membrane, VAMP2 associates with syntaxin4 and SNAP23 in a coiled structure which allows for the GSV's and plasma membrane to fuse. SNARE proteins have been found to be regulated by insulin signalling via kinase activity. In the absence of insulin signalling, Munc18c and Doc2*β* have been found to interact with SNARE proteins inhibiting their function. Phosphorylation of these SNARE binding proteins causes their dissociation with their target proteins.

1.3.4. HEPATOCYTES

With high glucose concentrations, insulin is released and liver cells respond by absorbing glucose from the surrounding blood in order to lower the blood glucose concentration. This occurs more rapidly in hepatocytes than adipocytes and myocytes since hepatocytes house GLUT2 instead of GLUT4 glucose transporters (Vaulont *et al.,* 2000). GLUT2 is not recruited to the plasma membrane under the influence of insulin as is seen with GLUT4. Instead GLUT2 expression is upregulated as a result of sterol regulatory element-binding protein (SREBP) transcription factor activation during high glucose conditions (Im *et al.,* 2005). This ensures that a rapid equilibrium is achieved between the blood glucose levels and hepatocyte cytoplasmic glucose concentrations (Vaulont *et al.,* 2000). Assimilated glucose is stored in the liver cells as glycogen and lipids for use when the glucose concentration decreases below the required limit (4

mM). Along with glycogen (figure 1.7A) and lipid production, the liver reduces glucose release and production through the suppression of gluconeogenesis (figure 1.7B). In order for this to be accomplished, the insulin signal is required to affect hepatocyte proteins involved in the processes by either activation or repression of expression levels (Dipl-Pharm and Zierath, 2005).

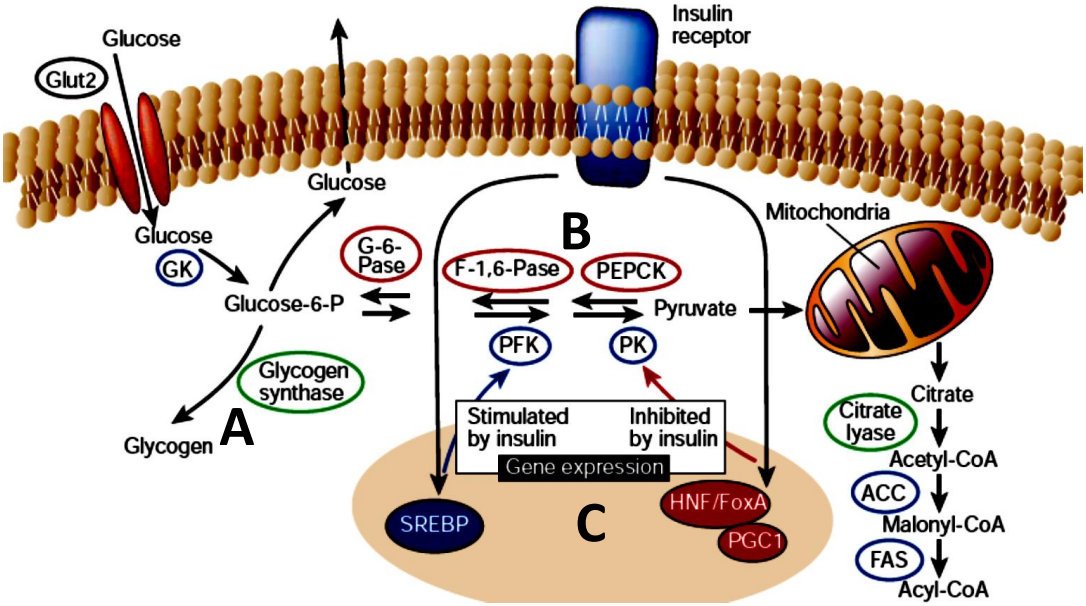

Figure 1.7: A diagram illustrating the signal transduction through a hepatocyte due to the activation of the IR by insulin. Enzymes activated by insulin are circled in blue (glycolytic and lipid synthesis) while those repressed are circled in red (B) (gluconeogenic) (Dipl-Pharm and Zierath, 2005). Glycogen synthesis and the nucleus are represented by A and C, respectively. (GLUT2=Glucose transporter 2, GK=Glucokinase, G-6-Pase=Glucose-6-phosphatase, F-1,6-Pase=Fructose-1,6-bisphosphatase, PEPCK=Phosphoenolpyruvate carboxykinase, PFK=Phosphofructokinase, PK=Pyruvate kinase, SREBP= Sterol regulatory element-binding protein, HNF/FoxA= Hepatocyte nuclear factor/Forkhead box protein A, PGC1= Peroxisome proliferator-activated receptor-γ coactivator, ACC=Acetyl-CoA carboxylase, FAS=Fatty acid synthase, CoA=Coenzyme A).

Hepatocyte signalling of insulin functions occurs via a phenotypic shift by regulation of several processes such as activation of glycogen synthesis and lipid synthesis while suppressing gluconeogenesis and glycogenolysis (Michael *et al.,* 2000). Figure 1.7C shows how the insulin signal reaches proteins in the nucleus

(transcription factors: SREBP-1, FOX, PGC1 and HNF), activating them to elicit these responses.

1.4. PREADIPOCYE CELL DIFFERENTIATION

Adipocytes were initially regarded as a mass of tissue with little function in the human body (Greenberg and Obin, 2006). This has changed since the discovery of leptin more than a decade ago. It is now known as an important tissue which should be studied as it is involved in nutrient homeostasis and contributes to the development of T2DM (Rosen and MacDougald, 2006). Obese individuals are more susceptible to cardiovascular diseases and T2DM as concluded by several researchers (Grontved, 2011; Malik *et al*., 2010). Resistin, tumour necrosis factor-α (TNFα), interleukin-6 (IL-6) and peroxisome proliferator-activated receptor gamma (PPARγ) have all been implicated as linking adipose tissue to the development of T2DM (Dandona *et al.,* 2004; Greenberg and Obin, 2006; Spiegelman, 1998; Steppan *et al.,* 2001).

In figure 1.8 it can be seen that several factors play a part in adipocyte differentiation. Insulin triggers the adipogenesis signal transduction via the MAPK (A), mTOR (B) and PI3K (C) pathways. Research involving the MAPK pathway has been contradictory as it includes extracellular-signal-regulated kinase (ERK) which has been found to act as an inducer and repressor of adipogenesis. Early experiments involving ERK have shown that it allowed differentiation of preadipocytes to adipocytes. Later this was challenged as it was found that ERK also phosphorylates the essential transcription factor PPAR*γ* and thus inhibits differentiation (Burns and Vanden Huevel, 2007). In later years a better understanding of this molecule indicated that the ERK activity in cells was regulated through differentiation, which was confirmed as ERK is required in the proliferative step (mitotic clonal expansion or MCE) during which time PPARγ expression is low. When the differentiating cell has reached the final stages, ERK expression is decreased to prevent phosphorylation of PPARγ (Bost *et al.,* 2005).

Interestingly it has been shown that as inhibition of ERK1 increases, insulin sensitivity is increased.

ERK1 is known to act as an inhibitor of IRS1 which is essential in transduction of the insulin signal. This is accomplished by the serine phosphorylation of IRS1 and is now known to contribute to insulin resistance in obesity (Bost *et al.,* 2005). As shown in figure 1.8 insulin plays a vital role, however, it does so through IGF1 and not through IR. The final transcription factor which is activated and is essential for adipogenesis is PPARγ (Rosen and MacDougald, 2006).

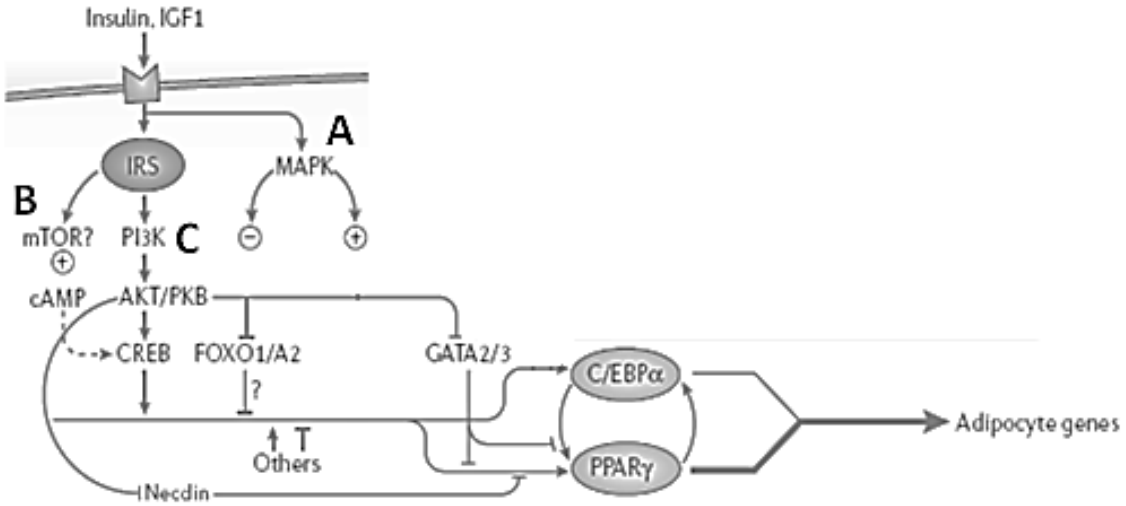

Figure 1.8: Adipogenesis signal transduction pathway illustrating the external factors which allow for the expression of adipocyte genes to be activated. (IGF1=Insulin growth factor receptor, IRS=Insulin receptor substrate, PI3K= Phosphatidylinositol 3-kinase, AKT/PKB=Protein kinase B, CREB= cAMP response element binding protein, mTOR=Mammalian target of rapamycin, cAMP=Cyclic adenosine monophosphate, FOXO1/A_2= Forkhead box protein O1/A_2, GATA2/3= GATA binging protein 2/3, C/EBP*α*= CCAAT-enhancer binding protein, PPAR*γ*= Peroxisome proliferator-activated receptor gamma).

Inhibition of p38 has been shown to decrease the rate of adipogenesis as a result of decreased CCAAT-enhancer binding protein (C/EBPα) phosphorylation and a lack of its post-translational modification. However, once again the function of p38 has been contradictory with several authors describing p38 as an inhibitor of adipogenesis as it acts as an activator of adipogenesis inhibitors. In T2DM p38

inhibits trafficking of GLUT4 to the cell membrane and thus has been implicated as a target of insulin resistance in adipocytes. More investigation is required to elucidate the process by which p38 reduces glucose uptake (Bost *et al.,* 2005).

PPARγ is the end point of all signalling which takes place in preadipocyte differentiation (Rosen *et al.,* 1999). When induced this transcription factor can cause the differentiation of preadipocytes to adipocytes (Rosen and MacDougald, 2006). All external factors which contribute to the differentiation of preadipocytes allow for the tight regulation of PPARγ as seen in figure 1.8. Insulin signalling is no exception to this as it is known that at three points in the signalling route, regulation of insulin signalling occurs. AKT/PKB is the activator of PPARγ and does so through activation of cAMP response element binding protein (CREB), yet AKT/PKB is also a deactivator of FOXO1/A_2, necdin and GATA binging protein 2/3 (GATA2/3) as seen in figure 1.8. These are known to inhibit the activation of PPARγ thus showing how essential insulin recognition is in adipogenesis (Rosen and MacDougald, 2006).

1.5. CURRENT AVAILABLE TREATMENTS FOR DM

1.5.1. COMMERCIALLY AVAILABLE TREATMENTS

In order for a patient to counteract the metabolic symptoms of DM, a complete change of lifestyle is essential. This includes correcting nutrition and exercise to manage weight gain. Numerous medical/pharmaceutical treatments are currently prescribed to better control blood glucose levels and the associated metabolic symptoms of DM. These can be administered as a single drug or as a cocktail of two or more drugs. Unfortunately most of these drugs have harsh side-effects and are expensive. In Sub-Saharan Africa DM is severely underestimated, not only in terms of morbidity, but also with the medical costs involved (Hall *et al.,* 2011). A survey was completed indicating the cost per diabetic patient would

reach 7% (4 993 394 international dollars) of the national budget annually for healthcare in Africa (Hall *et al.,* 2011; Zhang *et al*., 2010).

1.5.1.1. SULFONYLUREA (SU)

For insulin to be secreted from β-cells, the K_{ATP} channels are closed causing depolarisation of the plasma membrane of the β-cells (Henquin, 2000). SU influences this process by binding to a protein called sulfonylurea receptor (SUR) which is the regulatory subunit of the K_{ATP} channel (Gribble *et al.,* 1998). This ensures the closure of the K_{ATP} channel and thus depolarisation and consequent insulin release (Bryan *et al.,* 2005). Another mechanism through which SU acts on β-cells occur via interaction with exchange Protein directly affected by cAMP 2 (Epac2) which is a guanine nucleotide exchange factor for the G protein Rap (Gloerich and Bos, 2010; Zhang *et al.,* 2009). This was elucidated through fluorescence Resonance Energy Transfer (FRET) and the evidence that SU has a diminished effect on insulin secretion in mice lacking Epac2 (Zhang *et al.,* 2009). Independent of the mechanism, it is known that SU acts as an insulin secretagogue with hypoglycaemia often being a side-effect of SU use (Hassan Murad *et al.,* 2009). Other side-effects include weight gain which is a result of hyperinsulinemia as this condition can increase appetite (LeRoith *et al.,* 2004). The binding properties of SU have been investigated and were found to interact with K_{ATP} channels of other tissues including the brain and cardiac muscle (Garratt *et al.,* 1999; Riveline *et al.,* 2003). However clinical studies do not correlate any negative effects of SU with cardiovascular dysfunction (LeRoith *et al.,* 2004). Other insulin secretagogues have been developed which have a lower affinity for heart and skeletal muscle K_{ATP} channels (LeRoith *et al.,* 2004). Meglitinides such as nateglinide and repaglinide are structurally different from SU, but act in the same way as SUR1 and thereby facilitate insulin secretion. Meglitinides are generally used for patients with a more erratic lifestyle as these provide better control of blood glucose (Hamilton, 2012). This is due to their short

half-life and thus allows a shorter time of physiological action decreasing the possibility of hypoglycaemia (Scheen, 2007). Nateglinide has been found to have a lesser affinity for cardiac muscle K_{ATP} channels which is an improvement from older insulin secretagogues (Richard and Raskin, 2011).

1.5.1.2. THIAZOLIDINEDIONE (TZD)

TZDs act by initiating differentiation of preadipocytes to mature adipocytes. Adipocytes take up glucose which accumulates as lipids in lipid vacuoles and results in a lowering of blood glucose (Rosen and Spiegelman, 2006). TZDs like rosiglitazone and pioglitazone act as PPAR*γ* agonists which initiate preadipocyte differentiation into adipocytes, thereby enhancing insulin action and sensitization (Kahn *et al.,* 2000; Zhang *et al.,* 2007). TZDs are very efficient in reducing blood glucose levels but are accompanied by side-effects. Investigations have shown the potential of rosiglitazone to decrease bone density (Schwarts, 2008). Studies show post-menopausal women using this treatment are considered to be at a higher risk of osteoporosis than younger women and men (Fitzpatrick *et al.,* 2011). Hussein *et al.,* (2004) illustrated that the use of rosiglitazone and pioglitazone significantly increase cholesterol levels in patients. On 23rd September 2010, the U.S. Food and Drug Administration (FDA) began restricting the use and availability of rosiglitazone as a treatment for DM as investigations and clinical trials had proven rosiglitazone to be a dangerous oral hypoglycaemic drug (http://www.fda.gov/Drugs/DrugSafety). In a study done by Lipscombe *et al.* (2007) which investigated the effects of TZDs on an elder community of diabetics, it was concluded that TZDs significantly increased the patient's risk of congestive heart failure and acute myocardial infarction.

1.5.1.3. METFORMIN (MET)

MET is an insulin sensitizing agent which increases glucose uptake in peripheral tissues, especially hepatocytes (Zhang *et al*., 2009). MET acts by stimulating AMPK activation and decreasing glucose-6-phosphatase expression and thereby decreasing glucose output from the liver (Ota *et al*., 2009; Ouyang *et al.,* 2011). Unlike TZDs and SU, MET does not cause an increase in body weight when administered to patients and acts as an appetite suppressant (Kirplchnikov *et al.,* 2002).

The side-effects associated with MET include abdominal pain, flatulence and diarrhoea. Due to its effects in the intestine, MET also inhibits vitamin B_{12} absorption (Kirplichnikov *et al.,* 2002). The most serious side-effect induced is lactic acidosis which is potentially life threatening, but is not a common occurrence (Kirplichnikov *et al.,* 2002).

1.5.1.4. INSULIN TREATMENT

The administration of insulin is used routinely as a treatment for DM alongside the use of other anti-hyperglycaemic drugs (Holman *et al.,* 2009). Provision of insulin in poorer countries is limited as the national health budgets of these countries make substantial provision for infectious diseases such as human immunodeficiency virus and acquired immunodeficiency syndrome (HIV/AIDS) and malaria (Gill *et al.,* 2011). Access to insulin within the rural areas of poorer countries is a known issue while the cost of insulin as treatment is an expensive means of DM treatment for the general population of third world countries (Gill *et al*., 2011).

1.5.2. USE OF *LEONOTIS LEONURUS* AS A THERAPEUTIC AGENT

As far back as 1939, MAR and its structure had been investigated (Holis *et al.,* 1939). MAR has been found in plants belonging to the family *Lamiaceae* to which the shrub *L. leonurus* belongs (Kenechukwu, 2004). *L. leonurus* is found indigenously in South Africa and has been used for centuries as a medicinal herb by the Zulus, Khoi-Khoi, Sothos and Xhosas. It is also known as “wild dagga”, “umunyane” and “umfincafincane” to the local South African population (Kenechukwu, 2004). It had been documented to be used medicinally for many ailments including: influenza, cramps, hypertension, sores, stings and bites. (Kenechukwu, 2004). In a survey done by Oyedemi *et al.,* (2009) on the traditional South African methods of treatment, 15 plant species were named by traditional healers and herbalists. The most common of the species named in the survey were *Strychnos henningsii* and *L. leonurus*. A second survey completed in the Eastern Cape, South Africa, found plants from the family *Asteraceae* comprised 50% of the medicinal plants used for DM treatment (Erasto *et al.,* 2005). Traditional healers are often consulted in Southern Africa as there is a lack of medical resources in the rural areas, as well as the fact that treatment for DM is too expensive for the rural population (Oyedemi *et al.,* 2009). Traditional healers identify DM by several symptoms including loss of body weight, excessive urination, fatigue and sweet urine (Awah *et al*., 2009). Treatment is medium term and ranges between 6 months to one year. Reported results are often positive with a decrease in urination and patients becoming more energized. There were even reports of complete recovery after the treatment without other harmful side-effects (Oyedemi *et al.,* 2009). This evidence alone should justify investigations into the active compounds in medicinal plants as a potential treatment for DM (Oyedemi *et al.,* 2009).

1.5.3. MARRUBIIN AND MARRUBIIN DERIVATIVES AS POTENTIAL ANTIDIABETIC TREATMENTS

MAR is a labdane diterpene and is isolated from *Marrubium vulgare* which belongs to the family *Lamiaceae* (figure 1.9) (Knoss *et al.,* 1997). Currently, the purified form of MAR is predominantly in research phase. The potential applications for MAR and compounds derived from MAR include the medicinal use as an analgesic, insecticide, antiedematogenic, antidiabetic and for cardiovascular problems including hypertension (Novaes *et al.,* 2001; Stulzer *et al.,* 2006; Mnonopi *et al*., 2011; Mnonopi *et al.*, 2012).

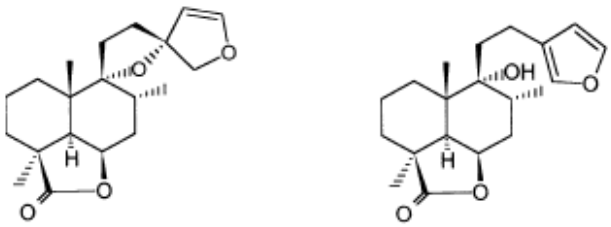

Figure 1.9: Chemical structures of MAR and premarrubiin (Knoss *et al.,* 1997).

Diterpenoids are naturally produced by plants from many genera. Investigations into the *in vitro* cytochemical effects of these compounds have been extensive, since natural plant compounds would benefit patients as they may elicit less unwanted side-effects when used as treatments. Completed experiments include cytotoxic testing, PTP1*β* inhibition studies (*in vitro*) and their antimicrobial potential to name a few (Kuzma *et al.,* 2007; Na *et al.,* 2006; Roengsumran *et al.,* 2001).

Diterpenoids of interest would be those which have been implicated as antidiabetic agents such as regulators of PTP1*β* activity. An investigation was completed on the inhibitory effect of diterpenoids isolated from *Acanthopanax koreanum*, traditionally used in Korea as a diabetic treatment (Na *et al.,* 2006). Isolation and screening of these compounds from the plant led to the discovery of

diterpenoids which were able to inhibit PTP1*β* (a target for antidiabetic therapy in T2DM). Initially CH_2-Cl_2 soluble root extracts were screened and contained PTP1*β* inhibitors (72% inhibition at 30 µg/mL), later identification of 3 diterpenoid compounds in the root extract was associated with the inhibition of PTP1*β* (Na *et al.,* 2006). One of these compounds had an IC_{50} value of 7.1 ± 0.9 µM and displayed non-competitive inhibition (Na *et al.,* 2006). Although *Acanthopanax koreanum* does not belong to the same botanical family as *L. leonurus*, the structural similarity between the diterpenoids is comparable (Na *et al.,* 2006).

Oyedemi *et al.,* (2011) illustrated the antidiabetic effects of an aqueous leaf extract of *L. leonurus* in a streptozotocin (STZ)-induced diabetic rat model. Rats were treated with STZ after which they displayed elevated blood glucose, water intake and cholesterol levels associated with DM. However during the 15 day time study with administration of the *L. leonurus* aqueous extract, the rats began displaying lower blood glucose, HDL and reduced intake of water (Oyedemi *et al.,* 2011). Organic extracts of *L. leonurus* and MAR were tested for their antidiabetic properties on rats with high fat diet-induced DM (Mnonopi *et al*., 2012). The obese control had illustrated high cholesterol levels which were indicative of a patient with cardiac risk whereas obese rats treated with MAR had illustrated decreased LDL levels with an increase in HDL. Rats treated with *L. Leonurus* organic extract had shown decreased cholesterol profile compared to the obese control. However MAR-treated rats displayed a significant decrease in cholesterol levels (Mnonopi *et al*., 2012). In correlation with decreased cholesterol levels, treatments had also increased insulin secretion compared to the obese control. The obese control insulin level was 1.24 ± 0.02 ng/mL while the MAR obese and obese *L. leonurus*-treated rats displayed 4.75 ± 0.01 ng/mL and 2.75 ± 0.03 ng/mL, respectively (Mnonopi *et al*., 2012). These results clearly show the abilities of *L. leonurus* extracts and MAR to act as insulin secretagogues, and thus improve the DM state through changes in cholesterol, insulin and blood glucose levels.

This study aims to investigate the effects of MAR and MAR derivatives on PTP1*β* inhibition, glucose uptake in hepatocytes, myocytes and adipocytes and the molecular basis associated with the improved glucose uptake.

CHAPTER 2: AIMS AND OBJECTIVES

This investigation aims to elucidate the anti-diabetic potential of MAR and MAR derivatives. It is to be accomplished through analysis of the interactions between PTP1*β* and the respective treatments by *in silico* and *in vitro* inhibition studies (Chapter 3, 4 and 5). This will be followed by *in vitro* screening of the treatments for cytotoxicity and glucose uptake analysis in Chang, C2C12 and 3T3-L1 cell lines. Screening of the treatments will provide an indication of the cell lines most suitable for further investigation at the molecular level. Molecular analysis will be completed using western blotting and RT-PCR. The study will include the following objectives using MAR and MAR derivatives.

1. *In silico* inhibition screening of MAR and MAR derivatives (20 compounds) on PTP1*β* using AutoDockTools 4.2 (ADT).
2. Conduct *in vitro* enzyme inhibition studies using PTP1*β* and alkaline phosphatase (ALP).
3. Perform *in vitro* analysis C2C12, 3T3-L1 and Chang cell lines with regards to cytotoxicity and glucose uptake studies.
4. Using the compounds eliciting the highest glucose uptake effect the following molecular studies will be conducted:
    4.1. Determine IRS1, phospho-IRS1, PI3K, phospho-PI3K and PTP1*β* levels, with *β*-actin as a reference protein, using Western blotting.
    4.2. Determine GLUT4 and IRS-1 expression levels using RT-PCR.

PART II: *IN SILICO* COMPUTATIONAL MODELLING AND *IN VITRO* ENZYME INHIBITION STUDIES OF PTP1β

CHAPTER 3: METHODS AND MATERIALS

3.1. *IN SILICO* COMPUTATIONAL MODELLING

3.1.1. 3D CONSTRUCTS OF MAR AND MAR DERIVATIVES

Chemical structures of MAR and MAR derivatives were constructed in ACD/Chemsketch 11.01 (figure 3.1). Using the software provided, two dimensional (2D) drawings were converted to three dimensional (3D) simulations (refer to ACD/Chemsketch reference manual). Chemsketch utilises a 3D optimisation function which takes into account bond stretching, van der Waals forces, bond angles and internal rotation. This 3D optimisation function is based on CHARMM parameterisation but is modified in order to increase the stability and speed of the computation (figure 3.1).

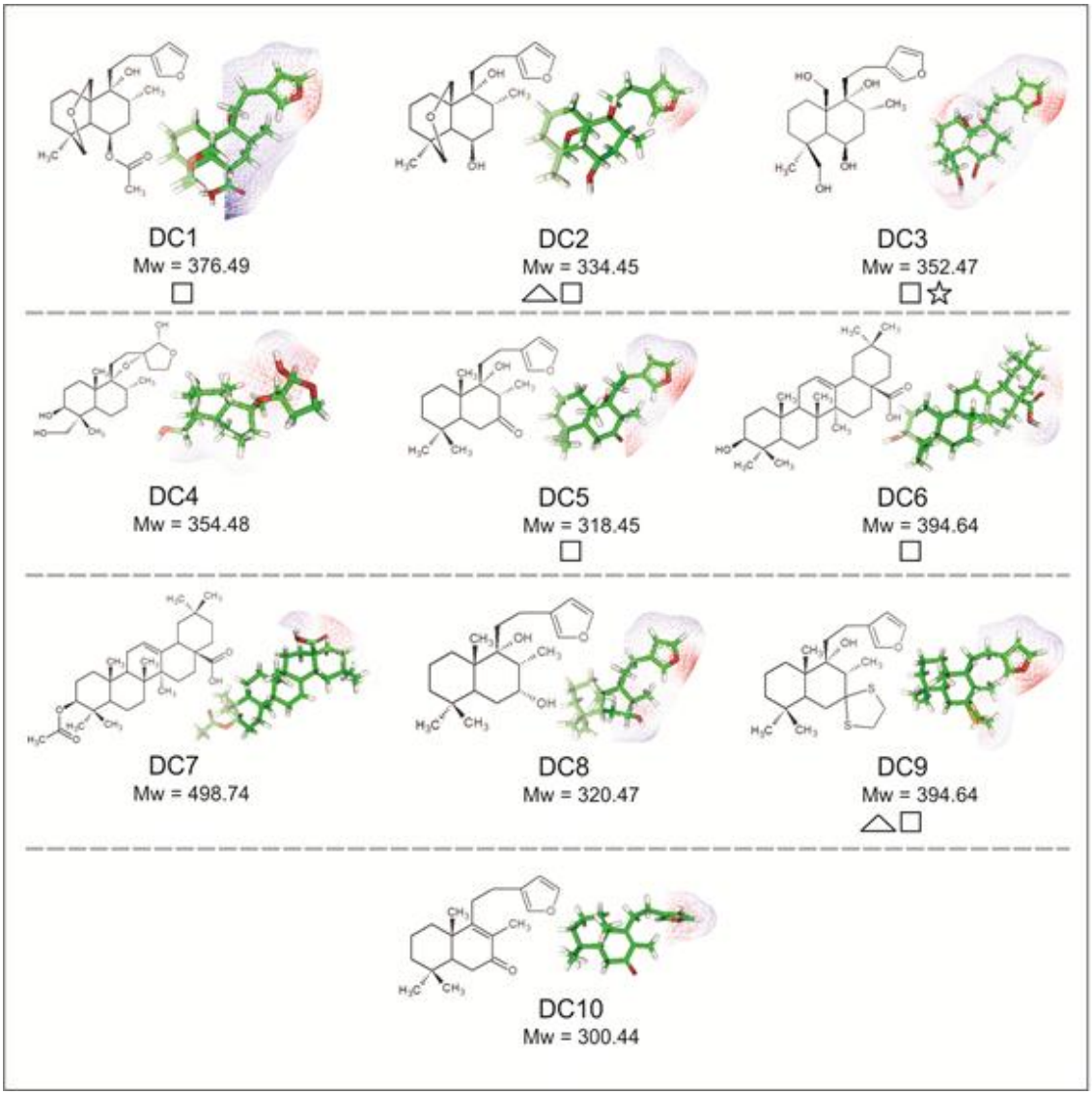

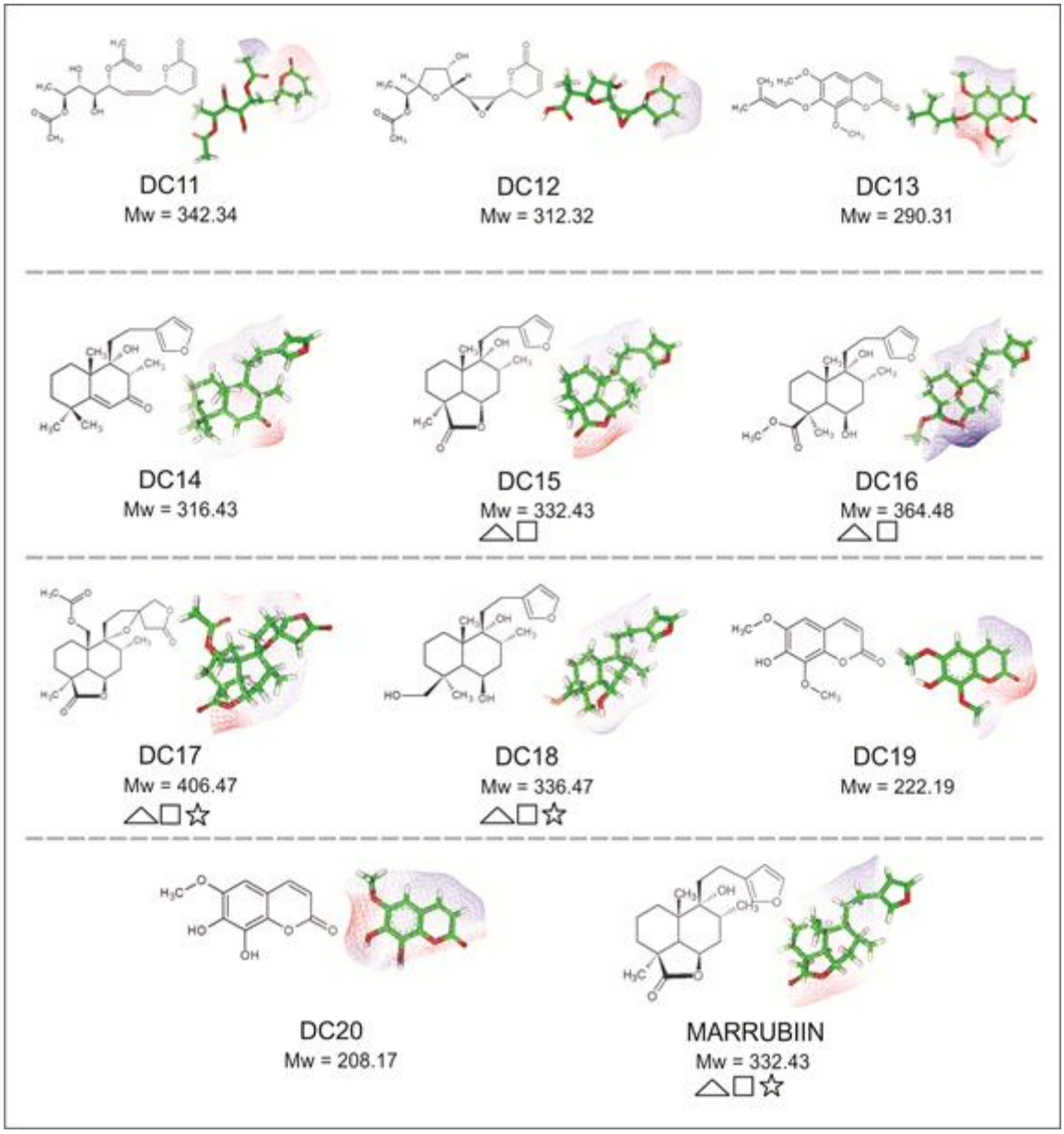

Figure 3.1: Two-dimensional (2D) drawings and three-dimensional (3D) constructs of MAR and MAR derivatives drawn in ACD/Chemsketch 11.01 and DSV, respectively. Molecular weights (Mw) and symbols are added for each compound which elicited a significant glucose uptake (see section 6.2) for Chang (△), C2C12 (□) and 3T3-L1 adipocytes (☆). The colours denote specific atoms, i.e. red=oxygen, white=hydrogen, yellow=sulphur and green=carbon. Molecule structures were provided by Prof. Mike Davis-Coleman from the Department of Chemistry, Rhodes University.

3.1.2. PTP1*β* DOCKING STUDIES WITH MAR AND MAR DERIVATIVES.

The constructs in figure 3.1 were converted to *.mol files, compatible for analysis in Accelrys Discovery Studio Visualizer 2.5 (DSV), and subsequently were converted to *.pdb files. From the PDB databank, a digital crystalline 3D structure of PTP1*β* was uploaded (PDB ID: 3EB1). The structure was formatted as a *.pdb file in DSV by removing the ligand (4-[3-(dibenzylamino)phenyl]-2,4-dioxobutanoic acid) as well as any water molecules surrounding the protein which could affect the docking result (Lui *et al*., 2008).

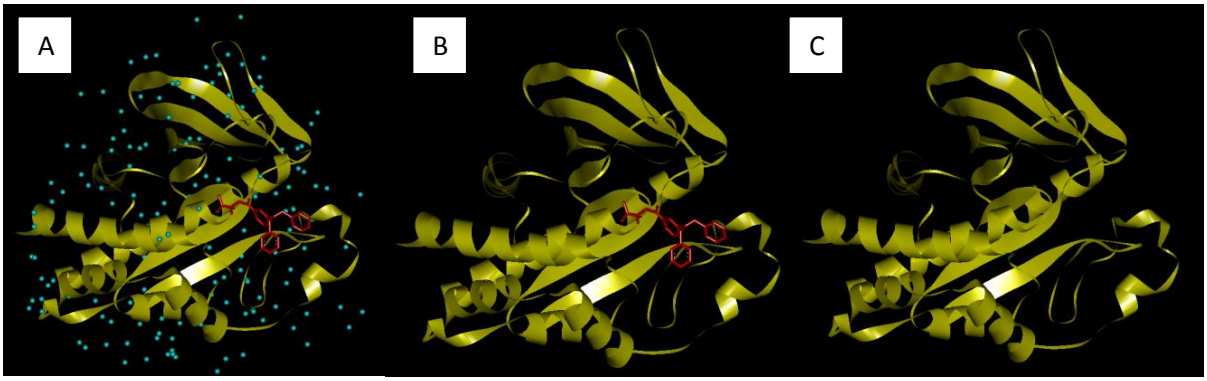

Figure 3.2: A representation of the removal of water molecules and the inhibitor which was imbedded in the active site of PTP1*β*. This was conducted using DSV. A) Raw structure downloaded from the PDB website. B) Waters (blue) have been removed. C) Ligand (red) has been removed to provide the PTP1*β* structure ready for docking procedures.

Once the digital PTP1*β* was successfully formatted and all MAR derivatives were in the 3D and *.pdb format, computational molecular docking was completed using ADT. ADT enables the conversion of *.pdb files to *.pdbqt files which allows for the inclusion of charge and torsion of a ligand or protein. A standard protocol for molecular screening was completed based on the methodology devised by Rao *et al.,* (2006) as explained below. A grid was placed at the active site of PTP1*β* with a spacing of 0.375 Å and 40 grid points per x, y and z axis. An initial population of 50 randomly placed individuals, a maximum of 2 x 10^6 energy evaluations, a mutation rate of 0.02, a crossover rate of 0.8 and an elitism value of 1 was set up for the docking protocol. Three flexible residues, Cys 215, His 214, and Arg 221, were selected based on their importance in phosphatase activity in the active site. Oleanolic acid (DC6) (figure 3.1) is known to be a potent inhibitor of PTP1*β* and was used as a positive control in this investigation (Zhang *et al*., 2008).

3.2. *IN VITRO* INHIBITION STUDIES WITH MAR AND MAR DERIVATIVES

3.2.1. ALKALINE PHOSPHATASE (ALP)

ALP is a zinc metalloenzyme and is found in several tissue types in humans as well as other organisms. There are many isozymes of ALP which all fall under the class of hydrolases. As the name suggests, it has an alkaline pH optimum known to be at pH 9.5 and catalyses the hydrolysis of phosphomonoesters. The physiological importance of ALP was discovered when a high level of ALP was found in bone more than 80 years ago. It is now known that ALP functions in the mineralization of bone (Golub and Boesze-Battaglia, 2007). MAR, MET and MAR derivatives will be tested for their potential to inhibit the action of PTP1*β* and ALP. In this experiment ALP is regarded as a potential candidate for cross reactivity *in vivo* which is undesired as the treatments should be specific to PTP1*β*.

Intestinal calf ALP (Roche) standard curve assays were conducted in clear, non-sterile, 96-well plates (Lasec). This was done in order to establish the concentration of ALP required for following experiments. ALP assay buffer was formulated by mixing 0.1 mM Na_2CO_3 and 0.1 mM $NaHCO_3$, pH 9.5. On the day of the experiment ALP and para-nitrophenylphosphate (*p*NPP) was diluted in ALP assay buffer to 20 mU and 20 mM, respectively. A standard curve was constructed as seen in table 3.1 and plotted in appendix 1, figure A.1.

Table 3.1: Volumes and concentrations of the added components in the generation of the ALP standard curve.

Components	20 mU	10 mU	5 mU	2.5 mU	1.25 mU	BLANK
ALP (µL), [ALP] (20 mU)	20	10	5	2.5	1.25	0
ALP assay buffer	0	10	15	17.5	18.75	20
*p*NPP (µL) stock [pNPP] (20 mM) in assay buffer	180	180	180	180	180	180
Total (µL)	200	200	200	200	200	200
Pre-heat the Biotek Powerwave plate reader to 25^0C						
Plate shake, 5 seconds						
Read at 405 nm, 1 minutes intervals for 7 minutes						

For the generation of double Dixon (DD) plots and determination of K_i, *p*NPP was added at various concentrations for each concentration of compound (table 3.2). The

reaction was initiated by addition of 10 mU ALP. DD plots are given in appendix 1, E figures.

Table 3.2: Volumes and concentrations of the added components in the investigation of ALP inhibition due to DC1 compound. The same procedure was followed for all other compounds

Final [DC1] (µM)	10			5			2.5			BLANK		
DC1 (µL)	2	2	2	2	2	2	2	2	2	2 µL 0.01% DMSO	2 µL 0.01% DMSO	2 µL 0.01% DMSO
pNPP (µL)	178	178	178	178	178	178	178	178	178	178	178	178
pNPP (µM)	*20*	*10*	*5*	*20*	*10*	*5*	*20*	*10*	*5*	*20*	*10*	*5*
ALP assay buffer	10	10	10	10	10	10	10	10	10	10	10	10
ALP [10 mU] (µL)	10	10	10	10	10	10	10	10	10	10	10	10
Total	200	200	200	200	200	200	200	200	200	200	200	200
Pre-heat the Biotek Powerwave plate reader to 25^{0}C												
Plate shake, 5 seconds												
Read at 405 nm, 1 minutes intervals for 7 minutes												

3.2.2. PTP1*β*

Assays were performed in clear, non-sterile, 96-well plates (Lasec). PTP1*β* (Sigma) was reconstituted and frozen in aliquots (4 U/mL) at -80^{o}C. Assay and storage buffers were made according to manufacturer's specifications. An enzyme activity standard curve was constructed as shown in table 2 and the results plotted in appendix1, figure A.2.

Table 3.3: Volumes and concentrations of the added components in the generation of the PTP1*β* standard curve.

Components	**320 mU**	**240 mU**	**160 mU**	**80 mU**	**40 mU**	**BLANK**
PTP1*β* (µL), [PTP1*β*] (20 mU)	80	60	40	20	10	0
PTP1*β* assay buffer	0	20	40	60	70	80
*p*NPP (µL) stock [pNPP] (50 mM) in assay buffer	120	120	120	120	120	120
Total (µL)	200	200	200	200	200	200
Pre-heat the Biotek Powerwave plate reader to 30^{0}C						
Plate shake, 5 seconds						
Read at 405 nm, 5 minutes intervals for 60 minutes						

DD plots were to be used to determine the K_i values of the potential inhibitors. The conditions for the determination of compound inhibition potential on PTP1*β* are shown in table 3.4. Oleanolic acid (DC6) was used as a positive control for PTP1*β* inhibition, using a concentration range of 25, 50 and 100 nM of DC6.

Table 3.4: Volumes and concentrations of the added components in the investigation of PTP1*β* inhibition due to DC1 compound. The same procedure was followed for all other compounds except DC6.

Final [DC1] (µM)	10			5			2.5			BLANK		
DC1 (µL)	2	2	2	2	2	2	2	2	2	2 µL 0.01% DMSO	2 µL 0.01% DMSO	2 µL 0.01% DMSO
pNPP (µL)	118	118	118	118	118	118	118	118	118	118	118	118
pNPP (µM)	*75*	*50*	*25*	*75*	*50*	*25*	*75*	*50*	*25*	*75*	*50*	*25*
PTP1*β* assay buffer	10	10	10	10	10	10	10	10	10	10	10	10
PTP1*β* [320 mU] (µL)	80	80	80	80	80	80	80	80	80	80	80	80
Total	200	200	200	200	200	200	200	200	200	200	200	200
Pre-heat the Biotek Powerwave plate reader to 25^0C												
Plate shake, 5 seconds												
Read at 405 nm, 1 minutes intervals for 7 minutes												

Progress curves were used to plot DD plots from which K_i values were extrapolated, while Lineweaver-Burk (LB) plots were used to extrapolate the V_{max} and K_m under saturating substrate concentrations. Examples of the progress curves (appendix 1; B figures), DD plots (appendix 1; C figures) and LB plots (appendix 1; D figures) are shown.

CHAPTER 4: RESULTS AND DISCUSSION

4.1. COMPUTATIONAL MODELLING OF PTP1*β* AND MAR DERIVATIVES.

PTP1*β* negatively regulates glucose uptake in cells which are sensitive to insulin signalling. Its action is portrayed in its ability to deactivate phosphorylated proteins which are essential to insulin cell signalling, i.e. IRS-1 and insulin receptors (Galic *et al*., 2005). Thus inhibition of PTP1*β* in targeted cell lines like adipose tissue would be of great importance to allow for increased insulin sensitivity. All 20 MAR derivatives, MAR and MET were docked with PTP1*β*. Examples of docked ligands are illustrated in figure 4.1.

Among all the ligands which have been screened, DC6 and DC7 performed the best. DC6 can be seen bound tightly to PTP1*β* in figure 4.1. The amino acids which interact with DC6 through hydrogen bonds are Asp 48, Lys 116 and Lys 120 (figure 4.1). The orientation of DC4 can be compared to that of DC6 with hydrogen bonds as hydrogen bonding between PTP1*β* and DC4 is found on Lys 116 and Asp 48. Lys 116 is found to be part of the R-loop which has been shown to be of significance for PTP1*β* activity as the R-loop is known to move in conjunction with the WPD-loop which creates a better p-Tyr binding pocket once closed (Kamerlin, *et al.,* 2006). This suggests that the ligand bound to PTP1*β* does not bind directly to the active site, but binds to adjacent residues necessary for phosphatase activity and thus could potentially result in non-competitive inhibition. Figure 4.1 illustrates that the interaction between DC7 and PTP1*β* is found anchored directly to the active site residues Ala 217, Ile 219 and Gly 220 by hydrogen bonds. The active site is known to span from His 214 to Arg 221 residues of PTP1*β* (Kamerlin, *et al.,* 2006). Thus direct binding to this region suggests potential competitive inhibition could be displayed by DC7. A similar interaction is portrayed with DC17 as the ligand bound directly to the amino acids Cys 215 and Ala 217 via hydrogen bonds. With the active site occupied by the small molecule inhibitors like DC7 and DC17 the enzyme will not be able to accomplish its phosphatase activity on any surrounding p-Tyr residues. MET was also docked to establish any interaction with PTP1*β* and results indicate that metformin could interact with Asp 48 through hydrogen bonding (figure 4.1)

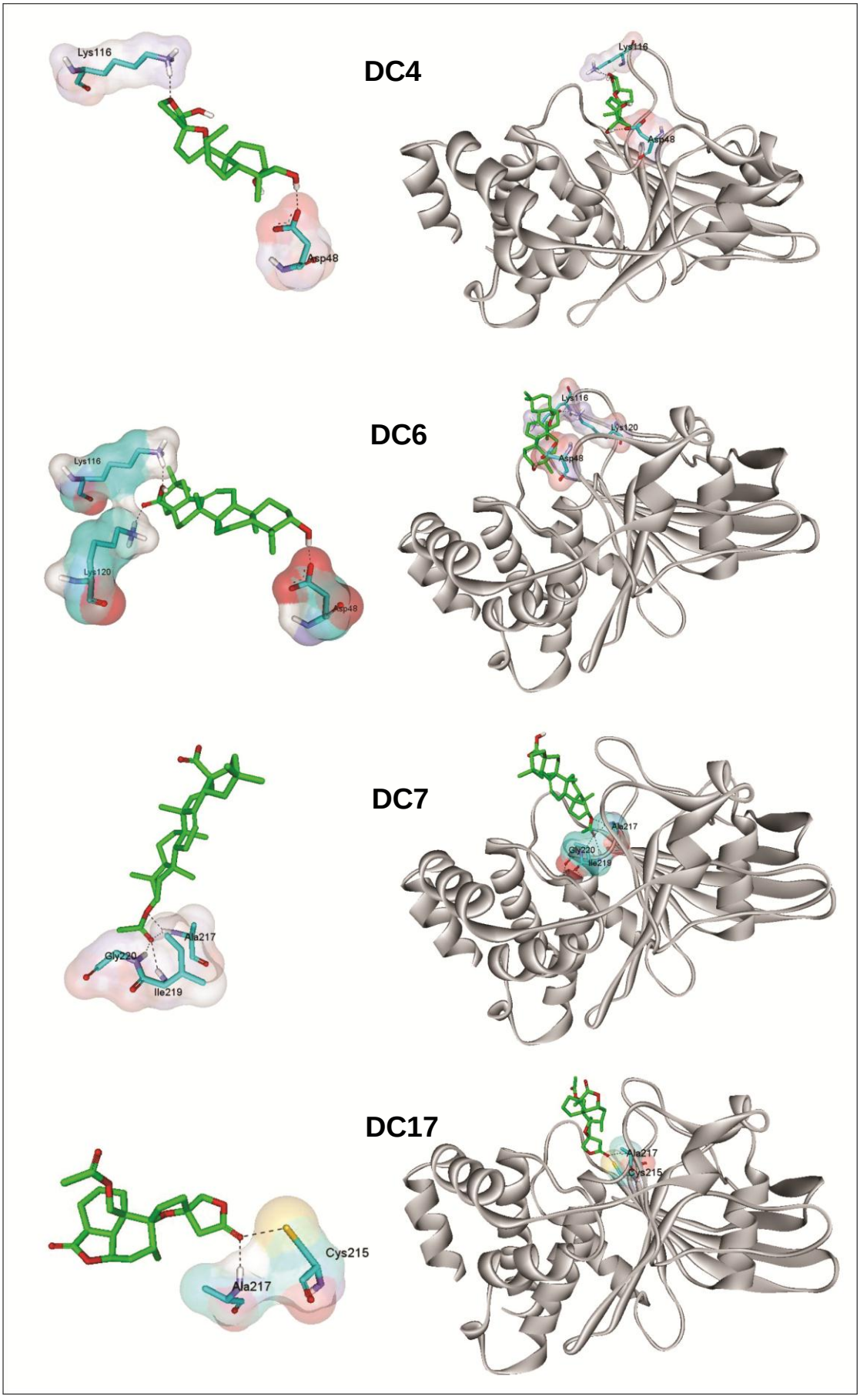
Lys116
Asp48
DC4
Lys116
Asp48
Lys116
Lys120
Asp48
DC6
Lys116
Lys120
Asp48
Ala217
Gly220
Ile219
DC7
Ala217
Gly220
Ile219
Cys215
Ala217
DC17
Ala217
Cys215

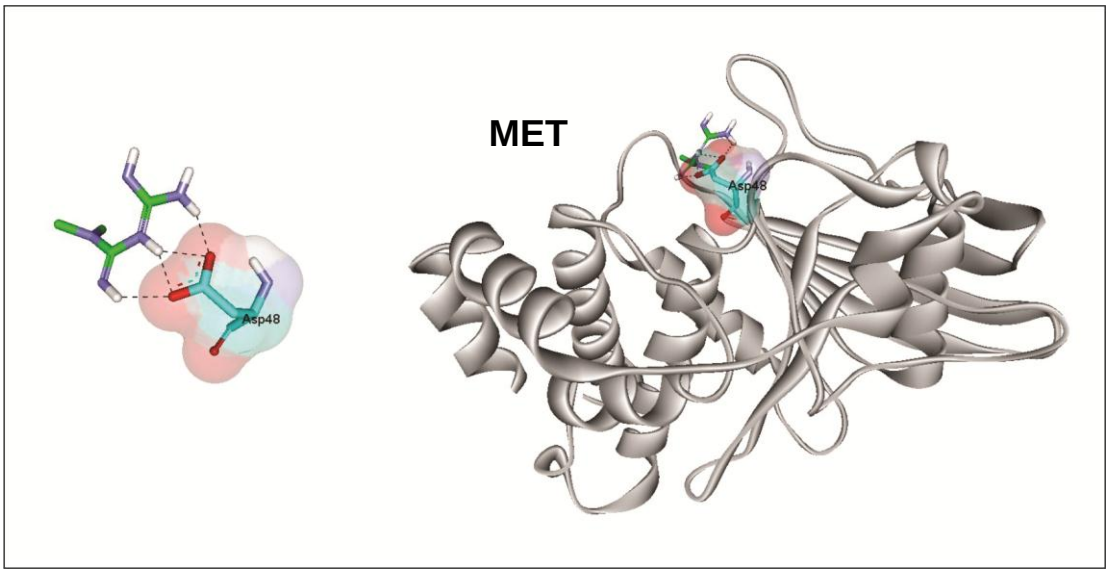

Figure 4.1: An illustration of the ligands DC4, DC6, DC7, DC17 and MET docked with PTP1*β* (white 3D protein structure). In the right pane, the ligands are shown docked to the complete protein; while in the left pane the ligand interaction is magnified to illustrate individual hydrogen bonding (black dotted lines) to the amino acids of PTP1*β* which have been annotated. Molecules have been colour coded as follows: hydrogen = white, oxygen = red, nitrogen = purple, Sulphur = yellow, ligand carbon = green, amino acid carbon = light blue.

Table 4.1 is a summary of the docking results for the 20 MAR derivative compounds tested. The best ranked result is shown for each compound with rankings based on binding energy and the calculated inhibition constant. Binding energies are calculated as the sum of intermolecular energy and torsional free-energy penalty (Huey and Morris, 2008). For efficient binding, the calculated binding energy should be as low as possible (comparable to the positive control) and thus the prerequisite for such a binding condition would be for the intermolecular energy and torsional free-energy penalty to both be low. Theoretical inhibition constants are shown and calculated by ADT using the following equation:

$$K_i = \exp(\Delta G \times 1000) / (Rcal \times TK)$$

ΔG = is the sum of intermolecular energy and the ligands internal energy

Rcal = 1.98719 $cal.K^{-1}.mol^{-1}$

TK (temperature in Kelvin) = 298.15 K.

Cluster analysis is a factor which plays a vital role in the rank of small molecule inhibitors. A cluster is generated by the selection of a single molecule conformation of good binding capacity and is referred to as the 'seed' (Huey and Morris, 2008). Once the seed has been chosen, it is compared to other docked conformations by root-mean squared deviation (RMSD). The RMSD value determines the similarity between the two conformations of the same ligand. If the RMSD is lower than 0.5, the two conformations will be placed together in a cluster (Huey and Morris, 2008). Molecule conformations in a cluster are ranked from lowest binding energy to the highest. An example is shown in figure 4.2 with ligand DC6 having 8 molecule conformations i.e. Rank: 1_1 to 1_8.

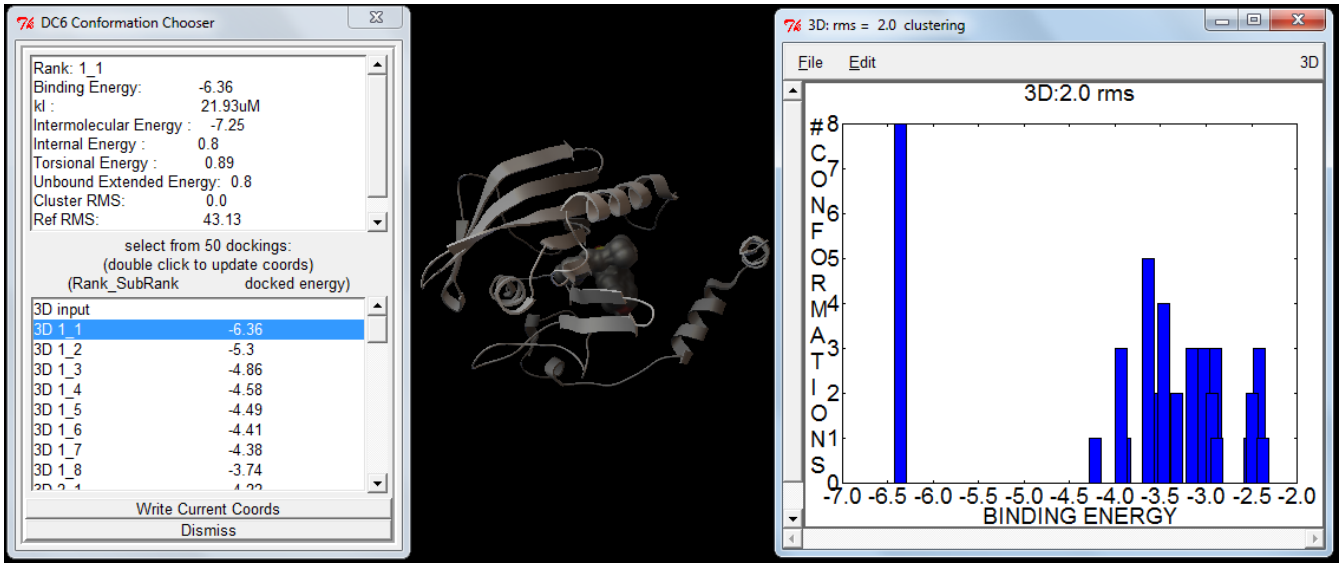

Figure 4.2: A window of the ADT program illustrating the result obtained for DC6. The windows shown summarize the results obtained for the docking of DC6 to PTP1*β* while also allowing for the visualization of the docked conformation selected (centre). Conformations are chosen from the docked conformations listed in the "DC6 conformation chooser" window (left). A complete summary is shown for any of the docked conformations chosen. The "3D: rms = 2.0 clustering" (right) pane plots the ligand conformations into clusters. It can be seen that 8 conformations of DC6 are similar with the lowest binding energy at -6.36.

Of the 2 000 000 that were completed for each compound, the best 50 conformations were chosen for each. Clusters were formed from the 50 best conformations which were selected. Even though DC7 was evaluated with the second best binding energy at -5.33 MeV, there was only one conformation in the cluster which is unfavourable. DC6 on the other hand, which showed the best binding energy at -6.36 also showed favourable cluster formation with 8 conformations in the cluster showing best binding energies ranging from -6.36 to -

3.74 MeV. DC17 which showed the third best binding energy at -4.16 MeV has 5 conformations in the cluster and ranges with binding energies of -4.16 MeV to -1.78 MeV.

Table 4.1: A summary of the results obtained from the 20 MAR derivatives *in silico* docking experiments conducted showing the intermolecular, torsional and binding energies achieved. The theoretical inhibition constants were calculated and are represented in mM.

Conformation number	Intermolecular energy	Torsional energy	Binding energy	K_i (mM)	Rank#
DC 1_1	-5.61	1.79	-3.82	1.6	7
DC 2_1	-5.22	1.49	-3.73	1.85	11
DC 3_1	-5.42	2.68	-2.73	9.89	18
DC 4_1	-5.52	1.19	-4.32	0.6785	3
DC 5_1	-5.4	1.19	-4.21	0.81983	4
DC 6_1	-7.25	0.89	-6.36	0.02193	1
DC 7_1	-6.52	1.19	-5.33	0.12378	2
DC 8_1	-4.36	1.49	-2.87	7.83	17
DC 9_1	-4.71	1.19	-3.52	2.62	14
DC 10_1	-4.67	0.89	-3.78	1.71	8
DC 11_1	-4.23	3.28	-0.95	200.18	21
DC 12_1	-5.56	1.79	-3.77	1.71	9
DC 13_1	-4.19	1.49	-2.7	10.5	19
DC 14_1	-4.84	1.19	-3.64	2.14	12
DC 15_1 (MAR)	-4.94	1.19	-3.74	1.81	10
DC 16_1	-3.95	2.39	-1.56	71.98	20
DC 17_1	-5.06	0.89	-4.16	0.88799	5
DC 18_1	-5.1	2.09	-3.01	6.19	16
DC 19_1	-4.51	0.89	-3.61	2.25	13
DC 20_1	-4.38	0.89	-3.48	2.79	15
MET	-3.88	0.0	-3.88	1.44	6

Rank is based on binding energy values.

The development of accurate computational molecular docking software has become a focus of drug discovery in the past decade. As a result, numerous docking software tools have been developed and are consistently being upgraded (Cross *et al.,* 2009). Investigations which compare and rank the developed software and methods used have become a necessity in order for researchers to make informed and educated decisions about the choice of software and method used when screening a library of ligands. Software such as GOLD, DOCK, GLIDE, FlexX, Autodock and Surflex are among the most popular software used (Onodera *et al.,* 2007; Agostino *et al.,* 2009). Software rankings have been investigated which were based on RMSD values of the ligands tested (Onodera *et al.,* 2007; Agostino *et al.,* 2009). Although the programs which have been tested outweigh each other in different facets, GLIDE has consistently been found to be the overall preferred choice of docking software available for procedures. GOLD and Autodock are rated lower than the above mentioned competitors, these are consistently being reviewed and upgraded (Onodera *et al.,* 2007; Cross *et al.,* 2009; Agostino *et al.,* 2009). ADT was chosen as the software package for our purposes as it rapidly allowed for the screening and was readily available for use.

The crystal structure of PTP1*β* used in this investigation was uploaded into the PDB by Lui *et al.* (2008). In their investigation, the use of p-Tyr mimetics was examined as these inhibitors have low bioavailability as a result of their overall negative charge. They had crystalized the structure of PTP1*β* with their inhibitor bound to the active site while PTP1*β* remained in the inactive conformation i.e. the WPD loop remained open and this conformation of PTP1*β* had been added to the PDB (accession number 3eb1). The 3eb1 conformation of PTP1*β* was therefore chosen to determine the potential of MAR and MAR derivatives to interact with inactive PTP1*β* at the active site with the WPD loop open (Lui *et al.,* 2008).

Researchers have revealed that the inclusion of specific water molecules in a protein lattice can be advantageous to small molecule docking in a protein active site (Huang and Shoichet, 2008). Water molecules have been shown to increase binding efficiency and stability of the bound ligand by acting as hydrogen bond bridges between specific amino acids and the ligand (Huang and Shoichet, 2008; de Beer *et al.,* 2010). It was previously thought that the addition of water molecules would negatively influence the docking result. It was later found that omission of specific

water molecules is of great importance to the docking of the ligand in some cases (Thilagavathi and Mancera, 2010). Unfortunately, ADT does not allow for the inclusion of water molecules and thus nullify all solvent effects.

4.2. *IN VITRO* INHIBITION STUDIES OF PTP1*β* AND ALP

Table 4.2 illustrates the varying degrees of cross reactivity between the two phosphatases (ALP and PTP1*β*) induced via *in vitro* exposure to the various MAR derivatives, MAR and MET. This is seen for treatments DC9 and DC16. Although inhibition of PTP1*β* was noted to be more potent than ALP, it suggests that these compounds would have a degree of cross reactivity on certain enzymes which are more similar to PTP1*β*, eg. TCPTP (T-cell Protein Tyrosine Phosphatase).

DC5 has an inhibitory effect on PTP1*β* with an inhibition constant of 33 μM, which is high compared to other compounds eliciting inhibition of PTP1*β*, with no cross reactivity associated with ALP. DC1, DC2, DC15 and DC17 on the other hand seem to display no inhibition of ALP nor PTP1*β* for the concentration ranges tested.

As a comparison, inhibition constants for the *in silico* computational modelling is displayed in table 4.2. Inhibition of PTP1*β* does not seem to correlate between most results obtained *in vitro* and *in silico*, except DC6 which showed to be the best candidate for PTP1*β* inhibition in the computational modelling and correlates with the results achieved for the *in vitro* inhibition study. This discrepancy may be due to the fact that ADT also considers interactions between non-specific amino acid residues and not necessarily the amino acid residues which are involved in catalysis or facilitation of enzyme function by mobility as in the case of the WPD loop, S-loop and R-loop of PTP1*β*.

Results achieved from the experiments conducted have shown that the positive control, DC6, had the best binding efficiency to the inactive form of PTP1*β*. This was demonstrated both *in vitro* and *in silico* as seen in table 4.2. DC18 had shown inhibition of PTP1*β* *in vitro* which had K_i values in the micromolar range and was specific to PTP1*β* with its inhibition activity. DC3, DC9, DC16 and MET illustrate good inhibition of PTP1*β* at a micromolar range, unfortunately illustrating non-

specific activity through inhibition of ALP. MAR (DC15) had illustrated no *in vitro* inhibition of either PTP1*β* or ALP.

Table 4.2: A summary of the inhibition constants achieved for the *in vitro* and *in silico* inhibition studies with alkaline phosphatase and PTP1*β*. *In vitro* inhibition constants were achieved by double Dixon plots.

		K_i (µM)		
Rank*	**Compound**	**ALP**	**PTP1*β***	**Docking**
1	DC6	No inhibition	0.047[c]	21
2	DC3	No inhibition	2.3[m]	9890
3	MET	No inhibition	4.1[c]	1440
4	DC18	No inhibition	15.5[c]	6190
5	DC5	No inhibition	33[c]	819
6	DC9	17	2.1[m]	2620
7	DC16	14	6[c]	71980
8	DC17	No inhibition	No inhibition	887
9	DC1	No inhibition	No inhibition	1600
10	DC15 (MAR)	No inhibition	No inhibition	1810
11	DC2	No inhibition	No inhibition	1850

c = Competitive mode of enzyme inhibition; m = mixed mode of enzyme inhibition.

*Rank based on K_i values of *in vitro* PTP1*β* inhibition studies and the cross reactivity of the compounds with ALP.

"No inhibition" indicates that the highest concentration, i.e. 10 µM tested for this study did not inhibit the enzymes.

Development of suitable PTP1*β* inhibitors has been problematic as the PTP1*β* active site is predominantly positively charged in nature, thus the development of pTyr mimetics have shown good inhibitory potential *in vitro*. Unfortunately, the overall negative charge of pTyr-like drugs has low *in vivo* bioavailability at the site of action. DC6 has no net charge which makes it a good candidate for *in vivo* studies as an anti-diabetic drug. Its activity on the PTP1*β* cannot be overlooked, but a single problem had arisen in that its activity was not specific to PTP1*β* as it also inhibits T-cell protein tyrosine phosphatase (TCPTP) (Zhang *et al.,* 2008). The effect of DC6 was investigated on animal models by de Melo *et al.* (2010) illustrated that normal mice treated with DC6 have a good tolerance to a high glucose diet and that mice treated with a high fat diet had shown to be resistant to obesity. The mice appeared

to show a healthy phenotype after 15 weeks of treatment. However the question involving the inhibitory potential of DC6 on TCPTP which is known to conduct important functions in the body remains. DC9 also holds no net charge and would thus be a good candidate for *in vivo* studies as its bioavailability would not be hindered through charge omission at the plasma membrane. Unfortunately its inhibitory activity against PTP1*β* is negligible compared to DC6 which is 44.7 times more efficient at inhibiting PTP1*β*. This is noted for all the MAR derivatives compared to DC6 tested *in vitro* (table 4.2). Thus, according to the *in silico*, MAR and its derivatives are not suitable candidates for PTP1*β* inhibition.

The testing of MAR and its derivatives for the treatment of T2DM was based on the traditional uses of *L. leonurus* as an antidiabetic medication in Southern Africa (Oyedemi *et al.,* 2009). *M. vulgare*, a botanical family member of *L. leonurus*, is used in Mexico as a traditional medication for diabetes-like symptoms (Vergara-Galicia, *et al.,* 2012). An investigation completed by Mnonopi *et al.,* (2012) demonstrated the antidiabetic effects of MAR on INS-1 cells through its ability to act by stimulating GLUT2 and insulin expression in the β-cells. It was therefore concluded that MAR acts as a potential antidiabetic agent in T1DM. In determining the effectiveness of MAR and its derivatives as a potential antidiabetic agent for T2DM, it was essential to determine their potential effects on the enzyme PTP1*β*. It can now be concluded that MAR does not have a significant inhibitory effect on PTP1*β*. PTP1*β*, however is not the only factor affecting insulin signalling, and it can therefore be hypothesized that MAR has its effect elsewhere in the insulin signalling pathway in peripheral tissues. In addition MAR may act as an inducer of protein expression which allows the signal to be transferred more efficiently for an additional period of time.

Although MAR and its derivatives were not efficient PTP1*β* inhibitors, further studies were completed to determine their effect on glucose uptake in peripheral tissues (part III), since reduced blood glucose levels were found in the *in vivo* study conducted by Mnonopi *et al*., (2012).

PART III: CELL CULTURE AND MOLECULAR ANALYSIS OF CELLS TREATED WITH MARRUBIIN AND MARRUBIIN DERIVATIVES

CHAPTER 5: METHODS AND MATERIALS

All materials and reagent preparation methods used in this section are listed in annexure A and B, respectively. All materials are of an analytical grade, unless otherwise stated.

5.1. CELL MAINTENANCE

Chang liver and C2C12 cells were grown and maintained in RPMI 1640 (Roswell Park Memorial Institute medium) (Gibco) supplemented with 10% FCS in a humidified incubator at 37^{o}C and 5% CO_2. 3T3-L1 preadipocytes were grown under the same conditions and maintained in DMEM (Dulbecco's Modified Eagle Medium) (Sigma) supplemented with 10% FCS. Growth of cells was conducted until 80% confluency was achieved and were consequently split or seeded for experiments to follow.

Rosiglitazone (BIOCOM biotech) is a known antidiabetic drug that forms part of the TZD class of drugs which has been used to initiate adipogenesis (Pisani *et al*., 2011). Rosiglitazone acts as a PPARγ agonist and thereby initiating lipogenesis and fat cell formation (Madsen *et al.,* 2003). Differentiation of 3T3-L1 preadipocytes was conducted by allowing cells to grow to 100% confluency. DMEM medium supplemented with 10% FCS and 1 µM rosiglitazone was added to the cells two days after post-confluence. Differentiating cells were then incubated for seven days with a medium change every 2-3 days.

All consequent experiments (n=3) were conducted in 96-well (Chang and C2C12) or 48-well plates (3T3-L1 adipocytes). MAR derivative and MET treatments were reconstituted in 10% DMSO (dimethyl sulfoxide) and exposed to cells at 10 µM and 1 µM, respectively; thus achieving a 0.1% DMSO exposure to the cells. A 0.1% vehicle control (CON) was thus used as an untreated control. The MAR derivatives used for *in vitro* cytotoxicity and glucose uptake studies were DC1, DC2, DC3, DC5, DC6, DC9, DC15 (MAR), DC16, DC17, DC18 and MET as the positive control. Selection for the treatments listed was based on availability of the purified compounds.

5.2. MTT CELL VIABILITY STUDIES

MTT (3-(4,5-dimethylthiazol-2-yl)-2,5-diphenyltetrazolium bromide) can be converted to a colour forming insoluble formazan compound by viable cells. This is accomplished by viable cells passing electrons to succinate dehydrogenase in the mitochondrial electron transport chain resulting in purple formazan proportional to the amount of viable cells (Freshney, 2000). Addition of DMSO solubilises the formazan allowing the purple colour intensity to be measured at an absorbance of 540 nm. In this study the MTT assay was used to determine the cytotoxic effects of MAR and its derivatives on the cells lines mentioned.

Chang liver and C2C12 cells were seeded at 30 000 cells/mL in 96 well plates (Costar) while 3T3-L1 cells were seeded at 40 000 cells/mL in 48 well plates (Costar). Blank wells contained no cells but were treated the same as the experimental wells throughout the experimental procedure. Cell density was determined by haemocytometer and the trypan blue cell exclusion method. 3T3-L1 cells were grown to 100% confluency and 2 days post-confluency cells were induced to differentiate (section 5.1). Cells were exposed to treatment concentrations ranging from 0.1 µM to 100 µM and 0.1% DMSO. This was accomplished by making a 1:100 dilution of a 10% DMSO solution containing treatment in the growth medium. In practice, 2 µL of a stock treatment was added to 200 µL growth medium in the 96-well plate or 5 µL of a stock treatment to 500 µL growth medium in 48-well plates achieving the desired concentration of treatment vehicle control (CON i.e. 0.1% DMSO). Cells were incubated for 48 hours, medium was removed and replaced with 200 µL (96-well plate) or 500 µL (48-well plate) of MTT (0.5 mg/mL) and incubated for 4 hours. The medium was removed and 200 µL or 500 µL 100% DMSO was added and incubated for 15 minutes to allow the purple formazan crystals to dissolve. The plate was shaken for 10 seconds and read at an absorbance of 540 nm using a Biotek Powerwave XS microtitre plate reader.

MTT assays were completed to determine cell viability which was used for normalisation of cell number during glucose uptake studies (section 5.3). MTT standard curves were created in triplicate for all cell lines used. Adipocytes (appendix 1; figure F.3) were differentiated (section 5.1) in 10 cm culture dishes prior to seeding at the specific concentrations required from 0 - 500 000 cells/mL, while

C2C12 (appendix 1; figures F.2) Chang liver (appendix 1; figure F.3) cells were seeded at a density range of 0 - 100 000 cells/mL.

5.3. GLUCOSE UPTAKE STUDIES

A glucose reagent was prepared for the detection of glucose in the experiment samples. The glucose reagent was comprised of phenol, 4-aminoantipyrine, horseradish peroxidase, EDTA, glucose oxidase and peroxidase (annexure B: reagent 1). The assay's principle is based on the conversion of glucose to gluconic acid and hydrogen peroxide by glucose oxidase followed by the interaction which occurs between hydrogen peroxide and 4-aminoantipyrine. This reaction is catalysed by peroxidase and causes a red oxidized dye and water which can be measured spectrophotometrically at an absorbance maximum of 492nm. Glucose uptake studies were completed on the cell lines mentioned in section 5.1.

Cells were counted by haemocytometer using the trypan blue exclusion method. Cells were seeded and differentiated as described in section 5.2 and treated with 10 µM MAR derivative treatments and 1 µM MET (positive control). Untreated cells were exposed to 0.1% DMSO and used as the CON. Blank wells contained no cells and were treated as experimental wells throughout the experimental procedure. Cells were exposed to the various treatments for 48 hours. Thereafter, the medium was replaced with glucose-free DMEM (for 3T3-L1 adipocytes) or glucose-free RPMI 1640 (for Chang liver and C2C12 cells) for 1 hour. The glucose-free media was aspirated and replaced with medium containing 6 mM glucose and 60 µU/mL insulin for 3 hours. From each well, 50 µL of the medium was aspirated and added to a nonsterile 96 well plate (Lasec) and diluted with 150 µL water. 50 µL of the dilution was added to 200 µL of glucose reagent, incubated at 37^{o}C for 30 minutes and read at an absorbance of 492nm using a Biotek Powerwave XS microtitre plate reader. The cell number was determined using the MTT assay described in section 5.2 and used to normalise cell number to 100 000 cells.

A standard curve using a glucose concentration range of 0 – 8 mM was used to determine the glucose utilised (figure 5.1).

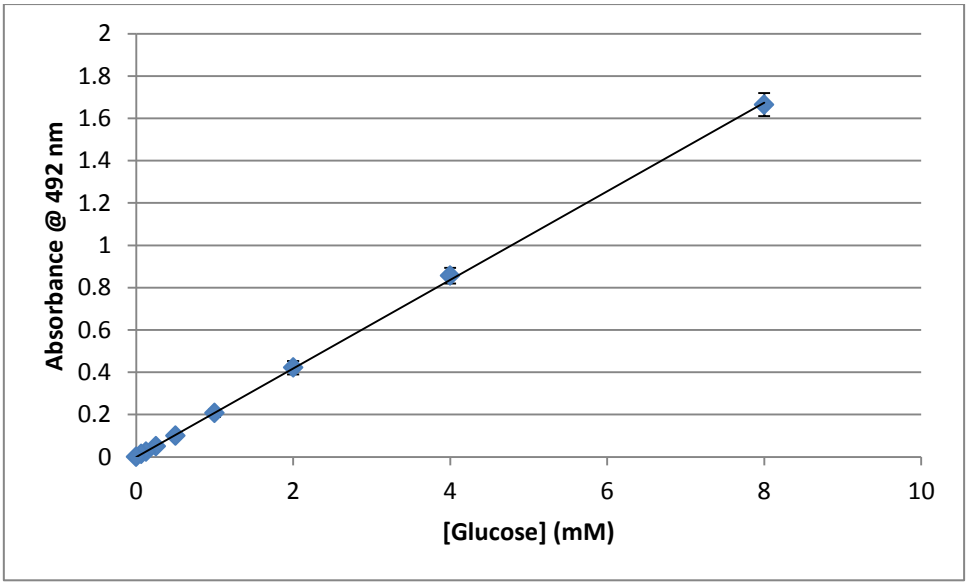

Figure 5.1: A glucose standard curve with a concentration range of 0–8 mM (R^2=0.9998; n=3).

5.4. TREATMENT OF 3T3-L1 ADIPOCYTES AND MOLECULAR ANALYSIS.

RNA was isolated using a NucleoSpin® RNA kit (Macherey-Nagel) according to the manufacturers instruction. 3T3-L1 preadipocytes were grown in 10 cm culture plates and differentiated to mature adipocytes once they were 2 days post-confluence using 1 µM rosiglitazone. Adipocytes were treated with 10 µM of 4 test compounds (DC6, DC15, DC17 and DC18) which elicited the best performance in the glucose uptake assays, 1 µM MET (positive control) and an untreated plate of cells as the CON. After 48 hours incubation at 37^{o}C, cells were treated with 60 µU/mL insulin for 3 hours. Medium was removed and cells washed briefly with 10 mL PBSA (phosphate buffered saline containing EDTA). The PBSA was discarded and replaced with 2 mL PBSA. Cells were lifted through cell scraping and gentle pipetting of the PBSA. The cell suspension was transferred to a 2 mL eppendorf tube and centrifuged for 2 min at 11 000 x *g* using an eppendorf minispin AG microfuge. The supernatant was discarded. 350 µL RP1 buffer and 3.5 µL β-mercaptoethanol was added to the pellet to facilitate cell lysis and was vortexed vigorously. Following lysis, the viscous cell lysate was added to a NucleoSpin® Filter and centrifuged for 2 minutes at 11 000 x *g* to remove any cell debris and the filter discarded. 350 µL 70% ethanol was added to the lysate and mixed by slow pipetting. The lysate was added to a NucleoSpin® RNA/Protein column and placed in a collection tube. The lysate was centrifuged at

11 000 x *g* for 30s and the column placed in a new collection tube. At this point the total cell RNA and DNA was bound to the column membrane while the total protein was in the collection tube flow-through (www.mn-net.com).

5.4.1. RNA PURIFICATION

The column membrane was desalted by addition of 350 µL membrane desalting buffer to the column in a new collection tube and centrifuged for 1 min at 11 000 x *g* to remove any salts to prevent inhibition of the action of the rDNase. The flow-through was discarded and 95 µL rDNase reaction mixture was added to the centre of the silica membrane and incubated for 15 minutes at room temperature to degrade any DNA present. 200 µL of buffer RA2 was added to the column and centrifuged for 30 seconds at 11 000 x *g* to remove DNA and deactivate the rDNase. After centrifugation the column was placed in a new collection tube and 600 µL of buffer RA3 was added to the column, centrifuged for 30 seconds at 11 000 x *g*, and the flow-through was discarded. A further 250 µL RA3 buffer was added to the column and centrifuged for 2 minutes at 11 000 x *g* to dry out the column. Finally the column was placed in a 1.5 mL RNase-free collection tube and the RNA was eluted out of the column with 60 µL RNase-free water by centrifugation for 2 minutes at 11 000 x *g* (www.mn-net.com). RNA was stored at -80^{o}C for further studies.

5.4.1.1. RNA QUANTIFICATION

Eluted RNA was quantified using an Agilent® 2100 bioanalyzer. This is an accurate and efficient means of determining RNA concentration and requiring only 1 µL of RNA containing material. The kit uses a specific set of reagents and chips which house interconnected channels. The Agilent® RNA kit quantifies and tests RNA based on RNA fragment size by electrophoresis within the chip. The Agilent® RNA kit was used to quantify RNA according to the manufacturer's specifications using Agilent® RNA 6000 Nano reagents. RNA is quantified electrophoretically within the RNA nano chip. A sample added into a well move through micro channels which separate the RNA based on size (figure 5.2). Separated bands are detected by fluorescence and reported as electropherograms. For eukaryotic RNA, two peaks

are characteristic: 18S RNA and 28S RNA. Sizes of the bands are compared to an RNA ladder which is analysed alongside the test wells (http://www.gene-quantification.de/rna-integrity.html).

Figure 5.2: The Agilent® RNA quantification chip has 16 loading wells. Gel-dye is added to the wells marked G, RNA ladder is added to thewell marked with a ladder which leaves 12 wells for isolated RNA samples (Trietsch *et al*., 2011).

5.4.1.2. cDNA SYNTHESIS

Conversion of RNA to cDNA was completed using a QuantiTect® Reverse Transcription kit (QIAGEN). The three requirements for RT-PCR are to ensure firstly, the integrity of the RNA should be at an acceptable level (relative integrity number greater than 8) and this is influenced by the RNA isolation protocol used. Secondly, genomic DNA (gDNA) should be removed from the RNA sample as gDNA may influence the RT-PCR result by acting as a template for the specific primers added into the real time RT-PCR reaction. Thirdly, the random oligo-DT primers added to the reverse transcriptase reaction in which cDNA is synthesized should allow for maximal conversion of RNA to cDNA (www.qiagen.com). The method for the use of the kit comprises of two main steps, 1) removal of all genomic DNA and 2) transcription of cDNA from RNA using the enzyme reverse transcriptase. Table 5.1 shows the composition of the gDNA wipeout mix.

Table 5.1: A representation of the components added to the isolated RNA to remove all gDNA. The final concentration of RNA is 71.42 ng/µL (www.qiagen.com).

Component	Volume (µL)
gDNA wipeout buffer 7x	4
Template RNA	2µg
RNase-free water	Variable
Final volume	28

The gDNA wipeout mix was incubated for 2 minutes at 42^{o}C and returned to ice directly after. A reverse transcriptase (RT) mastermix was made according the manufacturer's instructions as follows and 12 µL was added to the RNA mix to achieve a final volume of 40 µL.

Table 5.2: A representation of the components added to the RT mastermix which converts the RNA to cDNA with a final concentration of cDNA at 50 ng/µL (www.qiagen.com).

Mastermix	Volume (µL)
Quantiscript RT	2
Quantiscript RT Buffer	8
RT primer mix	2
Template RNA	28
Final volume	40

The solution was mixed by gentle pipetting and incubated at 42^{o}C for 15 minutes for cDNA synthesis to commence. Deactivation of the RT (reverse transcriptase) was at 95^{o}C for 3 minutes using a heating block. cDNA was cooled on ice and stored at -20^{o}C for later analysis using RT-PCR.

5.4.1.3. cDNA QUANTIFICATION

cDNA was quantified using a Thermo scientific NanoDrop® 2000c spectrophotometer. 2 µL of each cDNA sample was used to quantify the DNA content of the sample. Concentration and purity of the cDNA was measured using 260nm/280nm and 260nm/230nm absorbance ratios.

5.4.1.4. RT-PCR

Gene expression analysis was accomplished by RT-PCR. Selected genes GLUT4, IRS1 and tyrosine-3-monooxygenase/tryptophan-5-monooxygenase-activation protein, and zeta polypeptide (*Ywhaz*) expression were analysed. Analysis involved the use of an intercalating dye which binds double stranded DNA (SYBR Green I). This fluorescent dye has an excitation and emission spectrum of 494 nm and 521 nm, respectively (Dragan *et al*., 2012). Addition of this dye into the PCR mixture allows for increases in amplified DNA to be detected during the elongation phase of PCR. Both gene expression analysis and DNA melting temperature analysis was evaluated in real-time which allowed for the detection of undesired PCR products. Before the real time RT-PCR could be completed, annealing temperature and primer concentration needed to be established. Optimized annealing temperatures and primer concentrations are listed in table 5.3.

Table 5.3: Target genes for RT-PCR analysis with primer concentrations, optimized annealing temperatures and primer sequences.

Target gene	Annealing temperature (C^o)	[Primer] (nM)	Forward primer (5'- 3')	Reverse Primer (5' – 3')
GLUT4	58	300	CCAGCCTACGCCACCATAG	TTCCAGCAGCAGCAGAGC
IRS1	56	300	GCCCGTGTCATAGCTC	AAGCGCCTGGTGGCTC
Ywhaz	58	300	GAGTGTAGTCTGTGTGGGTAC	GCTGTGGTCAAGGGTGTG

REST 2009 (QIAGEN) software was used to analyse the results obtained from RT-PCR analysis. It uses the expression of reference genes to normalise any variation in expression levels of genes of interest due to loading differences. It also takes into account multiple reference genes and their efficiencies in order to make results more dependable. Standard curves of all genes were constructed with varying cDNA concentrations. Reaction efficiency was then calculated by the REST 2009 software which was used to determine expression of the target genes.

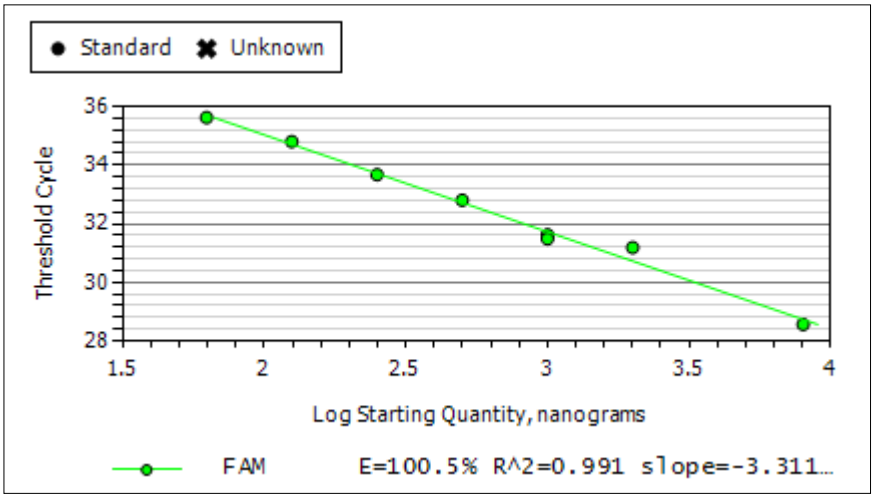

Figure 5.3: A typical standard curve for RT-PCR analysis. The standard curve is representative of the threshold cycle at which a specific concentration of template will begin amplifying. E, is the efficiency of the reaction which was found to be 100.5%.

Results were plotted as bar graphs. Significant statistical changes between controls and treated samples are represented by P-values.

5.4.2. TREATMENT OF 3T3-L1 ADIPOCYTES AND PROTEIN ISOLATION

3T3-L1 adipocytes were exposed to the various treatments DC6, DC15, DC17, DC18 and MET, respectively and insulin as per section 5.4. After the treatment period, the medium was removed; cells were washed with 10 mL PBSA to facilitate gentle lifting of the cell monolayer. The PBSA was removed and 2 mL of PBSA was added followed by gentle agitation and cell scraping to facilitate lifting. The cell suspension was transferred to a 2 mL eppendorf tube and centrifuged for 10 minutes at 2 000 x *g* in a benchtop microfuge. The supernatant was removed and replaced with 0.5 mL protein lysis buffer (annexure B: reagent 2.1) followed by vigorous vortexing for 3 minutes. The lysate was left on ice of 30 minutes and vortexed for an additional minute and centrifugation at 12 000 x *g* for 10 minutes. The supernatant was stored as 30 µL aliquots at -80^{o}C, for further analysis.

5.4.2.1. BCA ASSAY

The bicinchoninic acid (BCA) assay is a protein determination assay which uses the conversion of Cu^{2+} to Cu^{+} to react with peptide bonds under alkaline conditions. Two molecules of BCA chelates with one molecule of Cu^{+} creating an intense purple colour which is detected spectrophotometrically at 562 nm (Smith *et al*., 1985). One of the advantages of using the BCA assay include its tolerance to detergents, it can be completed in a single step therefore is not as labour intensive as the Lowry method. Furthermore, the Bradford assay is known to act on specific amino acids in proteins, thus if these amino acids are in low concentrations it can be expected that the protein concentration will be underestimated (Olson and Markwell, 2007).

Protein concentrations of cell lysates were determined using a BCA assay kit (Thermo Scientific). Diluted cell lysate or 25 µL cell lysate was added to 200 µL BCA reagent (annexure B: reagent A and reagent B at 50:1 ratio) and incubated at 37^{o}C for 30 minutes. A standard curve was completed using bovine serum albumin (BSA) ranging from 0 - 20 mg/mL (figure 5.4).

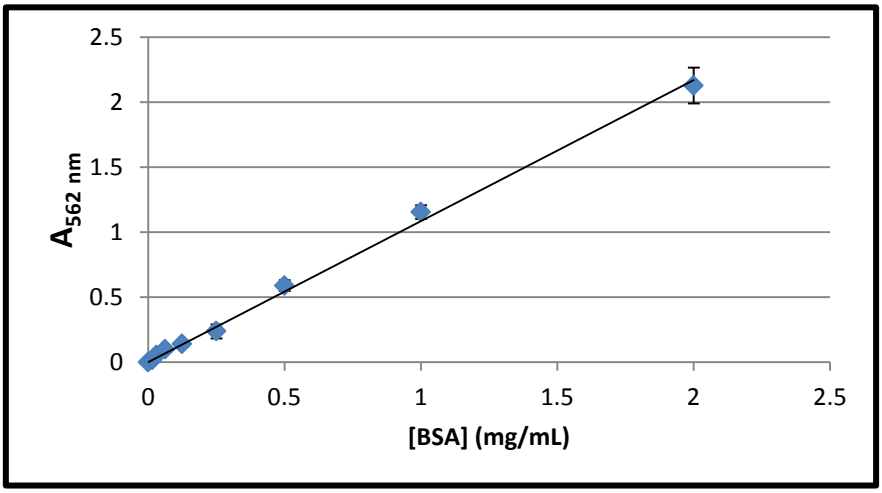

Figure 5.4: A typical BCA protein standard curve ranging from 20 µg/mL – 2 mg/mL (R^2=0.9973; n=3).

5.4.2.2. SDS-PAGE, ELECTRO TRANSFER AND WESTERN BLOTTING.

Protein lysate (20 µg) was separated on 10% SDS-PAGE (Sodium dodecyl sulphate polyacrylamide gel electrophesis) gels (annexure B: reagent 2.7) and electrophoresed at 100V for 90 minutes. SDS-PAGE allows for proteins to be

separated based on their mass alone. Once electrophoresed proteins were transferred to polyvinylidene difluoride (PVDF) membranes via electrotransfer from unstained SDS gels, duplicate gels and membranes were stained with Acqua Stain (VACUTEC).

Proteins in a duplicate gel were transferred to PVDF membranes through electrotransfer. PVDF membranes are suitable for western blotting as proteins are retained on these membranes even under harsh conditions. Electrotransfer was as follows:

- Membranes were washed in 100% methanol for 1-2 minutes and rinsed in ddH_2O for 5 minutes.
- Equilibration in cold transfer buffer (annexure B: reagent 3.1) was conducted for 30 minutes.
    - Fibre pads and filter paper were cut slightly larger than the gel itself and saturated in transfer buffer at 4^oC.
    - SDS-PAGE gels were soaked in transfer buffer for 30 minutes to remove salts and detergents associated with the SDS-PAGE separation procedure.
- The cassette holder was stacked from bottom to top as follows: Fibre pad, filter paper, gel, PVDF membrane, filter paper and lastly fibre pad.
- All air bubbles were carefully removed from the stack using a rolling pin.
- Protein transfer was done with a constant potential difference of 25 V for 2 hours using a Bio-Rad power pac 200 (www.bio-rad.com).

Membranes were washed in Tris buffered saline, 0.1% Tween 20 (TBS-Tween) (annexure B: reagent 3.2) for 5 minutes and repeated three more times. Membranes were soaked in membrane blocking agent (annexure B: reagent 3.3) overnight in order to block any non-specific binding of proteins or antibodies to the membrane. Membranes were briefly rinsed with TBS-Tween after the overnight block and incubated for 90 minutes at 4^oC with primary antibody in antibody dilution buffer (annexure B: reagent 3.4) diluted in ratios represented by table 5.4. Membranes were washed thrice in TBS-Tween and incubated with secondary antibody at the appropriate dilution ratio (see table 5.4) for 60 minutes at 4^oC and washed again in quadruplicate in TBS-Tween.

Table 5.4: Primary and secondary antibodies used in the western blot procedure along with dilutions used for detection.

Antibody	Dilution of primary antibody	Secondary antibody	Dilution of secondary antibody	Supplier
IRS-1 (L3D12) Mouse mAb	1:1000	Anti-mouse IgG, AP-linked antibody	1:3000	Cell signalling technology
Phopho-IRS-1 (Ser 612) (L7B8) mouse mAb	1:2000	Anti-mouse IgG, AP-linked antibody	1:3000	Cell signalling technology
PI3 kinase p85 (19H8) Rabbit mAb	1:1500	Anti-rabbit IgG, AP-linked antibody	1:3000	Cell signalling technology
Phospho-PI3 kinase p85 (Tyr 458)/p55 (Tyr 199) antibody	1:1000	Anti-rabbit IgG, AP-linked antibody	1:3000	Cell signalling technology
β-Actin (13E5) Rabbit mAb	1:10000	Anti-rabbit IgG, AP-linked antibody	1:3000	Cell signalling technology
PTP1*β* (N-19): SC-1718	1:500	Anti-rabbit IgG, AP-linked antibody	1:3000	Santa Cruz Biotechnology

Detection of secondary antibodies was completed by incubation of the membranes for 15 minutes in 5 mL 5-bromo-4-chloro-3-indolyl phosphate/ nitroblue tetrazolium (BCIP/NBT) (SIGMA*FAST*™) (annexure B: reagent 3.5). Images of detected bands were taken using an Alpha Imager 3400 while analysis was conducted using ImageJ 1.45s software. ImageJ is an image processing/analysis program which calculates area and pixel values from a defined area on an image. ImageJ creates density histograms which allow the user to define a set range to calculate the area of a designated peak on the histogram as illustrated in figure 5.5.

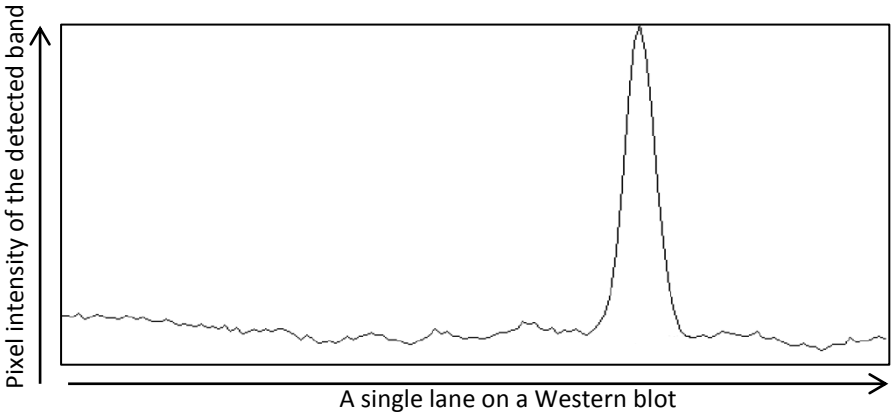

Figure 5.5: A histogram generated using ImageJ 1.45s. A peak can be identified for phospho IRS-1 with minimal background noise.

CHAPTER 6: RESULTS

6.1. MTT CELL VIABILITY STUDIES

Cell viability assays (MTT) were completed in Chang liver, C2C12 and 3T3-L1 cells. An initial screening of 10 µM to 100 µM of each compound was completed in each cell line (results not shown). Figure 6.1 illustrates the results at 10 µM for all compounds in the Chang liver cells. The highest toxicity was found for DC6 (oleanolic acid).

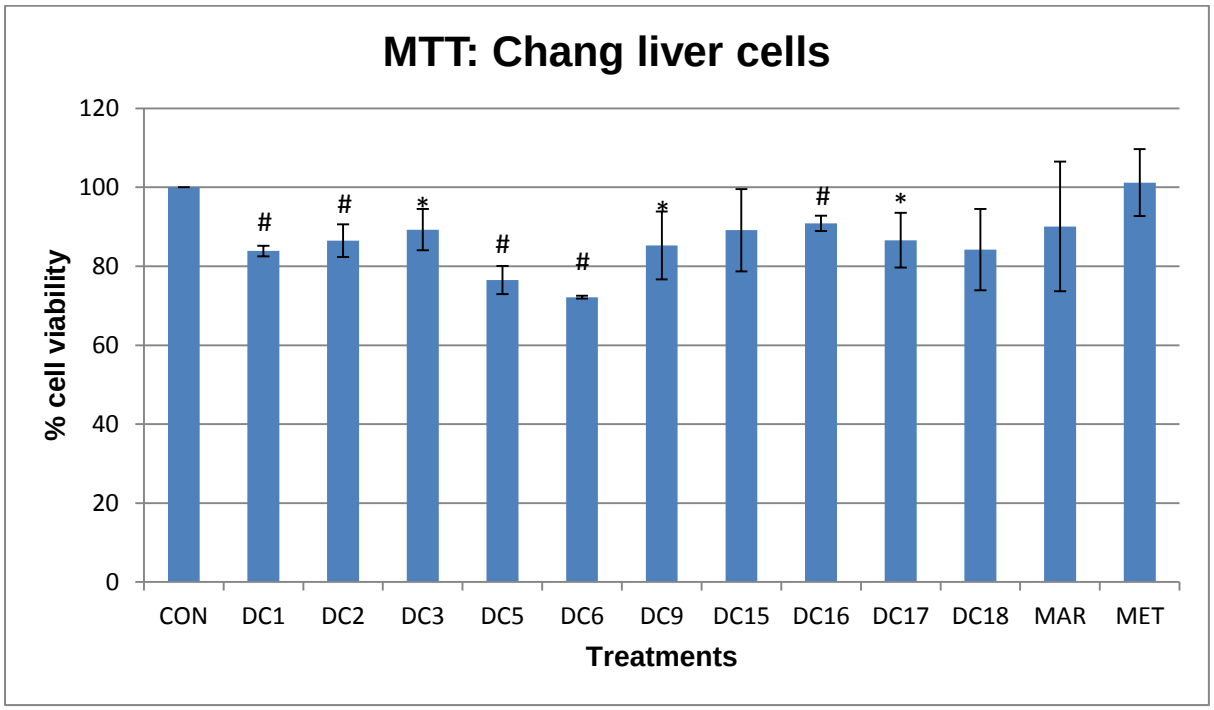

Figure 6.1: A graphical representation of the MTT assay on Chang liver cells (n=3). DC1, DC2, DC3, DC5, DC6, DC9, DC16, DC17 and MAR elicit a significant decrease cell proliferation at 10 µM in Chang liver cells and MET at 1 µM (* P<0.05 and # P<0.01 relative to the CON).

The C2C12 cells exhibited a similar trend with DC6 showing toxicity at concentrations exceeding 10 µM (results not shown). The results shown in figure 6.2 illustrates that the treatments DC1, DC6, DC9 and DC18 elicit a proliferative effect on C2C12 muscle cells as cell viability is increased compared to the CON.

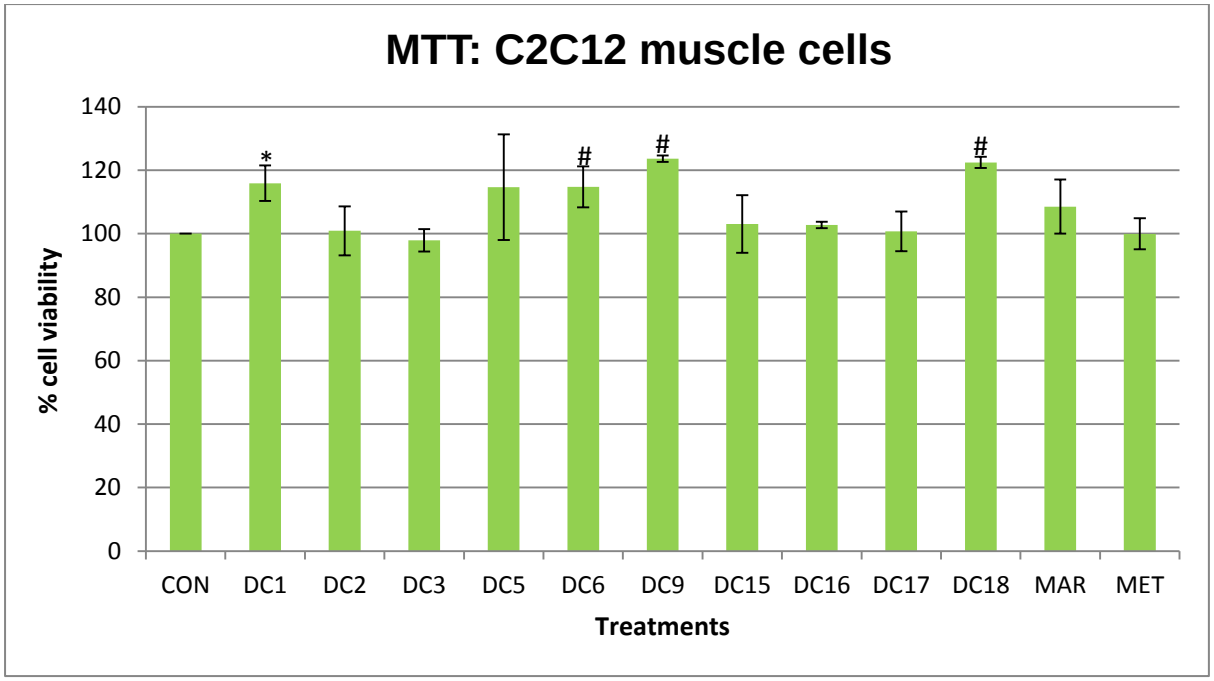

Figure 6.2: A graphical representation of the MTT assay on C2C12 muscle cells (n=3). DC1, DC6, DC9 and DC18 elicit a significant increase cell proliferation at 10 µM in C2C12 muscle cells (* P<0.05 and # P<0.01 relative to the CON).

3T3-L1 adipocytes displayed a higher tolerance to the respective treatments above 10 µM. Very little difference between the CON and treated cells was noted at 10 µM treatment (figure 6.3). The only exceptions were the effects of DC9 and DC15 which had shown an increase in cell viability (figure 6.3).

As a result of the above MTT viability results, a constant concentration of 10µM was chosen for each of the treatments to be utilised in subsequent glucose uptake experiments. MET, a known antidiabetic agent, was to be used as the positive control at a concentration of 1µM.

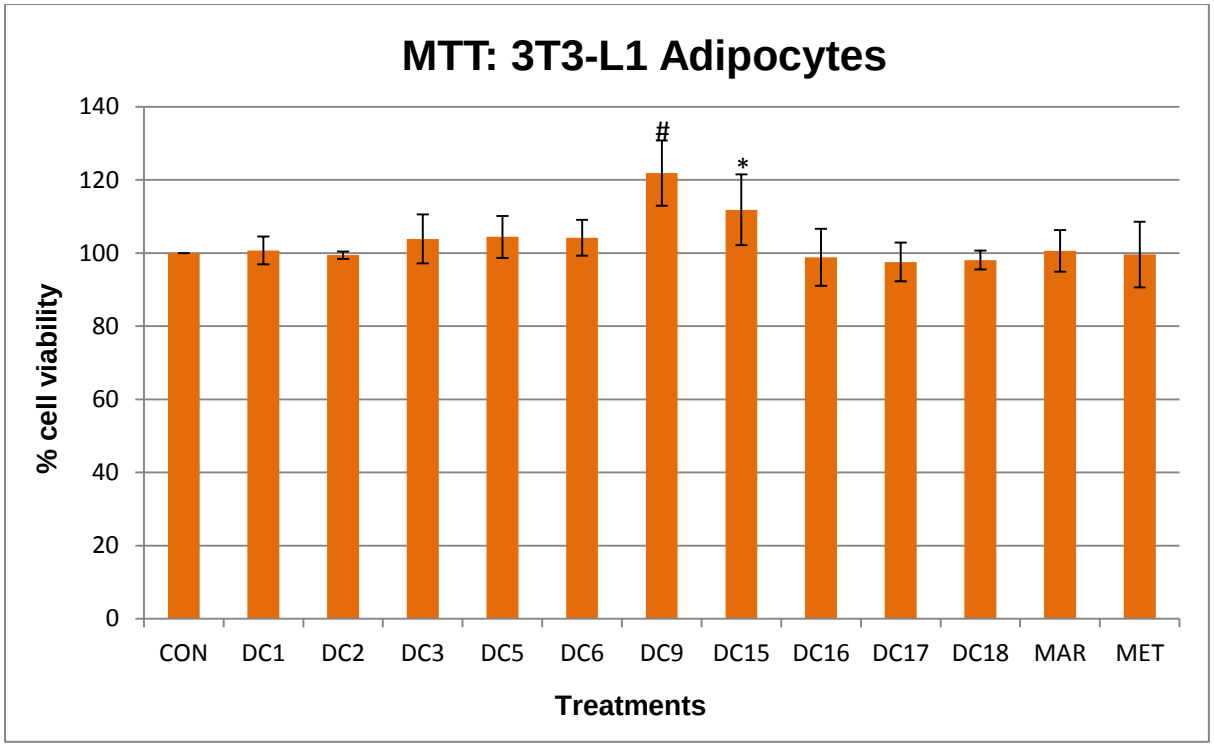

Figure 6.3: A graphical representation of the MTT assay on 3T3-L1 adipocytes. (n=3). DC9 and DC15 elicit a significant increase in cell proliferation at 10 µM in adipocytes (* P<0.05 and # P<0.01 relative to the CON).

6.2. GLUCOSE UPTAKE

Chang liver cells are slow growing compared to the rapid growth of C2C12 muscle cells and 3T3 preadipocytes and with a very distinct function which is to maintain glucose homeostasis in a body and many other functions which involve metabolism of foreign compounds in the body. They are also considerably different in their glucose metabolism as liver cells use GLUT2 instead of GLUT4 which is found in muscle and adipocyte cells. GLUT2 activity is unresponsive to insulin treatment and thus does not aid to increase the rate of glucose uptake. Figure 6.4 shows the results obtained for the glucose uptake experiments completed in Chang liver cells. It is evident that MET increased glucose uptake significantly in Chang liver cells as compared to the CON (2.5-fold increase) which was expected. A significant increase in glucose uptake was seen for DC9, DC15, DC16, DC17, DC18 and MAR however their effect was not as prominent as that of MET.

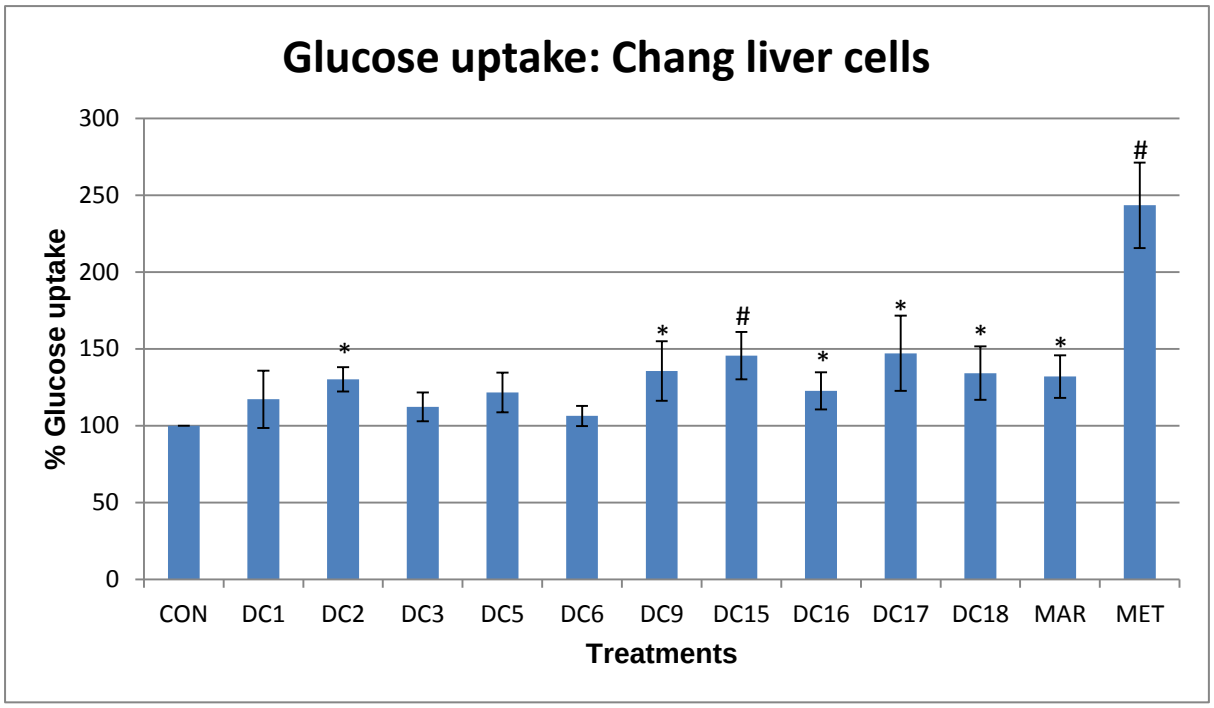

Figure 6.4: A graphical representation of glucose uptake performed on Chang liver cells. Glucose uptake is represented by the percentage glucose taken up compared to the CON (n=3). DC9, DC15, DC16, DC17, DC18, MAR and MET elicit a significant increase in glucose uptake at 10 µM in Chang liver cells (* P<0.05 and # P<0.01 relative to the CON).

MET acts predominantly by shifting glucose metabolism in the liver in presence of insulin to favour glucose uptake and glycogen production while also suppressing the effects of glucagon and glycogenolysis (Wiernsperger and Bailey, 1999; Kirpichnikov *et al.,* 2002). It has been reported that MET increases glucose uptake at least 2-fold in T2DM patients (Hundal *et al.,* 2000). This can be seen in figure 6.4 as MET induces a 2.5-fold increase in glucose uptake.

Glucose uptake results for the C2C12 muscle cells increased the glucose uptake significantly compared to the CON (figure 6.5). All treatments had a significant increase relative to the CON. DC16 and DC18 show a significant increase of glucose uptake from that of MET. DC16 and DC18 elicit a 4-fold and 3.5-fold increase of glucose uptake compared to the CON, respectively; while MET increases glucose uptake 3-fold. DC6 and DC9 show a similar glucose uptake profile compared to MET. MAR significantly increases glucose uptake, however to a lesser degree than all other treatments (1.5 fold increase).

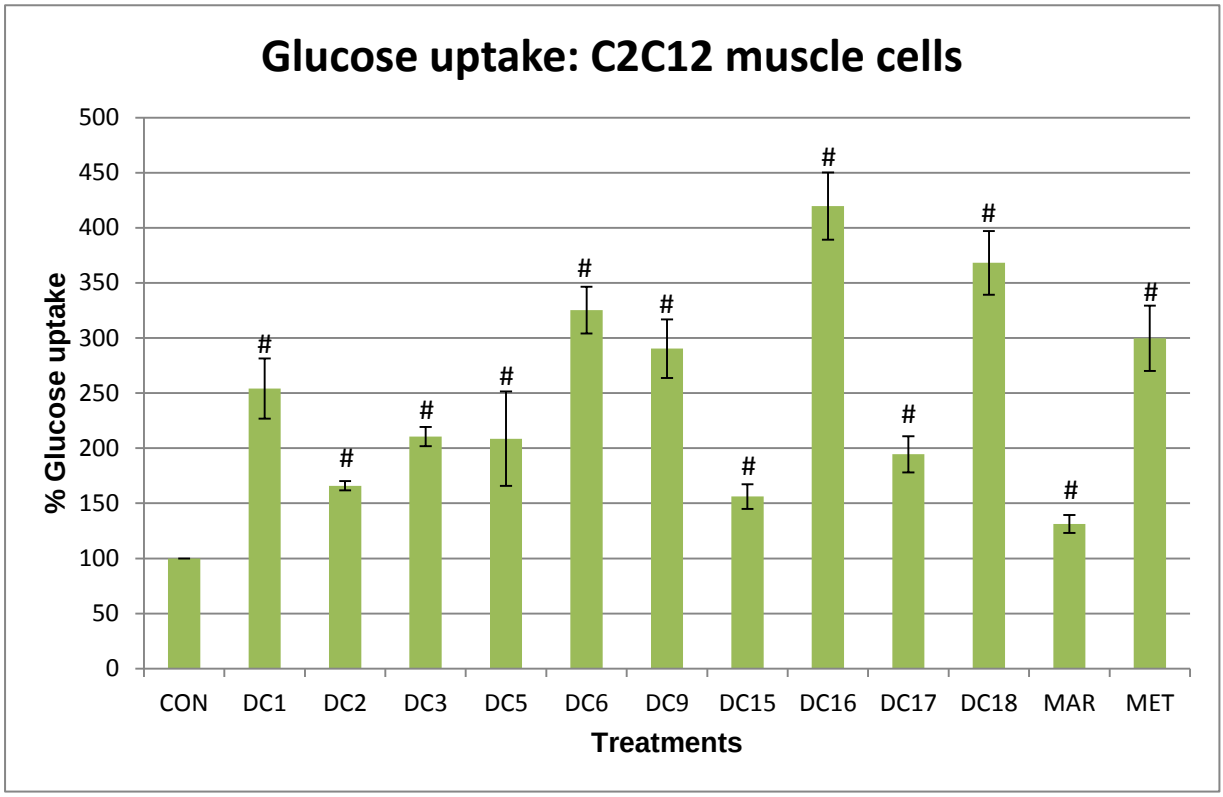

Figure 6.5: A graphical representation of glucose uptake performed on C2C12 muscles cells. Glucose uptake is represented by the percentage of glucose taken up compared to the CON (n=3). DC16 and DC18 elicits a significant increase in glucose uptake at 10 µM in adipocytes compared to MET (* P<0.05 and # P<0.01 relative to the MET positive control).

Figure 6.6 illustrates the glucose uptake profile of the treatments and their effects in 3T3-L1 adipocytes. DC1 and DC2 elicited a significant decrease in glucose uptake in adipocytes. As expected, MET significantly induced glucose uptake in the adipocytes in the presence of insulin compared to the CON. DC3, DC17, DC18 and MAR had also illustrated a significant increase in glucose uptake with DC17 comparing very well to the effects of MET in adipocytes. Based on all the findings DC17, DC18 and MAR were selected for further molecular studies (Western blotting and RT-PCR).

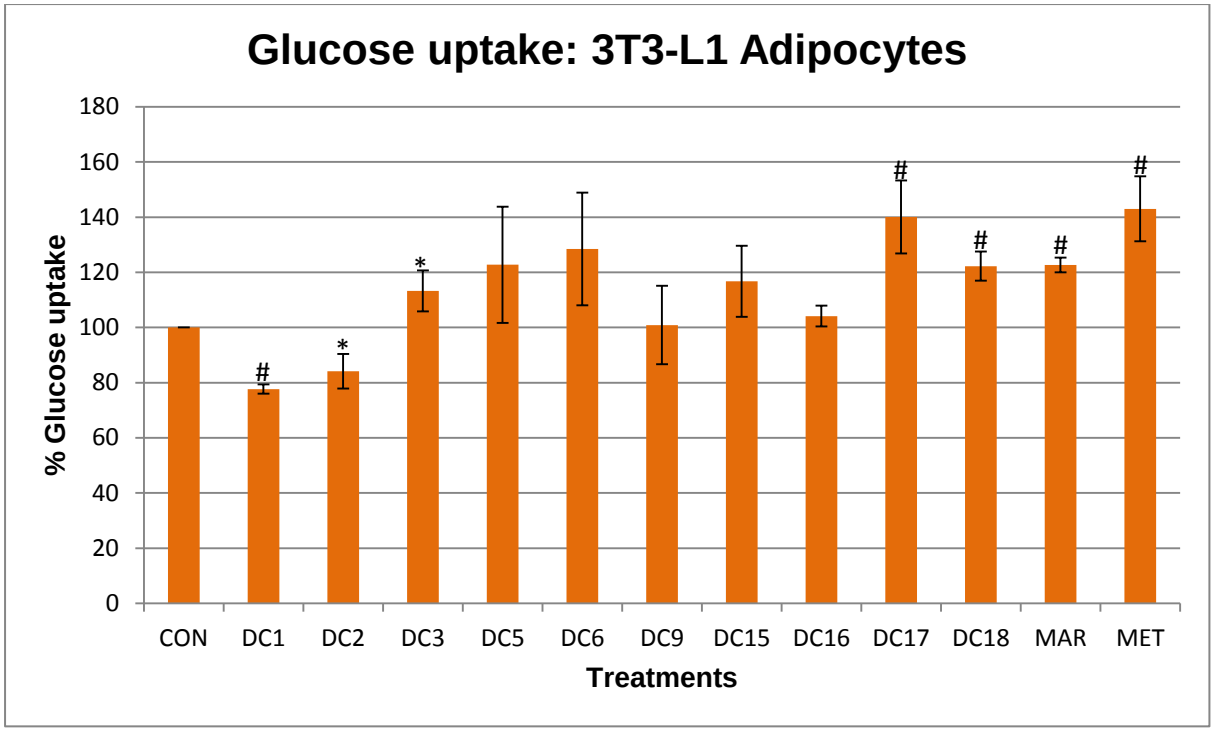

Figure 6.6: A graphical representation of glucose uptake performed on 3T3-L1 adipocytes. Glucose uptake is represented by the percentage of glucose taken up compared to the CON. (n=3). DC1 and DC2 elicits a significant decrease in glucose uptake at 10 µM in adipocytes and DC17, DC18, MAR and MET elicits a significant increase in glucose uptake at 10 µM in adipocytes (* P<0.05 and # P<0.01 relative to the CON).

Oleanolic acid (DC6) was also included as it is known to increase glucose uptake in adipocytes and to inhibit PTP1*β* activity *in vivo* and *in vitro* (de Melo *et al.,* 2010; Lin *et al.,* 2008; Pollier and Goossens, 2012; Zhang *et al.,* 2008). Adipocytes are known to play a vital role in diabetes control with drugs like TZD specifically targeting the adipocytes. Adipocytes were used as the model for molecular based studies during western blotting and RT-PCR as this cell type was responsive to DC17, DC18, MAR and MET treatments as well as portraying stability in viability studies after treatment.

6.3. SDS-PAGE AND WESTERN BLOTTING

3T3-L1 preadipocytes were successfully grown to confluence in 10 cm petri dishes, differentiated for 7 days to mature adipocytes, and then exposed to the respective treatments (DC6, DC17, DC18, MAR and MET) in triplicate for 48 hours. The adipocytes were lysed using the lysis buffer (annexure B; reagent 2.1). The protein concentration of samples (appendix 2) was quantified using the BCA assay (section

5.4.2.1). Figure 6.7 shows an example of one of the gels stained with Acqua stain. As can be seen there was an equivalent concentration of protein loaded in each well.

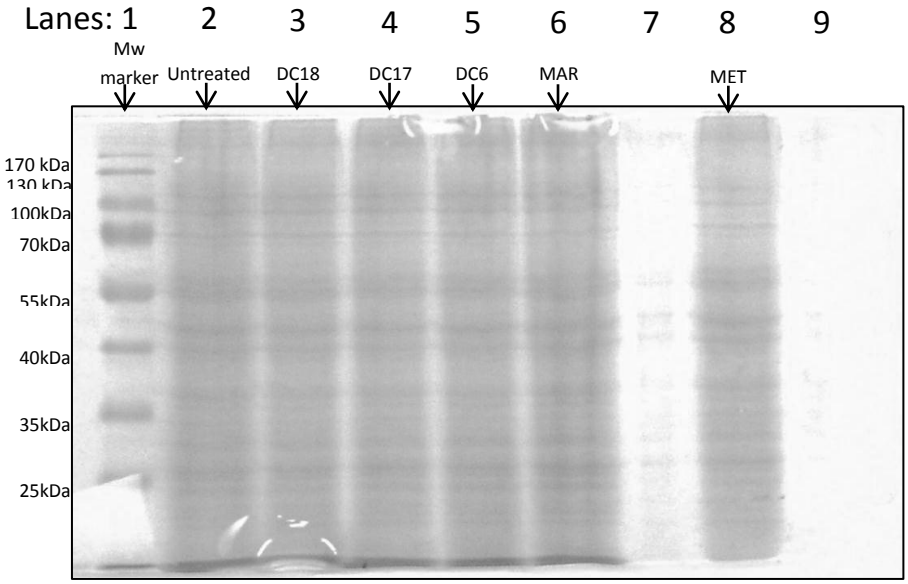

Figure 6.7: A typical SDS-PAGE (10%) polyacrylamide gel stained with Acqua stain. The Mw ladder in lane 1 is the peqGOLD IV prestained markers, lanes 2-6 and 8 are the protein lysates obtained for the various treatments.

To confirm even loading, western blotting was completed using β-actin as a reference protein (figure 6.8). There was no significant difference between detected β-actin levels from the specific treatments, as can be seen in figure 6.8 after densitometry analysis.

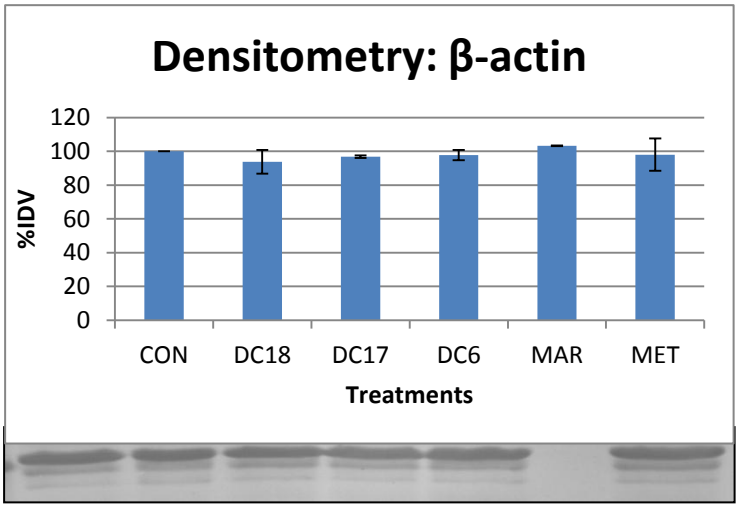

Figure 6.8: Densitometry analysis of β-actin using integrated density values (IDV) relative to the CON of the Western blot analysed (n=3).

Figure 6.9 illustrates the results obtained for densitometry analysis of phosphorylated-IRS1 (p-IRS). MET treatment had illustrated a significant increase in the level of p-IRS1. DC17 however had shown a significant decrease in IRS phosphorylation. DC6 had illustrated a decreased level of IRS1 phosphorylation however this was not significant.

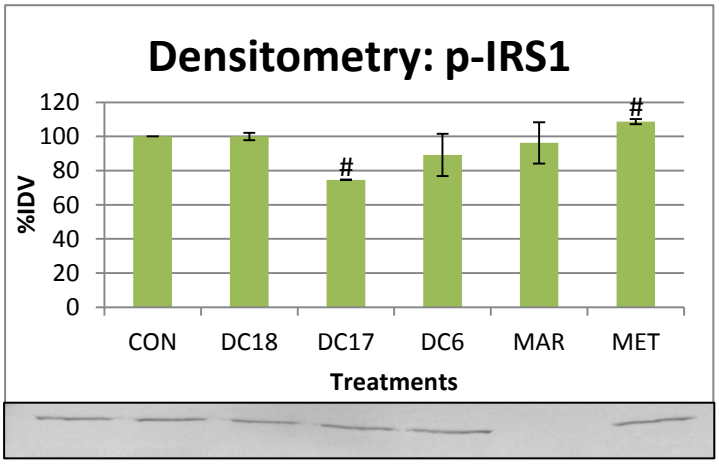

Figure 6.9: Densitometry analysis of p-IRS1 Western blot membrane using IDV relative to the CON of the Western blot analysed (n=3). (* P<0.05 and # P<0.01 relative to the CON).

For the antibodies listed in table 5.4, non-specific binding was only observed with the PTP1*β* which was a polyclonal primary rabbit antibody. The PTP1*β* band could be identified based on molecular mass and thus results could be achieved. PTP1*β* expression was the highest for DC17 and DC6 as seen in figure 6.10. DC18 and MET had shown a significant decrease in PTP1*β* expression.

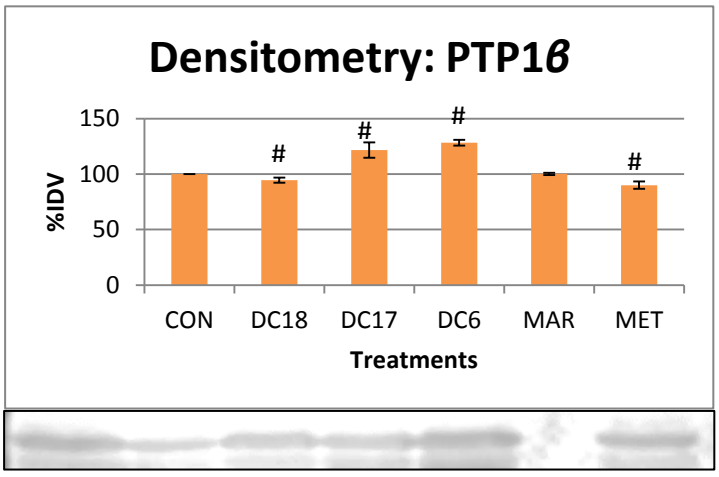

Figure 6.10: Densitometry analyses of PTP1*β* using IDV relative to the CON of the Western blot analysed (n=3). (* P<0.05 and # P<0.01 relative to the CON).

6.4. RNA QUANTIFICATION

RNA quantification was completed using the Agilent Bioanalyzer which required only 1 µL of sample to determine an accurate concentration and integrity determination.

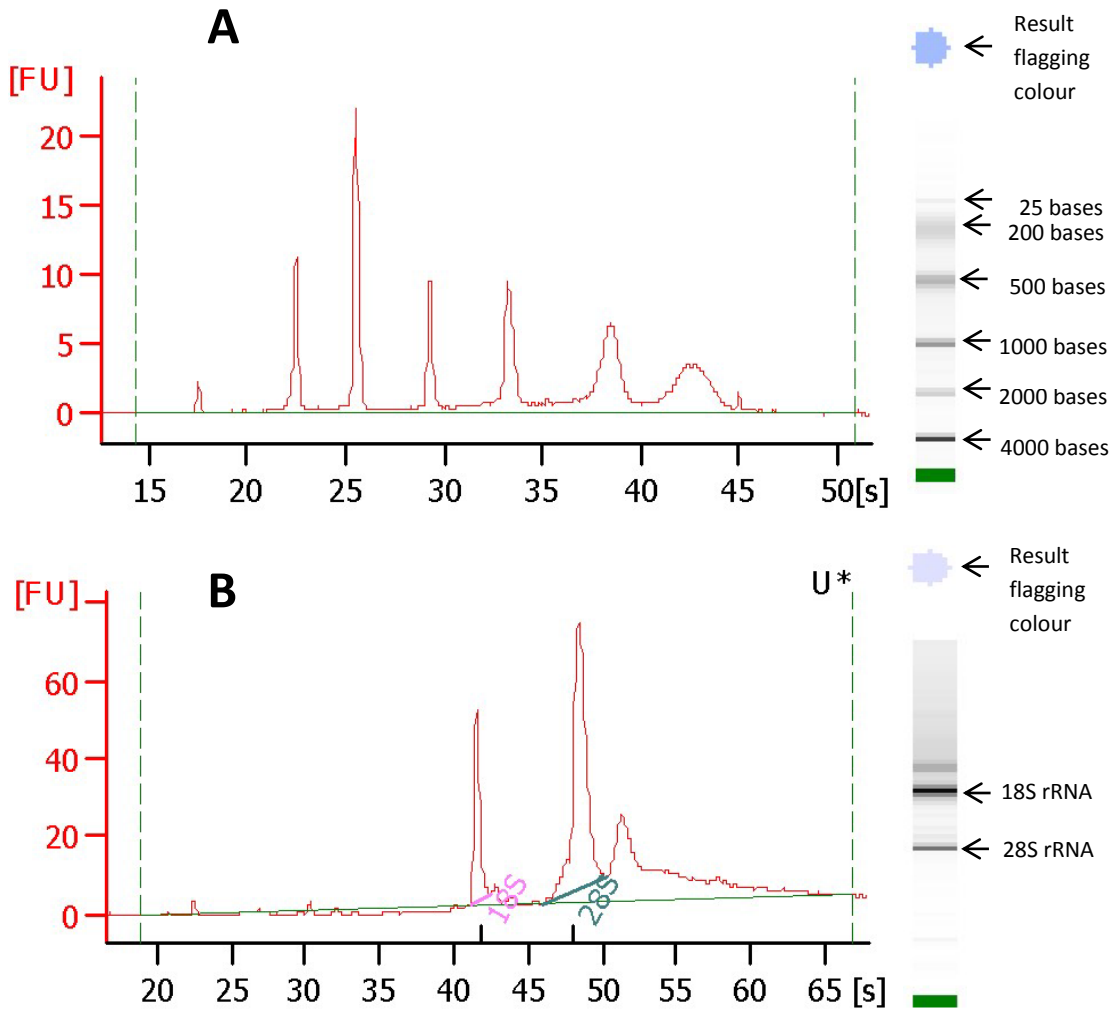

Figure 6.11: Electropherograms of a [A] RNA ladder standard curve and [B] a sample of the CON RNA. On the right of each image is a digital image of the electrophoresis corresponding to the respective peaks in the electropherograms. As the RNA in B was extracted from eukaryotic mouse cells (3T3-L1 adipocytes), the two detected peaks can be seen as 18S rRNA and 28S rRNA.

Results obtained from RNA quantification are tabulated in table 6.1. The integrity of RNA is represented by RIN which is a value associated to the level of RNA integrity. The Agilent 2100 Bioanalyzer has been shown to be a reliable means of measuring parameters of RNA (Schroeder *et al.,* 2006). RIN values range from 10, intact RNA, to 1, total degraded RNA. Results show that the RNA extracted had satisfactory integrity and concentration levels to proceed to cDNA synthesis.

Table 6.1: A summary of the RNA quantification and relative integrity results achieved. The experiment was completed in triplicate and therefore symbols ('-', '*' and 'o') have been assigned to the groups which correspond to the protein and cDNA groups.

Replicates	Sample ID	RIN (Relative integrity number)	[RNA] (ng/µL)
-	Untreated control	9.8	591
	DC18	10	537
	DC17	9.5	781
	DC6	9.9	1438
	MAR	10	1361
	MET	8.7	110
*	Untreated control	10	340
	DC18	9.6	1275
	DC17	10	977
	DC6	8.5	1742
	MAR	8	2058
	MET	N/A	2041
O	Untreated control	9.9	495
	DC18	10	654
	DC17	10	728
	DC6	10	562
	MAR	9.7	364
	MET	10	3590

6.5. cDNA QUANTIFICATION

cDNA concentrations were quantified using a NanoDrop 2000c. For each sample, a spectral scan was obtained as illustrated in figure 6.12 which is representative of a typical absorption spectrum for the presence of nucleic acid. RNA and DNA absorb UV light maximally at 260 nm (Wilson and Walker, 2005).

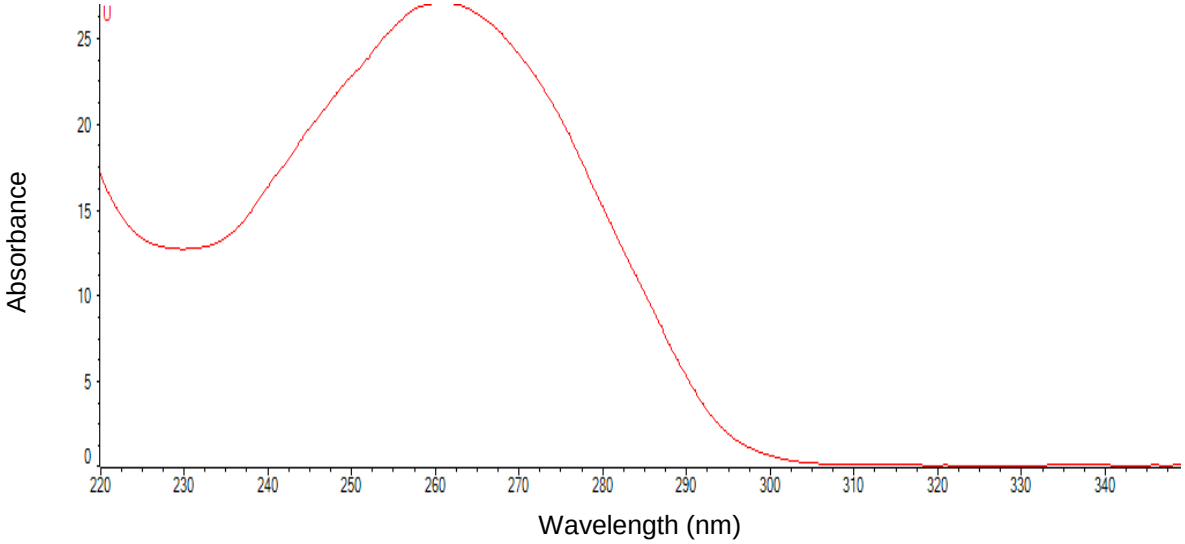

Figure 6.12: An absorption spectrum of cDNA synthesized from RNA isolated from the CON treatment of adipocytes.

Nucleic acids are measured at 260 nm as the nucleotides of DNA and RNA, adenine, guanine, cytosine, uracil and thymine all absorb light at 260nm with adenine and uracil absorbing light most efficiently (www.nanodrop.com). In order to establish the quality of the cDNA, the A_{260}/A_{280} and A_{260}/A_{230} ratio of the samples was measured. At 280 nm some protein amino acids can absorb light thus giving an indication of protein contamination in a sample using a 260/280 ratio (Wilson and Walker, 2005). A sample of nucleic acid is generally considered as pure once the ratio is higher than 1.8 and any value which is considerably lower should not be considered as pure. At 230 nm several chemicals and compounds have the potential to absorb light such as carbohydrates, phenolic compounds (TRIzol) and EDTA (www.nanodrop.com). Some phenolic compounds and EDTA are often used as detergents or stabilizing chemicals in the isolation of DNA or RNA and can thus be carried over in the sample which is to be quantified. Establishing an A_{260}/A_{230} ratio

can thus give an indication of this type of contamination and an acceptable level should be between 2 and 2.2. If the ratio which was calculated is considerably lower, the sample cannot be considered as pure.

Table 6.2: A summary of the cDNA concentration and purity achieved by NanoDrop analysis. Purity is shown here by 260/280 and 260/230 ratios. The experiment was done in triplicate and therefore symbols ('-', '*' and 'o') have been given to the groups which correspond to the protein (table A.1) and RNA (table 6.1) groups analyzed.

Replicates	Sample ID	[cDNA] (ng/µL)	260/280	260/230
-	Untreated control	1349.8	1.78	2.14
	DC18	1332.2	1.78	2.19
	DC17	1267.3	1.77	2.18
	DC6	1213.5	1.76	2.06
	MAR	1244.4	1.78	2.12
	MET	1437.1	1.76	2.16
*	Untreated control	2009.1	1.82	1.94
	DC18	1119.3	1.81	2.59
	DC17	1079.7	1.77	2.12
	DC6	2310.7	1.82	2.1
	MAR	1097.6	1.79	2.13
	MET	1510.9	1.83	2.06
O	Untreated control	1249.2	1.77	2.14
	DC17	1279.6	1.78	2.02
	DC18	1126.3	1.77	2.14
	DC6	1212.7	1.78	2.09
	MAR	1030.5	1.78	1.86
	MET	1135.4	1.78	2.23

As can be seen in table 6.2 the cDNA was determined to be adequate for RT-PCR analysis. The results showed that there is a low level of protein contamination in all samples as the 260/280 ratios are all near to or over 1.8. The 260/230 ratio also illustrate that samples were pure with only one sample being as low as 1.86 while all others were close to or over 2.

6.6. REAL TIME RT-PCR OF IRS1 AND GLUT4 GENES

Gene expression analysis was carried out with REST 2009 software. The program allows for the expression of target genes in experimental samples to be compared to the control sample using gene efficiencies for each gene analysed. Gene expression was analysed using *YWHAZ* as the housekeeping reference gene. A summary of the relative expression is displayed in figure 6.13.

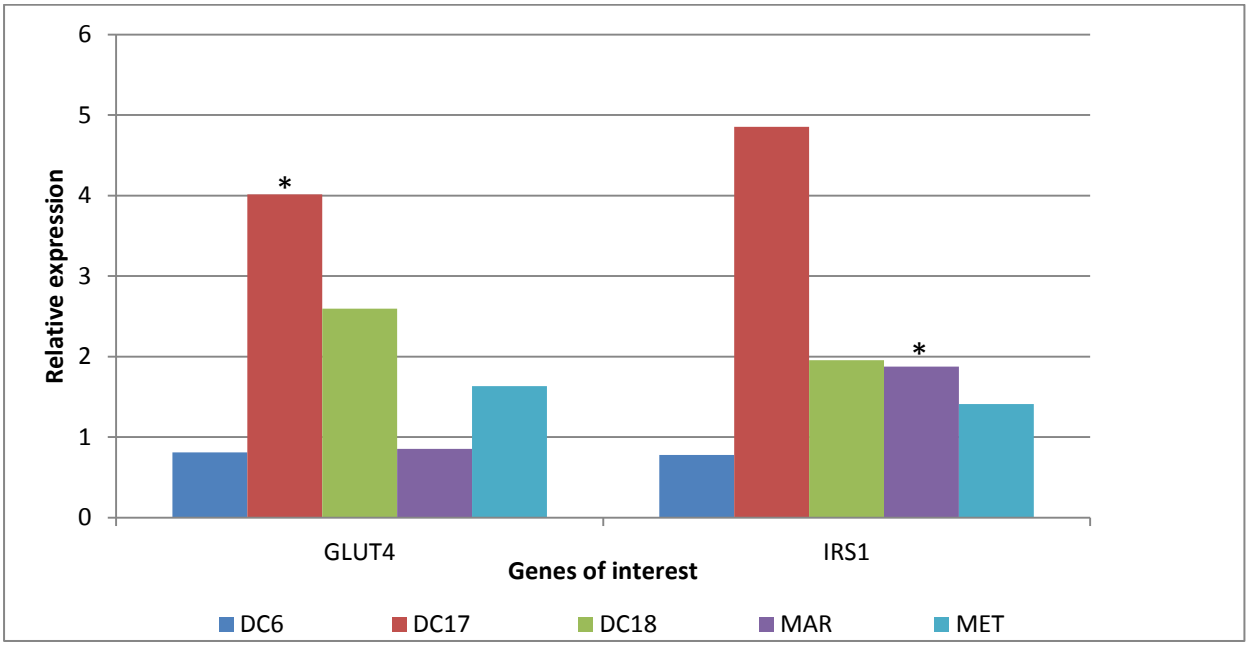

Treatment	Gene	Expression	Std. error	95% C.I.	P(H1)	Result
DC6	GLUT4	0.809	0.385-1.917	0.299-2.479	0.679	-
	IRS1	0.781	0.216-2.190	0.096-3.220	0.927	-
DC17	GLUT4	4.014	3.014-5.414	2.364-6.854	0	UP
	IRS1	4.854	3.316-7.884	2.438-10.635	0.07	-
DC18	GLUT4	2.594	1.232-4.502	0.948-5.590	0.11	-
	IRS1	1.955	1.024-4.157	0.723-4.843	0.22	-
MAR	GLUT4	0.853	0.544-0.1264	0.418-1.654	0.66	-
	IRS1	1.876	1.336-2.687	1.103-3.117	0.032	UP
MET	GLUT4	1.632	1.363-1.960	1.313-2.031	0.169	-
	IRS1	1.413	1.123-1.795	1.030-1.943	0.169	-

Figure 6.13: A graphical and tabular representation of the relative expression of target genes for the treatments listed. Significant increase in relative expression is denoted by *.

From the results obtained, DC17 (figure 6.13) elicits a significant increase in GLUT4 expression by a mean factor of 4.014 ($P<0.01$). DC17 was also shown to increase IRS1 expression by a mean factor of 4.854; however this is not a significant increase in expression. MAR (figure 6.13) was found to up-regulate IRS-1 expression significantly by a mean factor of 1.876 ($P<0.05$).

DC6, DC18 and MET had shown no significant difference in expression from the CON. DC18 and MET increased the expression of both IRS1 and GLUT4, however the was not found to be significant (figure 6.13).

CHAPTER 7: DISCUSSION

DM is a complex and intricate disease which involves many tissue types. Numerous tissue types including the pancreas and peripheral tissues such as the muscle, liver and fat are all known to malfunction in DM (Novack, 2010). Treatments to target these cell types are already in use however these can be too expensive and may have adverse side effects. An example of this saw rosiglitazone being withdrawn from the market in 2010. This is found mostly in the case of biguanides and TDZ's which can create the onset of lactic acidosis and cardiac disease, respectively, among others. Therefore there is a need for treatments which are more available and less harmful. Many countries in Africa are in need of affordable treatments, DM education, as well as quicker, easier and more affordable methods of detecting DM. In Africa and other third world countries which have rich heritage and the tradition of medicinal plant use, it may be possible to discover a means of treatment which could potentially provide a solution to the issues currently found with conventional DM treatments.

MAR is an example of a compound which was isolated from an indigenous Southern African plant (*L. leonurus*) where research has validated the traditional use of the plant as an antidiabetic treatment (Mnonopi *et al*., 2012). This was discovered in *M. vulgare*, a Mexican plant used for the treatments of DM like symptoms. Both *L. leonurus* and *M. Vulgare* extracts were investigated for their potential as DM treatment and it was concluded that both organic and aqueous extracts had antidiabetic effects (Herrera-Arellano *et al.,* 2004; Mnonopi *et al*., 2012; Oyedemi *et al.,* 2011; Vergara-Galicia *et al.,* 2012). MAR was then isolated from the extracts of these medicinal plants and found to possess a range of medicinal uses which include antioxidant, cardio-protective, hypertension, antiedematogenic and analgesic effects (Matkowski *et al.,* 2008; Meyre-Silva *et al.,* 2005; Mnonopi *et al*., 2012; Stulzer *et al.,* 2006). The most relevant of course would be its action in alleviating DM through insulin secretion from pancreatic β-cells (Mnonopi *et al.,* 2012). MAR has thus clearly shown potential to be used for several medical treatments however little is known about its effect on glucose uptake in peripheral cells. Most research completed has been on terpinoids other than MAR. Most of the articles published on *L. leonurus* and *M. vulgare* have been based on alcohol and aqueous extracts. This

study was aimed to discover the effect of MAR and the effects of several MAR derivatives on glucose uptake on peripheral cells.

Cell viability studies were successfully completed in the determination of the cytotoxic potential of the treatments on the cell lines. Initial screening of the treatments was started at 10 µM to 100 µM. Increased cytotoxicity was observed for oleanolic acid which decreased Chang liver cell viability in a dose dependant response manner (data not shown). Oleanolic acid was found to elicit a protective effect on the liver in low doses as an anti-inflammatory and antioxidant however at higher doses it is known to induce apoptosis (Lui, 2005). Due to its apoptotic potential, oleanolic acid was screened as a potential treatment against tumours. At 10 µM oleanolic acid had shown to have a decreased level of cytotoxicity and thus all treatments were decreased to 10 µM for consequent experiments. C2C12 myocytes tolerated the treatments showing no significant cytotoxicity compared to the CON. Treatments DC1, DC6, DC9 and DC18 elicited significant protective/proliferative effect on the C2C12 myocytes. Chang liver cells had illustrated increased cytotoxicity with increasing treatment concentration and at 10 µM treatment concentration, the Chang liver cells showed less than 100 % viability after 2 days of exposure. DC5, DC6, DC16 and DC17 all elicited a significant decrease in Chang liver cell viability compared to the CON. 3T3-L1 adipocytes were generally tolerant to the treatments at a 10 µM concentration as all treatments, except DC9 and DC15, had not affected cell viability significantly negatively or positively compared to the CON. Cell proliferation by DC9 and DC15 is hypothesized to be due to a protective effect from general environmental effects on the cells as mature adipocytes are unable to accomplish mitosis (Navarrete and Real, 2012).

At 10 µM, glucose uptake studies were completed. Although liver cells are known to be the primary target for MET it is also known to aid the effect of insulin induced glucose uptake in muscle and fat. MET is known to act on liver cells by decreasing glucose output through inhibition of gluconeogenesis while allowing for increased glucose uptake in skeletal muscle cells. This is known to be due to MET's action on AMPK which is an enzyme activated by AMP, signalling AMPK that there is a shortage of ATP or energy in the cell (Cheng and Fantus, 2005; Zhang *et al.*, 2012). MET treatment at 1 µM concentration was thus used as a control in this investigation.

Generally glucose uptake was increased in Chang liver cells for all treatments. MET had increased glucose uptake 2.5-fold compared to CON. Specifically DC15 increased glucose uptake 1.5-fold. All treatments had shown a significant increase in glucose uptake as compared to the CON for C2C12 myocytes. Two treatments had elicited a significant increase of glucose uptake above that of MET, i.e. DC16 and DC18, increased glucose uptake 4 and 3-fold, respectively. MET caused a 3-fold increase compared to the CON, while DC6 increased glucose uptake a level equivalent equal to that of MET. DC17, DC18, MAR and MET treatments increased glucose uptake significantly in 3T3-L1 adipocytes ($P<0.01$). DC6 had also shown an increase in glucose uptake which can be seen on figure 6.6., however this was not a significant increase.

DC16, DC17 DC18 and MAR are the most promising candidates to improve glucose uptake. Structurally these compounds differ substantially with DC17 and MAR having an intact furan ring however DC17 is conjugated with an acetoxy group (figure 3.1). DC18 and DC16 do not have a furan ring present and a single hydroxyl group is replaced with a methoxycarbonyl group. In the C2C12 muscle cells, DC18 (3T3-L1 and C2C12) and DC16 (C2C12) best induced glucose uptake. Based on the structural differences of the different MAR derivatives, i.e. the presence or absence of the furan ring, this plays a role in the peripheral tissue type affected. In the 3T3-L1 adipocytes, all these do have a significant effect on glucose uptake however DC17 and MAR elicits a greater response than DC16 which suggests that the furan ring's hydrophobicity contributes to the absorption of the treatment. The chemistry of DC16 is an overall positive charge which adds to the idea that it would not be suitable for bioactivity in the hydrophobic cytoplasmic environment of adipocytes.

DC6, DC17, DC18 and MAR treatments were selected for further investigation as a treatment for glucose uptake in 3T3-L1 adipocytes as these elicited glucose uptake *in vitro*. MET was again used as a positive control. DC6 was included as it has been previously documented to increase glucose uptake through a PTP1*β* inhibition based mechanism in 3T3-L1 adipocytes DC6 can therefore be useful to compare any treatments which may act in a similar manner (Lin *el al*, 2008; Zhang *et al.,* 2008; de Melo *et al.,* 2010).

Western blotting experiments of several target proteins included IRS1, PTP1*β* and *β*-actin (loading control). Blotting of these proteins gave an indication of the activation of insulin signalling pathway under insulin treatment. Figure 6.8 illustrates the expression levels of *β*-actin in response to the treatments and can be seen that the *β*-actin expression was consistent during the experimental treatments.

IRS1 is a protein involved in insulin signalling with several tyrosine and serine phosphorylation sites. Serine phosphorylation is known to be involved in insulin resistance as serine phosphorylation deactivates IRS1 proteins thus slowing insulin signalling. Thus detection of IRS1 Ser 612 phosphorylation would indicate the level of inactive IRS1 (Sykiotis and Papavassiliou, 2001). Figure 6.9 illustrates the level of Ser 612 phosphorylation in the 3T3-L1 adipocytes for the various treatments. DC17 generate a significant decrease in phospho-Ser 612 while DC6 displayed a similar trend, although not statistically significant. MET illustrates a significant increase in phospho-Ser 612 while MAR and DC18 were both comparable to the CON. Detection of PTP1*β* expression had allowed for insight into the level of activation of the insulin signalling pathway through IR and IRS1 tyrosine phosphorylation. The results illustrate a significant increase in PTP1*β* expression for DC17 and DC6 while MET and DC18 shows a significant decrease in PTP1*β* expression. DC6 is a known inhibitor of PTP1*β* and *in silico* studies have shown that DC17 also acts as an inhibitor of PTP1*β* (table 4.1). As treatments do not decrease PTP1*β* expression it may be that their action as PTP1*β* inhibitors would cause a cell to express more PTP1*β* in order to achieve glucose homeostasis similar to that of the CON. DC18 and MET on the other hand appear to act in the decrease of PTP1*β* expression. As explained previously, MET acts by activating AMPK which signals the cell that there is a decrease in ATP and thus induces the cell to express a “starved” phenotype and this promotes glucose uptake. It may be that DC18 acts in a similar manner by activating certain cellular signals thereby inducing a starved phenotype, however further investigation would be required to conclude on this statement. DC18 presents as a good candidate for future studies involving insulin resistant cells as it was found that PTP1*β* was up-regulated in T2DM patients (Zabolotny *et al.,* 2008). PTP1*β* is up-regulated as a result of inflammatory cytokines which are present in higher concentrations when in the obese state thus leading to insulin resistance through a direct increase in PTP1*β* expression (Vazquez *et al*., 2008). DC18 has shown

potential to decrease PTP1*β*, this effect should therefore be investigated on insulin resistant cells or an insulin resistant animal model. From the phospho-Ser 612 of IRS1 results it can be explained that DC17 and DC6 show a decreased level in inactive IRS1 due to the presence of less active PTP1*β* as compounds like DC6 inhibit PTP1*β.* The IR therefore remains active and available for longer allowing IRS1 docking and further activation of the insulin signalling pathway resulting in glucose uptake. MAR shows no deviation from the CON with regards to both PTP1*β* and IRS1 deactivation. It may be that MAR's mechanism of action for glucose uptake is based on an alternative signal transduction pathway such as the Cbl/CAP or MAPK pathway.

Expression analysis of GLUT4 and IRS1 was completed and normalised using the *YWHAZ* housekeeping gene in Rest software. MAR is seen to have expression mean factors at 1.876 (*YWHAZ*) for IRS. Therefore it can be concluded that MAR increases expression of IRS1. DC17 is seen to have an expression mean factor of 4.014 (*YWHAZ*) for GLUT4. DC17 can be concluded to have increased GLUT4 expression.

CHAPTER 8: CONCLUSION AND FUTURE RESEARCH

The *in silico* inhibition and *in vitro* studies did not correlate, therefore a new model needs to be completed in software which allows for solvent effects (i.e. water molecules) to be taken into account (eg. GLIDE) as this may yield more accurate results. Refining the *in silico* model would reduce the research cost of screening numerous potential compounds.

Mnonopi *et al*., (2012) and Oyedemi *et al*., (2011) have both revealed that *L. leonurus* extracts have antidiabetic properties through insulin secretion and glucose uptake in rat models, respectively. In addition, Vergara-Galicia *et al*., (2012) illustrated that *M. vulgare* extracts has hypoglycaemic effects in rat models. MAR, a compound found in both of these plants, and MAR derivatives were tested in this investigation. MAR, DC6, DC17, DC18 stimulated glucose uptake in adipocytes while DC16 and DC18 both induced glucose uptake in myocytes to a level higher than metformin. This investigation proves that MAR acts as an insulin sensitizer of myocytes and adipocytes *in vitro* and can be concluded to be the active compound in *L. leonurus.*

The mechanism underlying the action of the selected MAR and MAR derivatives in increasing glucose uptake is still vague. However from the investigations conducted the following can be concluded:

1. DC6 was shown to act as an inhibitor of PTP1*β in vitro*, therefore acting as sensitizer of the insulin signal in adipocytes and myocytes.
2. DC17 was found to elicit a decrease in Ser 612 phosphorylation of IRS1, increase IRS1 expression (not significant) and an increase in GLUT4 expression (significantly).
3. DC18 elicited a significant decrease in PTP1*β* expression *in vitro*. A decrease in PTP1*β* expression facilitated an increase in the insulin signal.
4. MAR was found to increase IRS-1 expression which led to a better transfer of the signal through the insulin signalling pathway.

Further investigation would include construction of a MAR derivative with maximal glucose uptake associated bioactivity in adipocytes, myocytes and hepatocytes. A compound of this nature would need to have the correct pharmacokinetics, such as

the ability to be absorbed into target cells, have bioavailability and not be cytotoxic. In this investigation, DC1 and DC3 did not perform effectively which may have been as a result of their net charge and thus lack of bioavailability. DC5 elicited glucose uptake in myocytes alone and can be attributed to its hydrophobic nature which would potentially not allow for interaction with hydrophilic/charged active sites (figure 3.1). DC16 (myocytes) and DC18 (myocytes and adipocytes) both lack the furan ring however both increase glucose uptake. This can be credited to the added methoxycarbonyl group on DC16 and the added hydroxyl group on DC18 (figure 3.1). DC17 and MAR both have an intact furan ring however and were found to increase glucose uptake in all cell types tested (figure 3.1). The proposed MAR derivative would be composed of the diterpene and furan ring scaffold of MAR yet not be charged. A functional group similar to that of DC16 (methoxycarbonyl group), DC17 (acetoxy group) and DC18 (hydroxyl) would also be required, therefore adding to the polarity of the molecule.

This investigation focused on the ability of the various MAR derivative treatments to act on the target PTP1*β*. Although this study has shown that the MAR derivatives are not very suitable for inhibition of PTP1*β*, an investigation could be focused on the ability for these compounds to elicit an inhibitory effect in other targets. The Wortmannin insensitive and MAPK pathways were not investigated and could hold evidence to the mechanism of action of several of the treatments. In addition, there are many negative regulators of the insulin signalling pathways which could be affected (i.e. SOCS proteins) which have a similar function to PTP1*β*. PPARγ provides another target as compounds which act as PPARγ agonists are known to alleviate DM symptoms. As this investigation focussed on the glucose uptake potential in normoglycaemic cells, a future investigation may be considered to discover the effect the MAR derivatives would have on glucose uptake in insulin resistance. This will provide additional insight on the potential of these compounds.

CHAPTER 9: REFERENCES

Agostino, M., Jene, C., Boyle, T., Ramsland, P.A. and E. Yuriev. (2009) Molecular docking of carbohydrate ligands to antibodies: Structural validation against crystal structures. ***Journal of Chemical Information and Modelling.*** **49,** 2749-2760.

Ahren, B. (2005) Type 2 diabetes, insulin secretion and β-cell mass. ***Current Molecular Medicine*****. 5**, 275-286.

Amin, S., Khattak, M.I., Shabbier, G. and M.N. Wazir. (2012) Frequency of pulmonary tuberculosis in patients with diabetes mellitus. ***Gomal Journal of Medical Sciences.*** **9**, 163-165.

Awah, P.K., Unwin, N.C. and P.R. Phillimore. (2009) Diabetes mellitus: Indigenous diagnosis and self-management in an African setting: the example from Cameroon. ***BioMed Central Endocrine Disorders*****. 9**, 5-16.

Baker, M.A., Lin, H., Chang, H. and M.B. Murray. (2012) The risk of tuberculosis disease among persons with diabetes mellitus: A prospective cohort study. ***Oxford Journals*****. 54**, 818-825.

Bakhitiyari, S., Meshkani, R., Taghikhani, M. and B. Larijani. (2010) The effects of PTP-1*β* knockdown on glucose uptake and triglyceride levels in C2C12 skeletal muscle cells. ***Iranian Journal of Diabetes and Lipid disorders.*** **9**,1-8.

Bayascas, J.R. and D.R. Alessl. (2005) Regulation of AKT/PKB Ser 473 phosphorylation. ***Molecular cell.*** **18**, 143-145.

Bhattarai, A.R., Kafle, B., Hwang, J., Khadka, D., Lee, S., Kang, J., Ham, S.W., Han, I., Park, H. and H. Cho. (2009) Thiazolidinedione derivatives as PTP1*β* inhibitors with antihyperglycaemic and antiobesity effects. ***Bioorganic and medicinal chemistry letters.*** **19**, 6161-6165.

Bitzur, R. (2011) Diabetes and cardiovascular disease. ***Diabetes Care*****. 34**, 5380-5382.

Bost, F., Aouadi, M., Caron, L. and B. Binetruy. (2005) The role of MAPK's in adipocyte differentiation and obesity. ***Biochimie.* 87**, 51-56.

Boura-Halfon, S. and Y. Zick. (2009) Phosphorylation of IRS proteins, insulin action, and insulin resistance. ***American Journal of Physiology - Endocrinology and Metabolism.* 296**, 581-591

Burns, K.A. and J.P. Vanden Heuvel. (2007) Modulation of PPAR*γ* via phosphorylation. ***Biochimica et Biophysica Acta (BBA) – Molecular and Cell Biology of Lipids*. 1771**, 952-960.

Bryan, J., Crane, A., Vila-Carriles, W.H., Babenko, A.P. and L. Aguilar-Bryan. (2005) Insulin secretagogues, sulfonylurea receptors and K_{APT} channels. ***Current pharmalogical design.* 11**, 2699-2716.

Carr, M.E. (2001) Diabetes mellitus a hypercoagulable state. ***Journal of diabetes and its complications.* 15**, 44-45.

Cheng, A.Y.Y. and I.G. Fantus. (2005) Oral antihyperglycemic therapy for type 2 diabetes mellitus. ***Canadian Medicinal Association Journal.* 172**, 213-226.

Combs, A.P. (2010) Recent advances in the discovery of competitive protein tyrosine phosphatase 1*β* inhibitors for the treatment of diabetes, obesity, and cancer. ***Journal of Medicinal Chemistry.* 53**, 2333-2344.

Cross, J.B., Thompson, D.C., Rai, B.K., Baber, J.C., Fan, K.Y., Hu, Y. and C. Humblet. (2009) Comparison of several molecular docking programs: Pose prediction and virtual screening accuracy. ***Journal of Chemical Information and Modelling.* 49,** 1455-1474.

Dandona, P., Aljada, A. and A. Bandyopadhyay. (2004) Inflammation: The link between insulin resistance, obesity and diabetes. ***TRENDS in Immunology.* 25,** 4-7.

de Beer, S.B.A., Vermeulen, N.P.E. and C. Oostenbrink. (2010) The role of water molecules in computational drug design. ***Current topics in medicinal chemistry.* 10,** 55-66.

de Melo, C.L., Queiroz, M.G.R., Fonseca, S.G.C., Bizerra, A.M.C., Lemos, T.L.G., Melo, T.S., Santos, F.A. and V.S. Rao. (2010) Oleanolic acid, a natural triterpenoid improves blood glucose tolerance in normal mice and ameliorates visceral obesity in mice fed a high-fat diet. ***Chemico-biological interactions*****. 185**, 59-65.

de Oliveira, A.P., Santin, J.R., Lemos, M., Junior, L.C.K., Couto, A.G., de Silva Bittencourt, C.M., Filho, V.C. and S.F. de Andrade. (2011) Gastroprotective activity of methanol extract and marrubiin obtained from *Marrubium vulgare* L. (Lamiaceae). ***Journal of Pharmacy and Pharmacology*****. 63**, 1230-1237.

Dipl-Pharm, S.G. and J.R. Zierath. (2005) Tackling the insulin signalling cascade. ***Canadian Journal of Diabetes.*** **29**, 239-245.

Dragan, A.I., Pavlovic, R., McGivney, J.B., Casas-Finet, J.R., Bishop, E.S., Strouse, R.J., Schenerman, M.A. and C.D. Geddes. (2012) SYBR green I: fluorescence properties and interaction with DNA. ***Journal of Fluorescence.*** **22**, 1189-1199.

Draznin, B. (2006) Molecular mechanisms of insulin resistance: serine phosphorylation of insulin receptor substrate-1 and increased expression of p85α. ***Perspectives in Diabetes.*** **55,** 2392-2397.

Du, K., Herzig, S., Kulkarni, R.N. and M. Montminy. (2003) TRB3: A tribbles homolog that inhibits AKT/PKB activation by insulin in liver. ***Science*****. 300,** 1574-1577.

Erasto, P., Adebola, P.O., Grierson and A.J. Afolayan. (2005) An ethnobotanical study of plants used for the treatment of diabetes in the Eastern Cape province, South Africa. ***African Journal of Biotechnology.*** **4**, 1458-1460.

Fitzpatrick, L.A., Bilezikian, J.P., Wooddell, M., Paul, G., Kolatkar, N.S., Nino, A.J., Miller, C.G., Bogado, C.E., Arnaud, C.D. A.R. Cobitz. (2011) Mechanism of action study to evaluate the effect of rosiglitazone on bone in

postmenopausal women with type 2 diabetes mellitus: rationale, study design and baseline characteristics. ***Journal of drug assessment.*** **1**, 11-19.

Freshney, R.I. (2000) Culture of animal cells: a manual of the basic techniques. 4th ed. p. 336, Wiley-Liss, Inc., United States of America.

Galic, S., Hauser, C., Kahn, B.B., Haj, F.G., Neel, B.G., Tonks, N.K. and T. Tiganis. (2005) Coordinated regulation if insulin signalling by the protein tyrosine phosphatases PTP1*β* and TCPTP. ***Molecular and Cellular Biology,*** **25**, 819-829.

Garratt, K.N., Brady, P.A., Hassinger, N.L., Grill, D.E., Terzic, A. and D.R. Holmes. (1999) Sulfonylurea drugs increase early mortality in patients with diabetes mellitus after direct angioplasty for acute myocardial infarction. ***Journal of the American College of Cardiology*****. 33,**119-124.

Gill, G.V., Yudkin, J.S., Keen, H. and D. Beran. (2011) Insulin dilemma in resource-limited countries. A way forward? ***Diabetologia.*** **54**, 19-24.

Gloerich, M. and J.L. Bos. (2010) Epac: Defining a new mechanism for cAMP activation. ***Annual Review of Pharmacology and Toxicology.*** **50,** 355-375.

Golub, E.E. and K. Boesze-Battaglia. (2007) The role of alkaline phosphatase in mineralization. ***Current Opinion in Orthopaedics.*****18,** 44-448.

Greenberg, A.S. and M.S. Obin. (2006) Obesity and the role of adipose tissue in inflammation and metabolism. ***American journal of Clinical Nutrition*****. 83,** 461-465.

Gribble, F.M., Tucker, S.J., Seino, S. and F.M. Ashcroft. (1998) Tissue specificity of sulfonylureas: studies on cloned cardiac and β-cell K_{ATP} channels. ***Diabetes.*** **47**, 1412-1418.

Grontved, A. (2011) Television viewing and risk of type 2 diabetes, cardiovascular disease, and all-cause mortality. ***Journal of the American Medical Association.*** **305**, 2448-2455.

Gual, P., Marchand-Brustel, Y.L. and J. Tanti. (2005) Positive and negative regulation of insulin signalling through IRS-1 phosphorylation. ***Biochimie***. **87**, 99-109.

Gum, R.J., Gaede, L.L., Koterski, S.L., Heindel, M., Clampit, J.E., Zinker, B.A., Trevillyan, J.M., Ulrich, R.G., Jirousek, M.R. and C.M. Rondinone. (2003) Reduction of protein tyrosine phosphatase 1*β* increases insulin-dependent signalling in *ob/ob* mice. ***Diabetes*****. 52,** 21-28.

Gustavsson, N., Wang, X., Wang, Y., Seah, T., Xu, J., Radda, G.K., Sudhof, T.C. and W. Han. (2010) Neuronal Calcium Sensor Synaptotagmin-9 Is Not Involved in the Regulation of Glucose Homeostasis or Insulin Secretion. ***PLOS ONE*****. 5,** 1-8.

Hall, V., Thomsen, R.W., Henriksen, O. and N. Lohse. (2011) Diabetes in Sub Saharan Africa 1999-2011: Epidemiology and public health implications. A systematic review. ***BioMed Central public health*****. 11**, 1-12.

Hamilton, C.A. (2012) Pharmacological management of type 2 diabetes mellitus in patients with CKD. ***Journal of Renal Care.*** **38**, 59-66.

Hassan Murad, M., Coto-Yglesias, F., Wang, A.T., Sheidaee, N., Mullan, R.J., Elamin, M.B., Erwin, P.J. and V.M. Montori. (2009) Drug-induced hypoglycaemia: A systematic review. ***Journal of Clinical Endocrinology and. Metabolism.*** **94**, 741-745.

Heinonen, K.M., Bourdeau, A., Doody, K.M. and M.L. Tremblay. (2009) Protein tyrosine phosphatases PTP-1*β* and TC-PTP play nonredundant roles in macrophage development and INF-*γ* signalling. ***Proceedings of the National Academy of Sciences of the United States of America.*** **106**, 9368-9372.

Henquin, J. (2000) Triggering and amplifying pathways of regulation of insulin secretion by glucose. ***Diabetes*****. 49,**1751-1760.

Herrera-Arellano, A., Aguilar-Santamaria, L., Garcia-Hernandez, B., Nicasio-Torres, P. and J. Tortoriello (2004) Clinical trial of *Cecropia obtusifolia* and

Marrubiin vulgare leaf extracts on blood glucose and serum lipids in type 2 diabetics. ***Phytomedicine*. 11,** 561-566.

Holis, F., Richards, J.H. and A. Robertson. (1939) Marrubiin, a diterpenoid lactone. ***Nature.* 143,** 604-604.

Holman, R.R., Farmer, A.J., Davies, M.J., Levy, J.C., Darbyshire, J.L., Keenan, J.F. and S.K. Paul. (2009) Three-year efficacy of complex insulin regimens in type 2 diabetes. ***New England Journal of Medicine.* 391**, 1736-1747.

Huang, N. and B.K. Shoichet. (2008) Exploiting ordered waters in molecular docking. ***Journal of Medical Chemistry.* 51,** 4862-4865.

Hubbard, S.R. (1997) Crystal structure of the activated insulin receptor tyrosine kinase in complex with peptide substrate and ATP analog. ***European Molecular Biology Organisation Journal*. 16**, 5572-5581.

Huey, R. and G.M. Morris. (2008) Using AutoDock with AutoDockTools: A tutorial. U.S.A. Institute, Molecular Graphics Laboratory.

Hundal, R. S., Krssak, M., Dufour, S., Laurent, D., Lebon, V., Chandramouli, V., Inzucchi, S.E. Schumann, W.C., Petersen, K.F., Landau, B.R. and G.I. Shulman (2000) Mechanism by which metformin reduces glucose production in type 2 diabetes. ***Diabetes*. 49**, 2063-2069.

Hussein, Z., Wentworth, J.M., Nankervis, A.J., Proietto, J. and P.G. Colman. (2004) Effectiveness and side effects of thiazolidinediones for type 2 diabetes: real-life experience from a tertiary hospital. ***The Medical Journal of Australia.* 181**, 536-539.

Im, S.S., Kang, S.Y., Kim, S.Y., Kim, H.I., Kim, J.W., Kim, H.S. and Y.H. Ahn. (2005) Glucose-stimulated upregulation of GLUT2 gene is mediated by sterol response element-binding protein-1c in the hepatocytes. ***Diabetes*. 54**, 1684-1691.

International Diabetes Federation (2011). IDF Diabetes Atlas, 5th Edition, Brussels: IDF.

Iversen, L.F., Moller, K.B., Pedersen, A.K., Peters, G.H., Petersen, A.S., Andersen, H.S., Branner, S., Mortensen, S.B. and N.P.H. Mollers. (2002) Structure determination of T-Cell protein-tyrosine phosphatase. ***The Journal of Biological Chemistry*****, 277**, 19982-19990.

Kahn, C.R., Chen, L. and S.E. Cohen. (2000) Unravelling the mechanism of action of thiazolidinediones. ***Journal of Clinical Investigations.*** **106**, 1305-1307.

Kamerlin, S.C., Rucker, R. and S. Boresch. (2006) A targeted molecular dynamics study of WPD loop movement in PTP1*β*. ***Biochemical and Biophysical Research Communications*****. 345,** 1161-1166.

Kenechukwu, O. (2004) Cardiovascular effects of *Leonotis leonurus* extracts in normotensive rates and in isolated perfused rat heart. MPharm dissertation. University of Western Cape.

Kim, C. K., Lee, K.A., Zhang, H., Cho, H. and B. Lee. (2007) Docking studies on formylchromone derivatives as proteins tyrosine phosphatase 1*β* (PTP1*β*) inhibitors. ***Bulletin of the. Korean Chemical Society.*** **28**, 1141-1150.

Kirplichnikov, D., McFarlane, S.I. and J.R. Sowers (2002) Metformin: An update. ***Annals of Internal Medicine*****. 137,** 25-33.

Klaman, L.D., Boss, O., Kim, J.K., Martino, J.L., Moghal, N., Kim, Y.B., Sharpe, A.H., Stricker-Krongrad, A., Shulman, G.I., Neel, B.G., and B.B. Khan. (2000) Increased energy expenditure, decreased adiposity, and tissue-specific insulin sensitivity in protein-tyrosine phosphatase 1*β* deficient mice. ***Molecular Cell Biology.*** **20**, 5479-5489.

Knoss, W., Reuter, B. and J. Zapp. (1997) Biosynthesis of the labdane diterpene marrubiin in *Marrubium vulgare* via a non-mevalonate pathway. ***Biochemistry*****. 326,** 449-454.

Koren, S. and I.G. Fantus. (2007) Inhibition of the protein tyrosine phosphatase PTP1*β*: potential therapy for obesity, insulin resistance and type-

2 diabetes mellitus. ***Best practice & Research Clinical Endocrinology & metabolism*. 21,** 621-640.

Kramerlin, S.C.L. Rucker, R. and S.Boresch. (2006) A targeted molecular dynamics study of WPD loop movement in PTP1*β*. ***Biochemical and Biophysical Research Communications*. 345,** 1161-1166.

Kulkarni, R.N., Bruning, J.C., Winnay, J.N., Postic, C., Magnuson, M.A. and C.R. Kahn. (1999) Tissue-specific knockout of the insulin receptor in pancreatic *β*-cells creates an insulin secretory defect similar to that in type 2 diabetes. ***Cell Press.* 96,** 329-339.

Kumar, R., Shinde, R.N., Ajay, D. and M.E. Sobhia. (2010) Probing interaction requirements in PTP1*β* inhibitiors: A comparative molecular dynamics study. ***Journal of Chemical Information and Modelling.* 50,** 1147-1158.

Kuzma, L., Rozalski, M., Walencka, E., Rozalska, B. and H. Wysokinska. (2007) Antimicrobial activity of diterpenoids from hairy roots of *Salvia sclarea L.: Salvipisone* as a potential anti-biofilm agent active against antibiotic resistant *Staphylococci*. ***Phytomedicine*. 14**, 31-35.

Lee, J., Jung, K., Woo, E. And Kim. (2008) Docking study of biflavonoids, allosteric inhibitors of protein tyrosine phosphatase 1*β*. ***Bulletin of the Korean Chemical Society.* 29,** 1479-1484.

Leney, S.E. and J.M. Tavare. (2009) The molecular basis of insulin-stimulated glucose uptake: signalling, trafficking and potential drug targets. ***Journal of endocrinology.* 203,** 1-18.

LeRoith, D. Olefsky, J.M. and S.I. Taylor. (2004) Diabetes Mellitus: A fundamental and clinical text. 3rd edition. Philadelphia. Lippincott Williams and Wilkins.

Lin, Z., Zhang, Y., Zhang, Y., Shen, H., Hu, L., Jiang, H. and Z. Shen (2008) Oleanolic acid derivative NPLC441 potently stimulates glucose transport in 3T3-L1 adipocytes via a multi-target mechanism. ***Biochemical pharmacology*. 76**, 1251-1262.

Lipscombe, L.L., Gomes, T., Levesque, L.E., Hux, J.E., Juurlink, D.N. and D.A. Alter. (2007) Thiazolidinediones and cardiovascular outcomes in older patients with diabetes. ***Journal of American Medical Association.*** **298,** 2634-2643.

Loh, K., Merry, T.L., Galic, S., Wu., B.J., Watt, M.J., Zhang, S., Zhang, Z.Y., Neel, B.G. and T. Tiganis. (2012) T cell protein tyrosine phosphatase (TCPTP) deficiency in muscle cells does not alter insulin signalling and glucose homeostasis in mice. ***Diabetologia*****. 55,** 468-478.

Lopez, J.A., Burchfield, J.G., Blair, D.H., Mele, K., Ng, Y., Vallotton, P., James, D.E. and W.E. Hughes. (2009) Identification of a distal GLUT4 trafficking event controlled by actin polymerization. ***Molecular Biology of the Cell.*** **20**, 3918-3929.

Lui, J. (2005) Oleanolic acid and ursolic acid: Research perspectives. ***Journal of Ethnopharmacology*****. 100**, 92-94.

Lui, S., Zeng, L., Wu, L., Yu, X., Xue, T., Gunawan, A.M., Long, Y. and Z. Zhang. (2008) Targetting inactive enzyme conformation: Aryl diketoacid derivatives as a new class of PTP1*β* inhibitors. ***Journal of American Chemical Society.*** **130,** 17075-17084.

Madsen, L., Petersen, R.k., Sorgensen, M.B., Jorgensen, C., Hallenborg, P., Pridal, L., Fleckner, J., Amri, E., Krieg, P., Furstenberger, G., Berge, R.K. and K. Kristiansen. (2003) Adipocytes differentiation of 3T3-L1 preadipocytes is dependent on lipoxygenase activity during the initial stages of the differentiation process. ***Biochemical Journal.*** **375**, 539-549.

Malik, V.S., Popkin, B.M., Bray, G.A., Despres, J. and F.B. Hu. (2010) Sugar-sweetened beverages, obesity, type 2 diabetes mellitus, and cardiovascular disease risk. ***Journal of the American Heart Association*****. 121**, 1356-1364.

Matkowski, A., Tasarz, P. and E. Szypula. (2008) Antioxidant of herb extracts from five medical plants from *Lamiaceae*, subfamily *Lamioideae.* ***Journal of Medicinal Plant Research.*** **2**, 321-330.

Meltzer, D.D., Pels, S., Payne, W.G., Mannari, R.J., Ochs, D., Forbes-Kearns, J. and M.C. Robson. (2002) Decreasing amputation rates in patients with diabetes mellitus. ***Journal of American Podiatric Medical Association.*** **92**, 425-428.

Meyre-Silva, C., Yunes, R.A., Schlemper, V., Campos-Buzzi, F. and V. Cechinel-Filho (2005) Analgesic potential of marrubiin derivatives, a bioactive diterpene present in *Marrubium vulgare.* ***Il Farmaco*****. 60**, 312-326.

Michael, M.D., Kulkarni, R.N., Postic, C., Previs, S.F., shulman, G.I., Magnuson, M.A. and C.R. Kahn. (2000) Loss of insulin signalling in hepatocytes leads to severe insulin resistance and progressive hepatic dysfunction. ***Cell press.*** **6**, 87-97.

Miinea, C.P., Sano, H., Kane, S., Sano, E, Fukuda, M., Peranen, J., Lane, W.S. and G.E. Lienhard. (2005) AS160, the Akt substrate regulating GLUT4 translocation, has a functional Rab GTPase-activating protein domain. ***Biochemical Journal.*** **391**, 87-93.

Mnonopi, N., Levendal, R.A., Davies-Coleman, M.T. and C.L. Frost. (2011) The cardioprotective effects of marrubiin, a diterpenoid found in *Leonotis leonurus* extracts. ***Journal of Ethnopharmacology*****. 138(1)**, 67-75.

Mnonopi, M., Levendal, R-A., N. Mzilikazi, N. and C.L. Frost. (2012) Marrubiin, a constituent of *Leonotis leonurus*, alleviates diabetic symptoms. ***Phytomedicine.*** **19**, 488-493.

Montalibet, J. and B.P. Kennedy. (2005) Therapeutic strategies for targeting PTP1*β* in diabetes. ***Drug discovery today: Therapeutic strategies,*** **2**, 130-135.

Na, M., Oh, W.K., Kim, Y.O., Cai, X.F., Kim, S., Kim B.Y. and J.S. Ahn. (2006) Inhibition of protein tyrosine phosphatase 1B by diterpenoids isolated from *Acanthopanax koreanum*. ***Bioorganic and Medicinal Chemistry Letters*****. 16**, 3061-3064.

Navarrete, J.M.M. and J.M.F. Real. (2012) Adipocyte differentiation. ***Adipose Tissue Biology*. 1,** 17-38.

Novack, D.V. (2010) FOX (O1) blasts off. ***Cell Metabolism.* 11,** 175-176.

Novaes, A.P., Rossi, C., Poffo, C., Pretti, E.J., Oliveira E.A., Schlemper, V., Niero, R., Cechinel-Filho, V. and C. Burguer. (2001) Preliminary evaluation of effect of some Brazilian medicinal plants. ***Therapie.* 56,** 427–430.

Olson, B.J.S.C. and J. Markwell. (2007) Assays for determination of protein concentration. ***Current Protocols in Protein Science.* 3,** 1-29.

Onodera, K., Satou, K. and H. Hirota. (2007) Evaluations of molecular docking programs for virtual screening. ***Journal of Chemical Information and Modelling.* 47,** 1609-1618.

Ota, S., Horigome, K., Ishii, T., Nakai., M., Hayashi, K., Kawamura, T., Kishino, A., Taiji, M., and T. Kimura. (2009) Metformin suppresses glucose-6-phosphatase expression by a complex I inhibition and AMPK activation-independent mechanism. ***Biochemical and Biophysical Research Communications.* 388,** 311-316.

Ouyang, J., Parakhla, R.A., and R.S. Ochs. (2011) Metformin activates AMP kinase through inhibition of AMP deaminase. ***The Journal of Biological Chemistry.* 286,** 1-11.

Oyedemi, S.O., Bradley, G. and A.J. Afolayan. (2009) Ethnobotanical survey of medicinal plants used for the management of diabetes mellitus in the Nkonkobe municipality of South Africa. ***Journal of medicinal plants research.* 3**, 1040-1044.

Oyedemi, S.O., Yakuba, M.T. and A.J. Afolayan. (2011) Antidiabetic activities of aqueous leaves extract of *Leonotis leonurus* in streptozotocin induced diabetic rats. ***Journal of Medicinal Plants Research.* 5**, 119-125.

Patel, D.K., Prasad, S.K., Kumar, R. and S. Hemalatha. (2012) An overview on antidiabetic medicinal plants having insulin mimetic property. ***Asian Pacific Journal of Tropical Biomedicine.* 2**, 320-330.

Pederson, T.M., Kramer, D.L. and C.M. Rondinone. (2001) Serine/threonine phosphorylation of IRS-1 triggers its degradation, possible regulation by tyrosine phosphorylation. ***Diabetes*****. 50**, 24-31.

Pessin, J.E. and A.R. Saltiel. (2000) Signalling pathways in insulin action: molecular targets of insulin resistance. ***The Journal of Clinical Investigation.*** **106**, 165-169.

Pisani, D.F., Djedaini, M., Beranger, G.E., Elabd, C., Scheideler, M., Ailhaud, G. and E. Amri. (2011) Differentiation of human adipose-derived tissue stem cells into “brite” (brown-in-white) adipocytes. ***Frontiers in Endocrinology.*** **2**, 1-9.

Pollier, J. and A. Goossens (2012) Oleanolic acid. ***Phytochemistry*****. 77**, 10-15.

Rao, G.S., Ramachandran, M.J. and J.S. Bajaj. (2006) *In silico* structure-based design of a potent and selective peptide inhibitor of protein tyrosine phosphatase 1*β*, a novel therapeutic target for obesity and type 2 diabetes mellitus: a computer modelling approach. ***Journal of Biomolecular Structure and Dynamics.*** **23**, 377-384.

Renstrom, E., Barg, S., Thevenod, F. and P. Rorsman. (2002) Sulfonylurea-mediated stimulation of insulin exocytosis via an ATP-sensitive K^+ channel-independent action. ***Diabetes.*** **51**, 33-36.

Richard III, J.W. and P. Raskin. (2011) Updated review: Improved glycemic control with repaglinide-metformin in fixed combination for patients with type 2 diabetes. ***Clinical Medicine Insights: Endocrinology and Diabetes.*** **4**, 29-37.

Rieusset, J., Bouzakri, K., Chevillotte, E., Ricard, N., Jacquet, D., Bastard, J., Laville, M. and H. Vidal. (2004) Suppressor of cytokine signalling 3 expression and insulin resistance in skeletal muscle of obese and type 2 diabetic patients. ***Diabetes*****. 53**, 2232-2241.

Riveline, J.P., Danchin, N., Ledru, F., Varroud-Vial, M. and G. Charpentier. (2003) Sulfonylureas and cardiovascular effects: from experimental data to clinical use. ***Diabetes.* 29**, 207-222.

Roengsumran, S., Petsom, A., Kuptiyanuwat, N. Vilaivan, T., Ngamrojnavanich, N., Chaichantipyuth, C. and S. Phuthong. (2001) Cytotoxic labdane diterpenoids from *Croton oblongifolius*. ***Phytochemistry*. 56**, 103-107.

Rorsman, P., L. Eliasson, E. Renstrom, J. Gromada, S. Barg and S. Gopel. (2000) The physiology of biphasic insulin secretion. ***News in Physiological Sciences*. 15**, 72-77.

Rosen, E.D., Sarraf, P., Troy, A.E., Bradwin, G., Moore, K., Milstone, D.S., Spiegelman, B.M. and R.M. Mortensen. (1999) PPARγ is required for the differentiation of adipose tissue *in vivo* and *in vitro.* ***Molecular cell*. 4,** 611-617.

Rosen E.D. and B.M. Spiegelman. (2006) Review article: Adipocytes as regulators of energy balance and glucose homeostasis. ***Nature*. 444**, 847-853.

Rosen, E.D. and O.A. MacDougald. (2006) Adipocyte differentiation from the inside out. ***Nature reviews: Molecular cell biology*. 7**, 885-896.

Saltiel, A.R. and R. Kahn. (2001) Insulin signalling and the regulation of glucose and lipid metabolism. ***Nature.* 414**, 799-806.

Sano, H., Eguez, L., Teruel, M.N., Fukuda, M., Chuang, T.D., Chavez, J.A., Lienhard, G.E., and T.E. McGraw. (2007) Rab10, a target of the AS160 Rab GAP, is required for insulin-stimulated translocation of GLUT4 to the adipocyte plasma membrane. ***Cell metabolism.* 5**, 293-303.

Schroeder, A., Mueller, O., Stocker, S., Salowsky, R., Leiber, M., Gassmann, M., Lightfoot, S., Menzel, W., Granzow, M. and T. Ragg (2006) The RIN: an RNA integrity number for assigning integrity values to RNA measurements. ***BioMed Central Molecular Biology*. 7**, 1-14.

Schwartz, A.V. (2008) TZD's and bone: A review of the recent clinical evidence. ***Hindawi publishing corporation.*** **2008**, 1-6.

Scheen, A.J. (2007) Drug-drug and food-drug pharmacokinetic interactions with new insulinotropic agents repaglinide and nateglinide. ***Clinical Pharmacokinetics.*** **46**, 93-108.

Silva, J.A.F., Lorencini, M., Reis, J.R.R., Carvalho, H.F., Cagnon, V.H.A. and D.R. Stach-Machado. (2008) The influence of type I diabetes mellitus in periodontal disease induced changes of the gingival epithelium and connective tissue. ***Tissue and cell.*** **40**, 283-292.

Smith, P.K., Krohn, R.I., Hermanson, G.T., Mallia, A.K., Gartner,F. H., Provenzano, M.D., Fujimoto, E.K., Goeke, N.M., Olson, B.J., and D.C. Klenk. (1985) Measurement of protein using bicinchoninic acid. ***Analytical Biochemistry.*** **150**, 76–85.

Sowattanangoon, N., Kotchabhaki, N. and K.J. Petrie. (2009) The influence of Thai culture on diabetes perceptions and management. ***Diabetes research and clinical practice.*** **84**, 245-251.

Spiegelman, B.M. (1998) PPAR-γ: Adipogenic regulator and thiazolidinedione receptor. ***Perspectives in diabetes.*** **47**, 507-514.

Steppan, C.M, Bailey, S.T., Bhat, S., Brown, E.J., Banerjee, R.R., Wright, C.M., Patel, H.R., Ahima, R.S. and M.A. Lazar. (2001) Hormone resistin links obesity to diabetes. ***Nature.*** **409**, 307-312.

Straub, S.G. and G.W. Sharp. (2002) Glucose-stimulated signalling pathways in biphasic insulin secretion. ***Diabetes/Metabolism Research and Reviews*****. 18**, 451-463.

Stulzer, H.K., Tagliari, M.P., Zampirolo, J.A., Cechinel-Filho, V. and V. Schlemper. (2006) Antioedematogenic effect of marrubiin obtained from *Marrubium vulgare*. ***Journal of Ethnopharmacology*****. 180**, 379-384.

Sykiotis, G.P. and A.G. Papavassiliou. (2001) Serine phosphorylation of the insulin receptor substrate-1: A novel target for the reversal of insulin resistance. ***Molecular Endocrinology*****. 15**, 1864-1869.

Tang, X., Powelka, A.M., Soriano. N.A., Czech, M.P. and A. Guilherme. (2005) PTEN, but not SHIP2, suppresses insulin signalling through the Phosphatidylinositol 3-kinase/AKT pathway in 3T3-L1 adipocytes. ***The Journal of Biological Chemistry.*** **280**, 22523-22529.

Taniguchi, C.M., Emanuelli, B. And C.R. Kahn. (2006a) Critical nodes in signalling pathways: Insights into insulin action. ***Nature Reviews.*** **7**, 85-96.

Taniguchi, C.M., Thien, T.T., Kondo, T., Luo, J., Ueki, K., Cantley, L.C. and Khan, C.R. (2006b) Phosphoinositide 3-kinase regulatory subunit p85*α* supresses insulin action via positive regulation of PTEN. ***Proceedings of the National Academy of Sciences*****. 103**, 12093-12097.

Taube, A., Lambernd, S., van Echten-Deckert, G., Eckardt, K. and J. Eckel. (2012) Adipokines promote lipotoxicity in human skeletal muscle cells. ***Archives of Physiology and Biochemistry.*** **118,** 92-101.

Thilagavathi, R. and R.L. Mancera. (2010) Ligand-protein cross-docking with water molecules. ***Journal of Chemical Information and Modelling.*** **50**, 415-421.

Tonks, N.K. (2003) PTP1*β*: From the sidelines to the front lines. ***Federation of European Biochemical Societies.*** **546,** 140-148.

Trietsch, S.J., Hankemeier, T. and H.J. van der Linden. (2011) Lab-on-a-chip technologies for massive parallel data generation in the life sciences: A review. ***Chemometrics and Intelligent Laboratory Systems.*** **108**, 64-75.

Ueki, K., Kondo, T. And C.R. Kahn. (2004) Suppressor of cytokine signalling 1 (SOCS-1) and SOCS-3 cause insulin resistance through inhibition of tyrosine phosphorylation of insulin receptor substrate proteins by discrete mechanisms. ***Molecular and Cellular Biology.*** **24,** 5434-5446.

Vaulont, S., Vasseur-Cognet, M. and A. Kahn. (2000) Glucose regulation of gene transcription. ***The Journal of Biological Chemistry.*** **275**, 31555-31558.

Vazquez, I.N., Veledo, S.F., Kramer, D.K., Bedmar, R. V., Guerra, L.G. and M. Lorenzo. (2008) Insulin resistance associated to obesity: the link TNF-alpha. ***Archives of Physiology and Biochemistry.*** **114**, 183-194.

Vergara-Galicia, J., Aguirre-Crespo, F., Tun-Suarez, A., Crespo, A.A., Estrada-Carrillo, M., Jaimes-Huerta, I., Flores-Flores, A., Estrada-Soto, S. and O. Rolffy. (2012) Acute hypoglycemic effect of ethanolic extracts from *Marrubium vulgare*. ***Phytopharmacology*****. 3**, 54-60.

Watson, R.T. and J.E. Pessin. (2006) Bridging the GAP between insulin signalling and GLUT4 translocation. ***TRENDS in biochemical sciences.*** **31**, 215-222.

Wiernsperger, N.F. and C.J. Bailey (1999) The antihyperglycaemic effect metformin: Therapeutic and cellular mechanisms. ***Drugs*****. 58**, 31-39.

Wilson, K. and J. Walker. (2005) Principles and techniques of biochemistry and molecular biology. 6th Edition. Cambridge. Cambridge University press.

Ye, D., Zhang, Y., Wang, F., Zheng, M., Zhang, X., Luo, X., Shen, X., Jiang, H and H. Liu. (2010) Novel thiophene derivatives as PTP1*β* inhibitors with selectivity and cellular activity. ***Bioorganic and Medicinal Chemistry.*** **18**, 1773-1782.

Zabolotny, M.J., Kim, Y., Welsh, L.A., Kershaw, E.E., Neel, B.G. and B.B. Khan. (2008) Protein-tyrosine phosphatase 1B expression is induced by inflammation *in vivo*. ***The Journal of Biological Chemistry.*** **283**, 14230-14241.

Zhang, B., Salituro, G., Szalkowski, D., Li, Z., Zhang, Y., Rovo, I., Vilella, D., Diez, M.T., Pelaez, F., Ruby, C., Kendall, R.L., Mao, X., Griffin, P., Calaycay, J., Zierath, J.R., Heck, J.V., Smith, R.G. and D.E. Moller. (1999) Discovery of a small molecule insulin mimetic with antidiabetic activity in mice. ***Science*****. 284**, 974-977.

Zhang, F., Lavan, B.E. and F.M. Gregoire. (2007) Selective modulators of PPAR-γ activity: Molecular aspects related to obesity and side-effects. ***Hindawi publishing corporation.*** **2007**, 1-7.

Zhang, S. and Z. Zhang. (2007) PTP1*β* as a drug target: recent developments in PTP1*β* inhibitor discovery. ***Drug Discovery Today.*** **12**, 373-381.

Zhang, Y., Zhang, W., Hong, D., Shi, L., Shen, Q., Li., J., Li, J. and L. Hu. (2008) Oleanolic acid and its derivatives: New inhibitor of protein tyrosine phosphatase 1*β* with cellular activities. ***Bioorganic and Medicinal Chemistry*****. 16**, 8697-8705.

Zhang, C.L., Katoh, M, Shibasaki, T., Minami, K., Sunaga, Y., Takahashi, H., Yokoi, N., Iwasaki, M., Miki, T., and S. Seino. (2009). The cAMP sensor Epac2 is a direct target of antidiabetic sulfonylurea drugs. ***Science*****. 325**, 607-610.

Zhang, B.B., Gaochao, Z., and C. Li. (2009) AMPK: An emerging drug target for diabetes and the metabolic syndrome. ***Cell Metabolism*****. 9,** 407-416.

Zhang, P., Zhang, X., Brown, J., Vistisen, D., Sicree, R., Shaw, J. and G. Nichols. (2010) Global healthcare expenditure on diabetes for 2010 and 2030. ***Diabetes Research and Clinical Practice.*** **87**, 293-301.

Zhang, Y., Wang, Y., Bao, C., Xu, Y., Chen, J., Yan, J. and Y. Chen. (2012) Metformin interacts with AMPK through binding to γ subunit. ***Molecular and Cellular Biochemistry*****. 368**, 69-76.

Zobolotny, J.M., Kim, Y., Welsh, L.A., Kershaw, E.E., Neel, B.G. and B.B. Kahn. (2008) Protein-tyrosine phosphatase 1*β* expression is induced by inflammation *in vivo*. ***The Journal of Biological Chemistry.*** **283**, 14230-14241.

INTERNET WEBSITE REFERENCES

Salowsky, R. 2010. Comply with MIQE guidelines for qPCR - Agilent 2100 Bioanalyzer assessment of RNA integrity. [online]. Available: http://www.gene-quantification.de/rna-integrity.html [3 January 2013].

Thermo Scientific. 260/280 and 260/230 ratios. [online]. Available: http://www.nanodrop.com/Library/T009-NanoDrop%201000-&-NanoDrop%208000-Nucleic-Acid-Purity-Ratios.pdf [5 October 2012].

McCumisky, M. 2010 Western Cape [online]. Available: http://www.diabetessa.co.za/BranchesContentsFull.aspx?bid=3 [14 August 2012].

International Diabetes Federation. 2011. Types of Diabetes [online]. Available: http://www.idf.org/types-diabetes [30 December 2012]

International Diabetes Federation. 2012. IDF Diabetes Atlas –Fifth edition [online]. Available: http://www.idf.org/atlasmap/atlasmap [14 August 2012]

International Diabetes Federation. 2012. IDF Diabetes Atlas –Fifth edition [online]. Available: http://www.idf.org/diabetesatlas/5e/healthcare-expenditures [14 August 2012]

U.S. Food and Drug Administration. 2010. Avandia (rosiglitazone): Ongoing Review of Cardiovascular safety [online]. Available: http://www.fda.gov/Safety/MedWatch/SafetyInformation/SafetyAlertsforHumanMedicalProducts/ucm201446.htm [7 February 2012]

Qiagen. 2009. QuantiTect Reverse Transcription [online]. Available: www.qiagen.com/literature/render.aspx?id=252 [2 March 2012]

Macherey-Nagel. 2012. Total RNA and protein isolation [online]. Available: http://www.mn-net.com/Portals/8/attachments/Redakteure_Bio/Protocols/RNA%20and%20mRNA/UM_TotalRNAProtein.pdf [3 January 2013]

ANNEXURE A: LIST OF REAGENTS AND KITS (PRODUCT, CATALOGUE NUMBER AND SUPPLIER)

1. KITS

Product	Catalogue number	Supplier
Agilent RNA 6000 Nano Assay kit	5067-1551	Agilent Technologies
Nucleospin RNA/Protein	740933.50	Separations
Pierce BCA assay kit	23227	Thermo Scientific
QuantiTect Reverse Transcriptase kit	205313	Qiagen

2. ANTIBODIES

Product	Catalogue number	Supplier
Anti-mouse IgG, AP-linked	7054	Cell Signalling Tech.
Anti-rabbit IgG, AP-linked	7056	Cell Signalling Tech.
IRS-1 (L3D12) Mouse mAb	3194	Cell Signalling Tech.
Phospho-IRS-1 (Ser 612) (L7B8) Mouse mAb	3193	Cell Signalling Tech.
PI3 Kinase p85 (19H8) Rabbit mAb	4257	Cell Signalling Tech.
Phospho-PI3 Kinase p85 (Tyr 485)/p55 (Tyr 199) Antibody	4228	Cell Signalling Tech.
PTP1β (N-19)	Sc-1718	Santa Cruz Biotech.

3. REAGENTS

Product	Catalogue number	Supplier
4-aminoantipyrine	06800	Fluka

10 x Protease inhibitor cocktail	P2714-1BT2	Sigma
40% Acrylamide/Bis solution	161-0148	Bio-Rad
Alkaline phosphatase	P0114-10kU	Sigma
Ammonium persulfate	1123760	Merck
β-mercaptoethanol	21985	Gibco
Sigma*Fast* BCIP/NBT tablets	B5655-5TAB	Sigma
Bromophenol blue	011002	Hopkin and Williams Ltd.
Dimethylsulfoxide	SAAR1865000KF	Merck
Dulbecco's modified eagles medium	D5648-10L	Sigma
Dithiothreitol	43819-5G	Fluka
Ethylenediaminetetra acetic acid	BB100935V	Anal AR
Elite fat free powdered milk		
Foetal calf serum	50613	Biochrom AG
Glucose oxidase from *A. niger*	G0543-10kU	Sigma
Glutathione reduced	1323393	Boehringer Mannheim
Glycerol	2676500LC	Merck
Glycine	1.04169.100	Merck
Horseradish peroxidase	P8375-5kU	Sigma
Hydrochloric acid 37%	UN1789	Merck
HEPES	H4034-100G	Sigma
Insulin, Human	11376497001	Merck
Potassium chloride	5042020EM	Merck
1,1-Dimethylbiguanide Hydrochloride	04635-500MG	Fluka
Methanol	SAAR4164060LP	Merck
Tetrazolium blue (MTT)	M1415.0005	Duchefa Biochemies

*p*NPP	71768-25G	Sigma
Phenol	P3653	Sigma
PTP1*β*	SRP0215	Sigma
Rosiglitazone	71740	Biocom Biotech
RPMI 1640	SH30255.01	Gibco
NaN_3	S2480	Minema
Sodium Chloride	779400	SMM instruments
Sodium dihydrogen phosphate anhydrous	S9820	Minema
di-Sodium hydrogen orthophosphate	5822860EM	Merck
SDS	161-0302	Bio-Rad
TEMED	161-0800	Bio-Rad
Triton X-100	93443	Fluka
Tris	1.08382.0500	Merck
Tween-20	P1379-100ML	Sigma

ANNEXURE B: REAGENT PREPARATION

1. Glucose assay reagent preparation

Phosphate buffer preparation:

1. Solution A: 7 g NaH_2PO_4 in 100 mL water
2. Solution B: 9.2 g Na_2HPO_4 in 200 mL water
3. Add 10 mL of solution A to 40 mL of solution B and dilute with water to achieve a final volume of 1.3 L.

Add the following to 100 mL phosphate buffer:

0.028 g	Phenol
0.008 g	4-aminoantipyrine
0.074 g	EDTA
0.01 g	Horseradish peroxidase
65 µL	Glucose oxidase

2. SDS-PAGE

2.1. Cell lysis buffer for protein isolation

50 mM	Tris-HCl at pH 8.0
150 mM	NaCl
0.02%	NaN_3
1%	Triton X-100
1%	Protease inhibitor

2.2. Solution A

40%	Acrylamide/Bis solution

2.3. Solution B

1.5 M	Tris-HCl, pH 8.8

2.4. Solution C

0.5 M Tris-HCl, pH 6.8

2.5. Solution D

10% (w/v) SDS

2.6. Stacking gel

3.213 mL dH_2O

1.25 mL Solution C

50 µL Solution D

0.488 Solution A

5 µL TEMED

25 µL 10% Ammonium persulfate

2.7. 10% polyacrylamide gel

4.849 mL dH_2O

2.5 mL Solution B

100 µL Solution D

2.5 mL Solution A

5 µL TEMED

50 µL 10% Ammonium persulfate

2.8. 5 x Electrode buffer

5 g Tris

43.2 g Glycine

3g SDS

600 mL dH_2O

2.9. Double strength sample buffer

2 mL Solution C

1.6 mL glycerol

3.2 mL Solution D

0.4 mL	0.2% Bromophenol blue
0.8 mL	β-mercaptoethanol

3. Western Blotting

3.1. Transfer Buffer

25 mM	Tris
192 mM	Glycine
20%	Methanol

3.2. TBS-Tween 20 (pH 7.4)

50 mM	Tris-HCl
0.9%	NaCl
0.1%	Tween-20

3.3. Blocking agent

2%	Fat free powdered milk
0.02%	NaN_3
1 L	TBS tween-20

3.4. Antibody dilution buffer

1 L	TBS
0.2%	Fat free powdered milk

3.5. BCIP/NBT detection reagent

2	BCIP/NBT tablets
50 L	dH_2O

4. PTP1*β* assay

4.1. PTP1*β* reconstitution buffer

45 mM	Tris-HCl, pH 8.0
124 mM	NaCl
2.4 mM	KCl
3 mM	DTT

18 mM	Glutathione
10%	Glycerol

4.2. PTP1*β* assay buffer

50 mM	HEPES, pH 7.4
2 mM	EDTA
3 mM	DTT
100 mM	NaCl
Adjustable	*p*NPP

5.1. BCA assay reagent A (1L)

10 g	BCA
20 g	Sodium carbonate
1.6 g	Sodium tartrate
9.5 g	Sodium bicarbonate
pH	11.25

5.2. BCA assay reagent B

4%	$CuSO_4$

APPENDIX 1: FIGURES NOT SHOWN IN TEXT

A Figures: Determination of optimal enzyme (PTP1*β* and ALP) concentrations for inhibition studies.

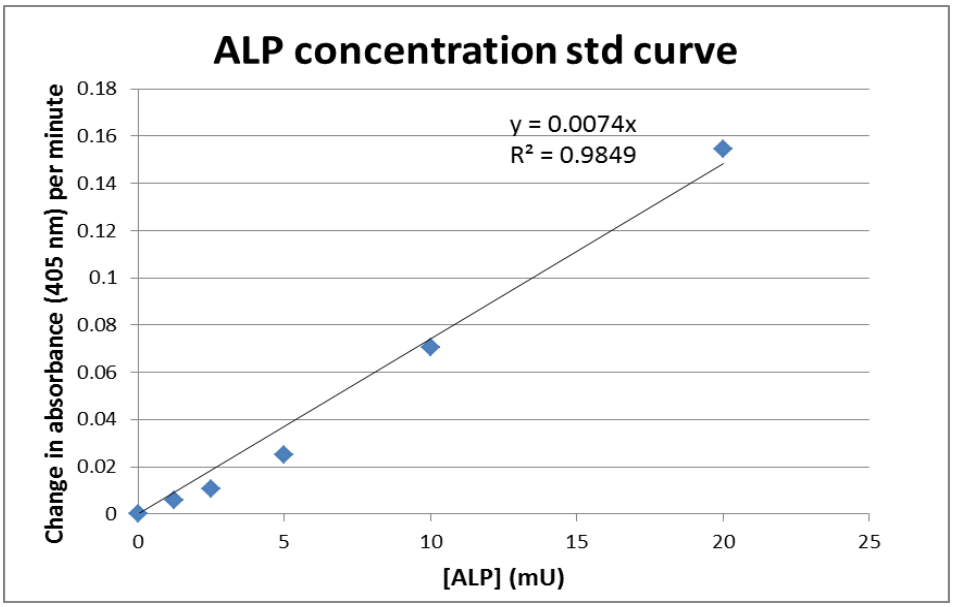

Figure A.1: A standard curve illustrating the increase in absorbance as a function of ALP concentration. A concentration of 10 mU was chosen for the completion of ALP inhibition studies

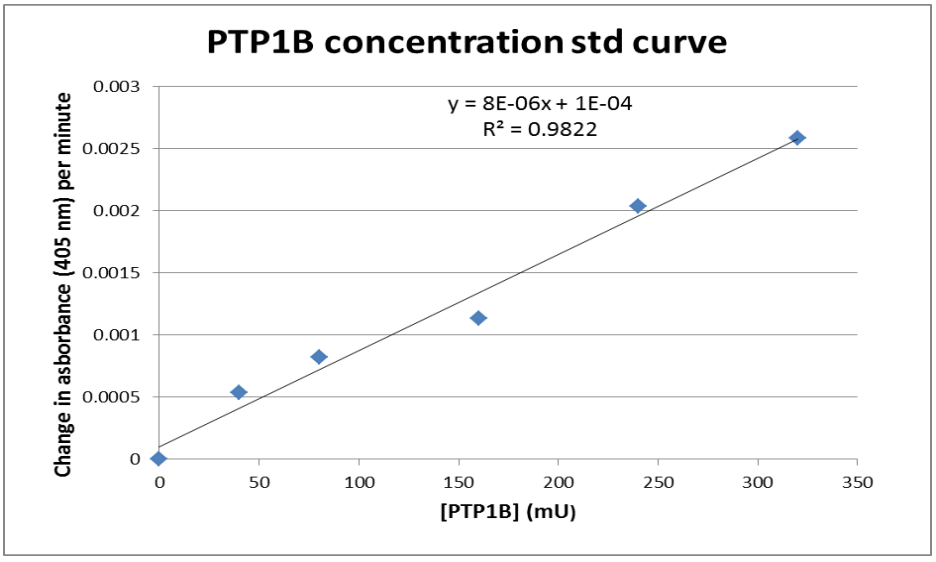

Figure A.2: A standard curve illustrating the increase in absorbance as a function of PTP1*β* concentration. A concentration of 320 mU was chosen for the completion of PTP1*β* inhibition studies.

B Figures: Examples of progress curves plotted for PTP1*β*.

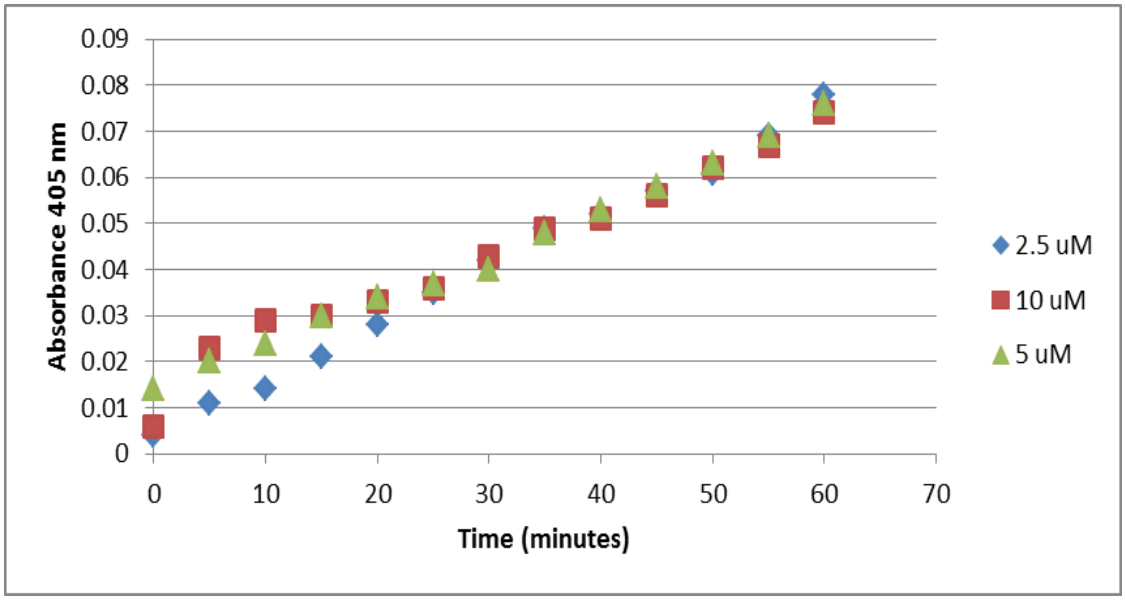

Figure B.1: Progress curves for PTP1*β* with DC9 as the inhibitor at 75 mM *p*NPP concentration. DC9 concentrations are shown in the key.

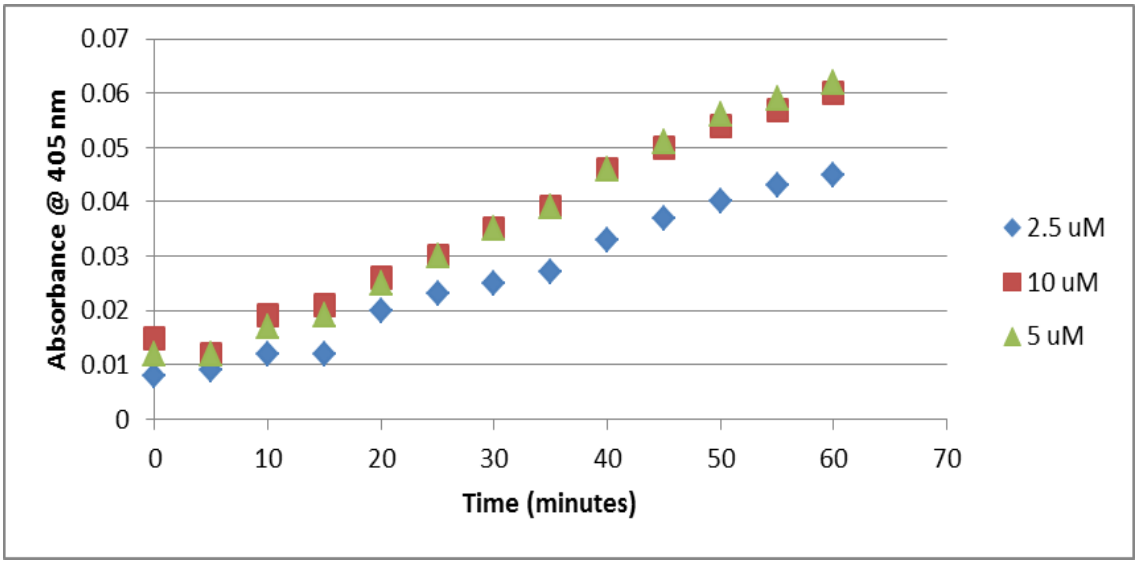

Figure B.2: Progress curves for PTP1*β* with DC9 as the inhibitor at 25 mM *p*NPP concentration. DC9 concentrations are shown in the key.

C Figures: Double Dixon plots were used in the determination of K_i values. Double Dixon plots are shown here for every inhibitor tested against PTP1*β*.

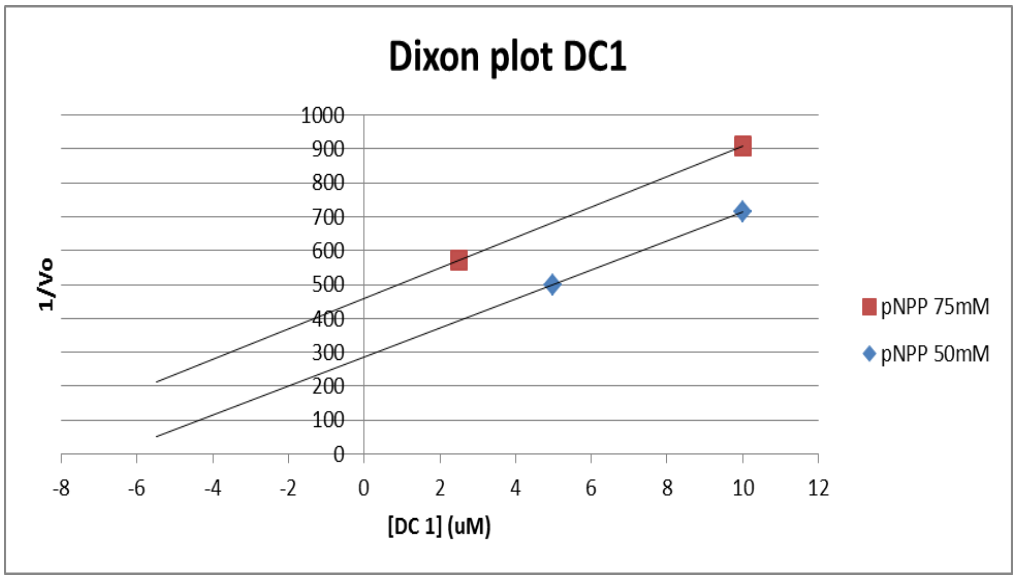

Figure C.1: A double Dixon plot for compound DC1 on PTP1*β*.

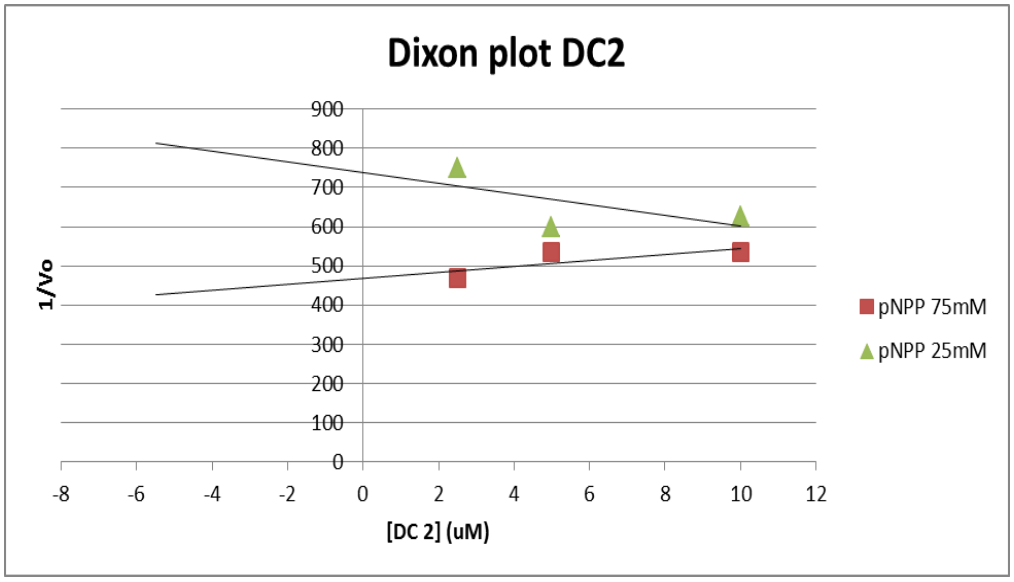

Figure C.2: A double Dixon plot for compound DC2 on PTP1*β*.

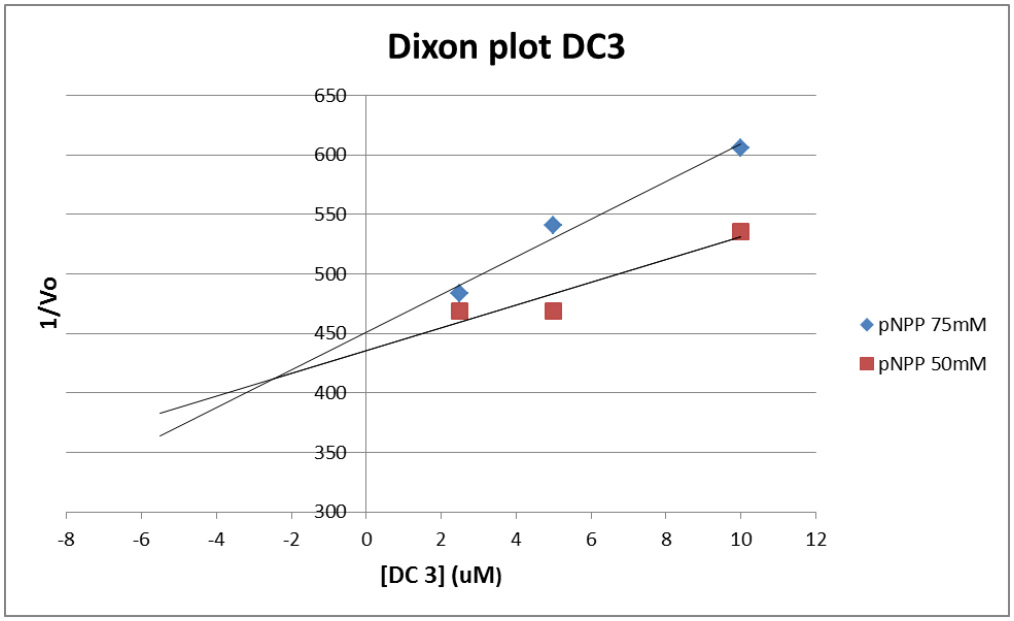

Figure C.3: A double Dixon plot for compound DC3 illustrating an inhibitory action on PTP1*β* (K_i = 2.3 µM).

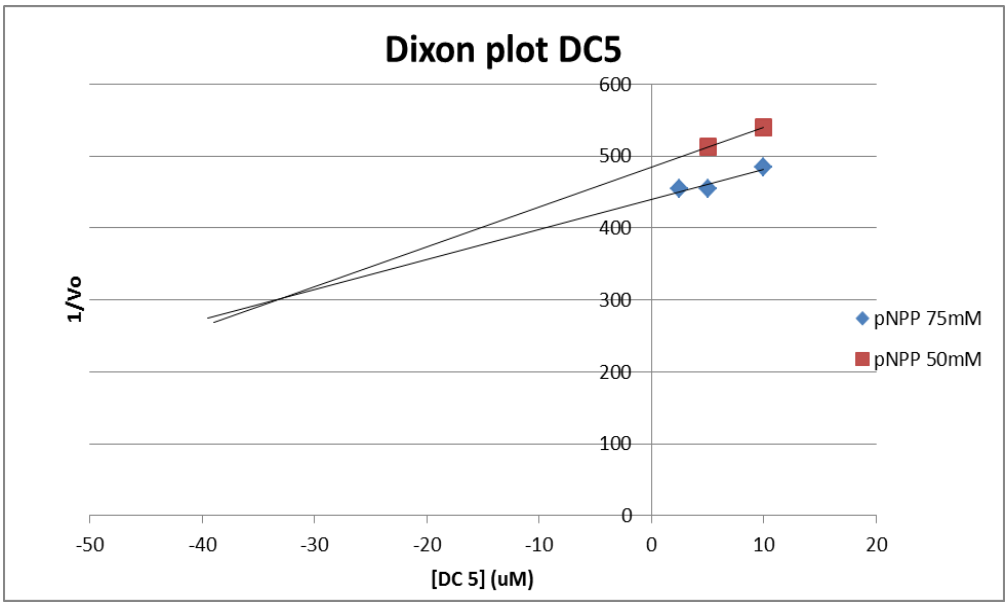

Figure C.4: A double Dixon plot for compound DC5 illustrating an inhibitory action on PTP1*β* (K_i = 33 µM).

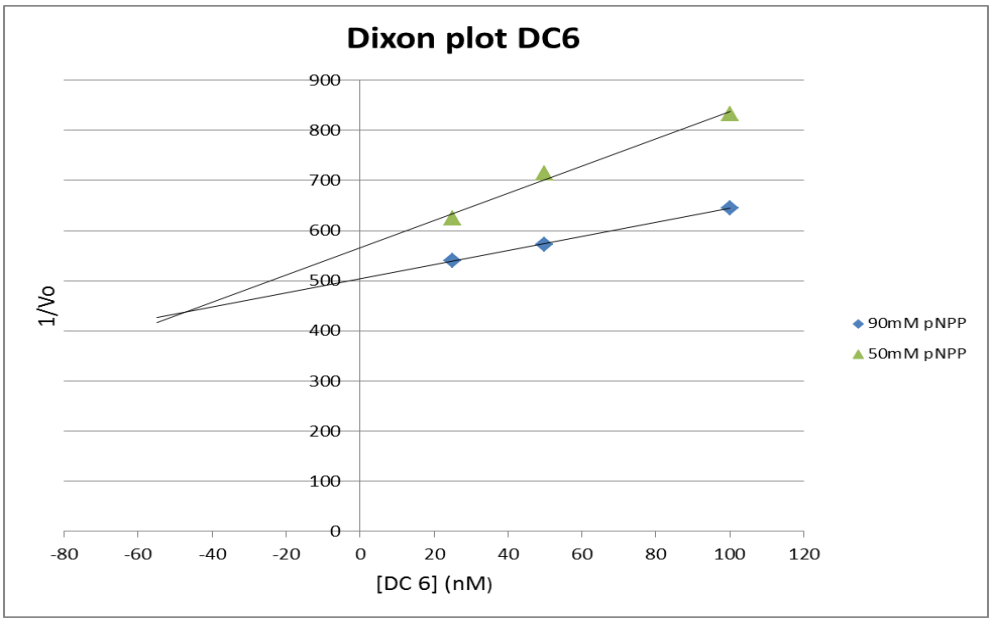

Figure C.5: A double Dixon plot for compound DC6 illustrating an inhibitory action on PTP1*β* (K_i = 0.047 µM).

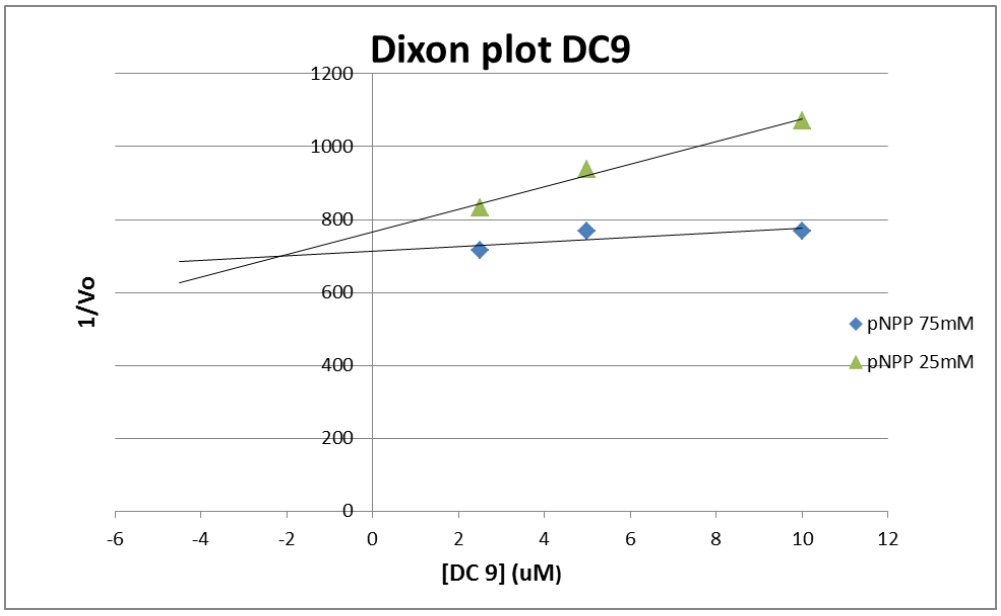

Figure C.6: A double Dixon plot for compound DC9 illustrating an inhibitory action on PTP1*β* (K_i = 2.1 µM).

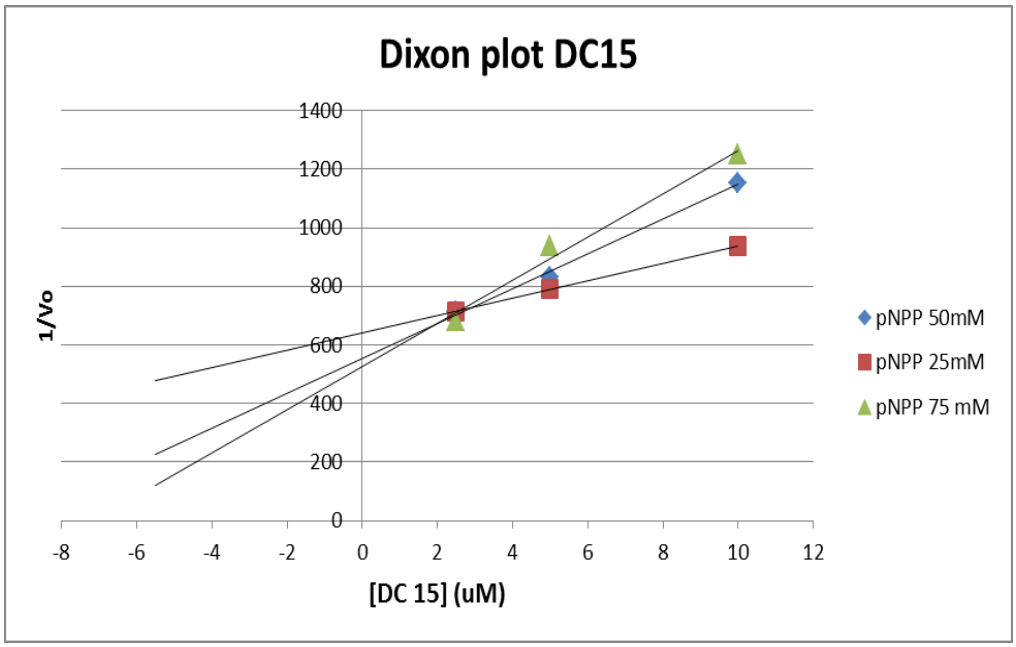

Figure C.7: A double Dixon plot for compound DC15 (MAR) on PTP1*β*.

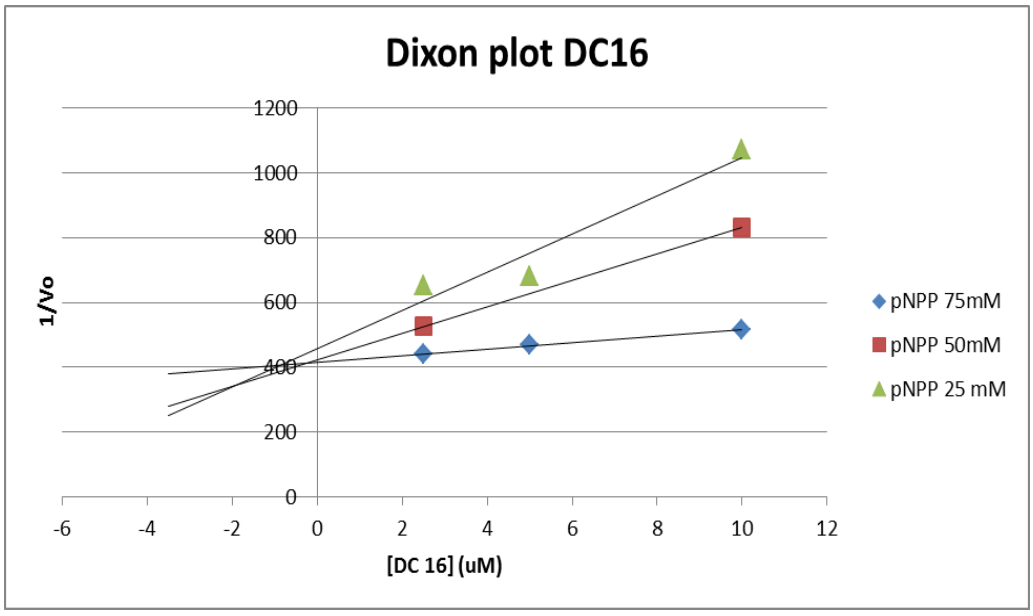

Figure C.8: A double Dixon plot for compound DC6 illustrating an inhibitory action on PTP1*β* (K_i = 6 µM).

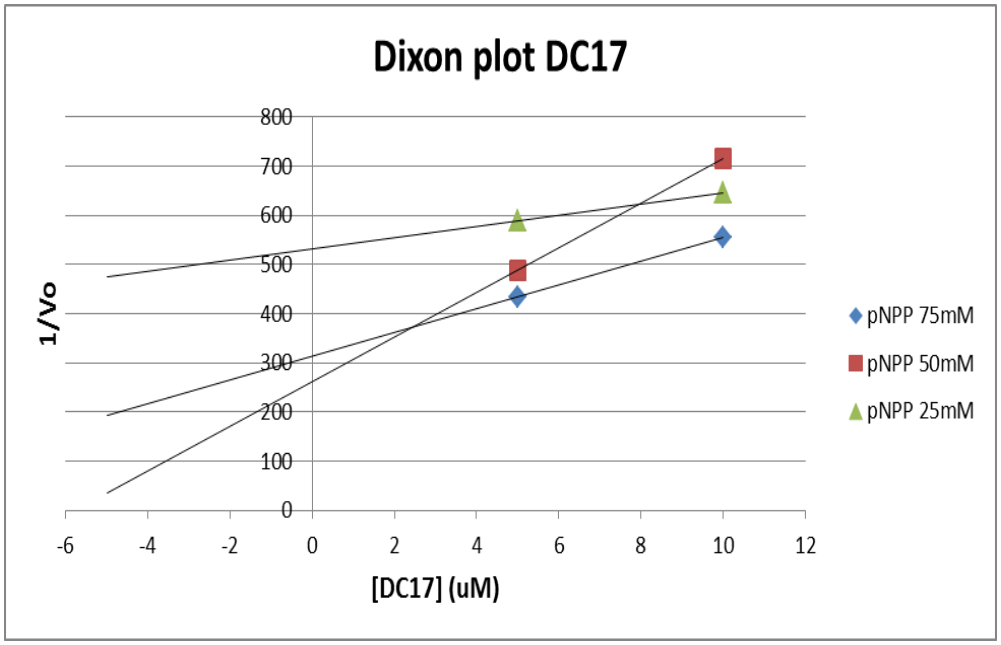

Figure C.9: A double Dixon plot for compound DC17 on PTP1*β*.

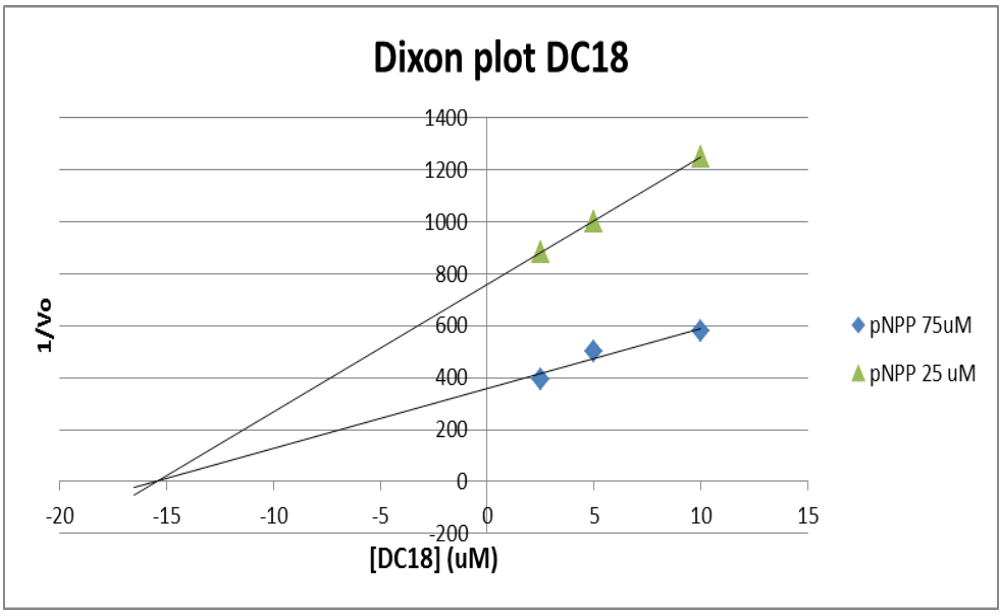

Figure C.10: A double Dixon plot for compound DC18 illustrating an inhibitory action on PTP1*β* (K_i = 15.5 µM).

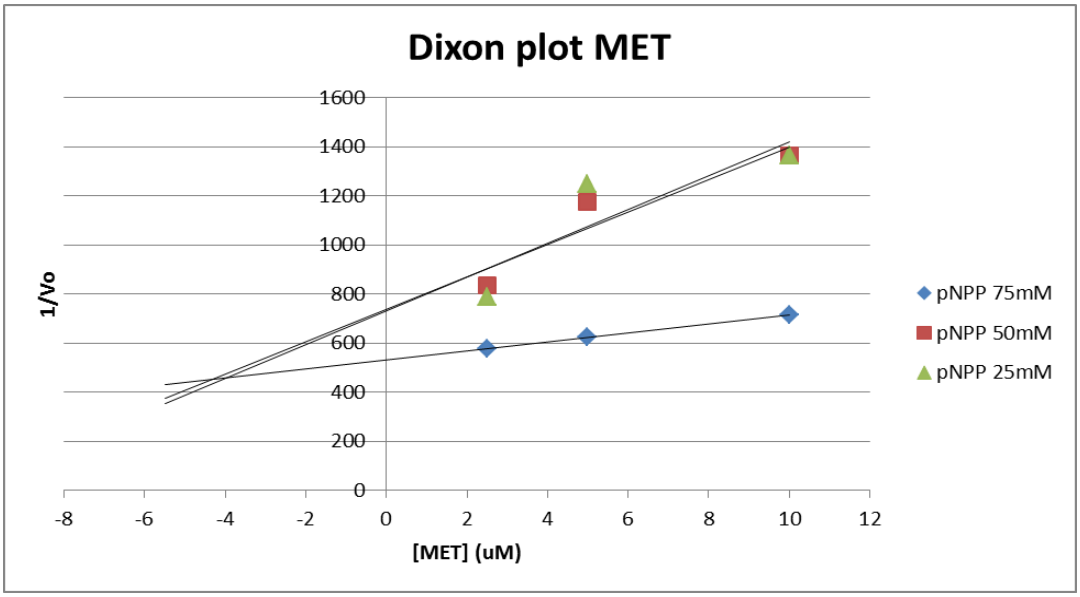

Figure C.11: A double Dixon plot for MET illustrating an inhibitory action on PTP1*β* (K_i = 4.1 μM).

D Figures: LB plots were used to investigate the mode of enzyme inhibition displayed. LB plots are shown for all those which exhibit an inhibition against PTP1*β*.

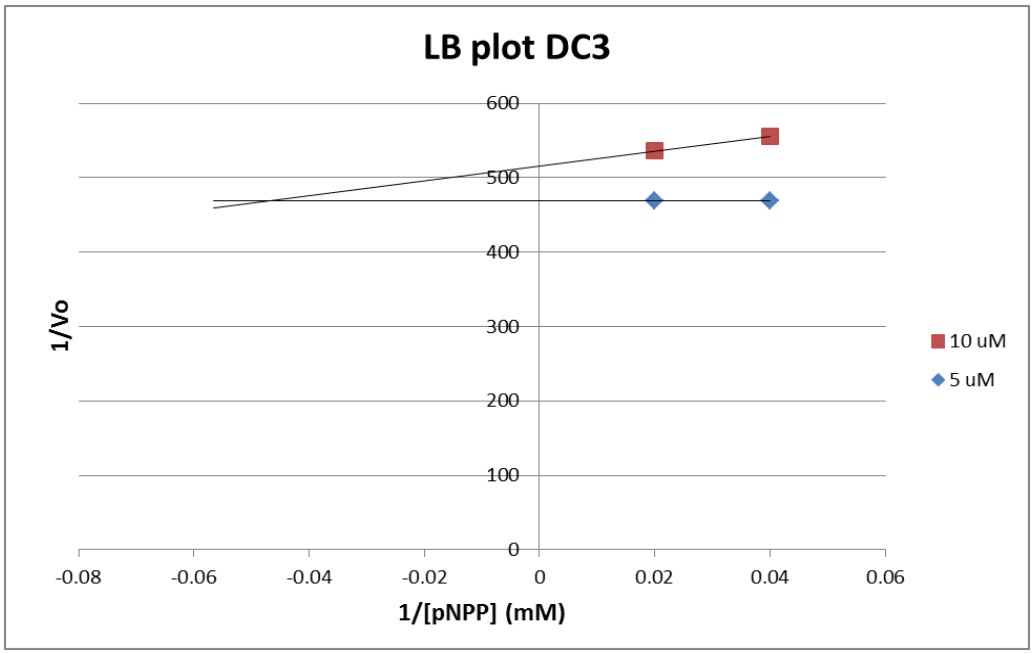

Figure D.1: An LB plot illustrating the mixed mode of inhibition on PTP1*β* by compound DC3.

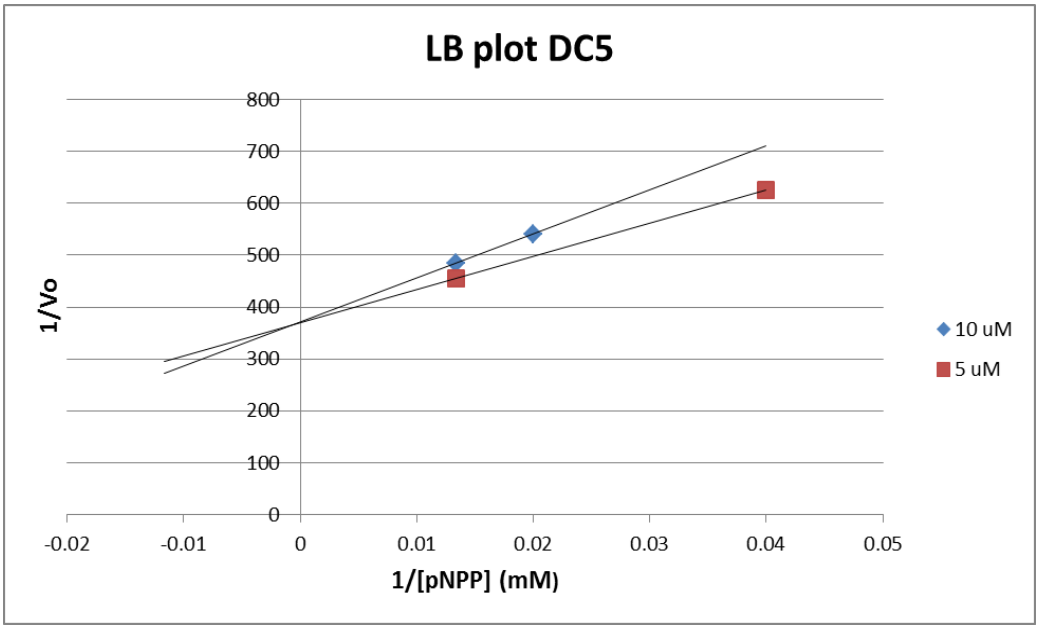

Figure D.2: An LB plot illustrating the competitive mode of inhibition on PTP1*β* by compound DC5.

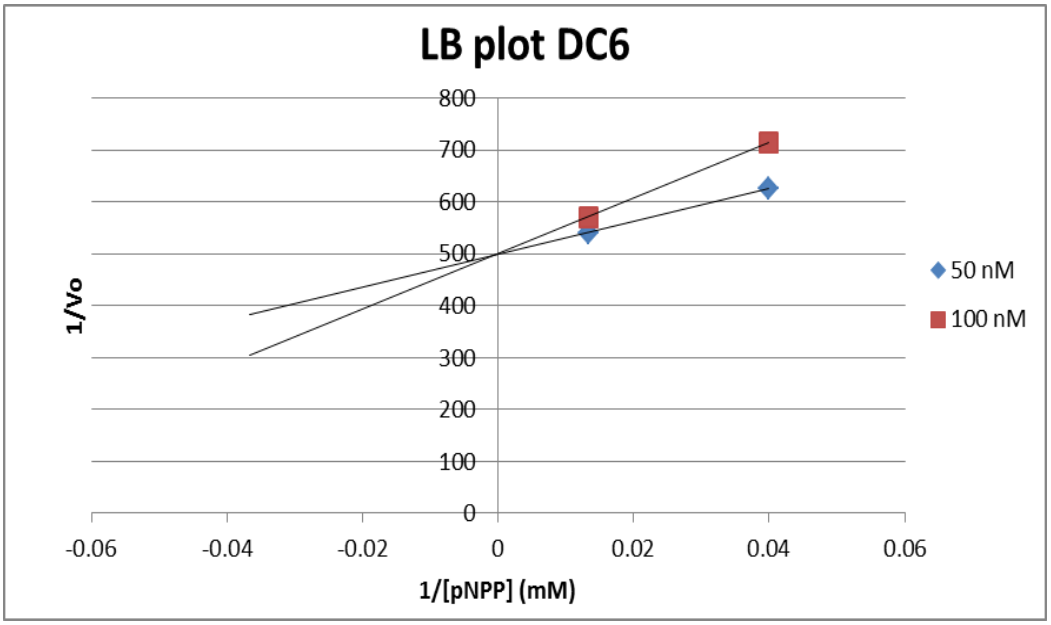

Figure D.3: An LB plot illustrating the competitive mode of inhibition on PTP1*β* by compound DC6.

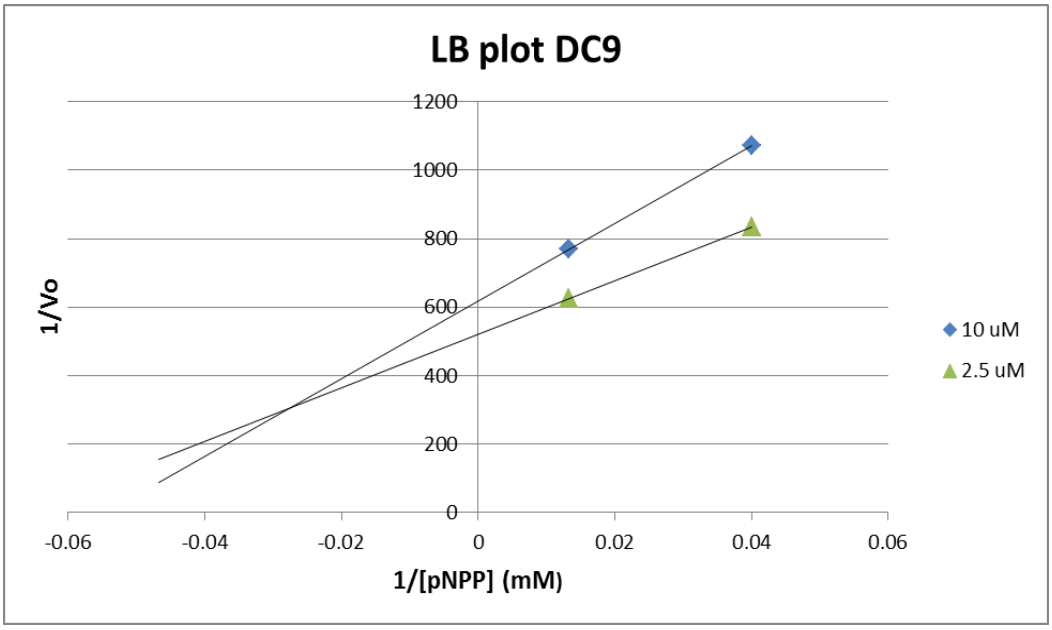

Figure D.4: An LB plot illustrating the mixed mode of inhibition on PTP1*β* by compound DC9.

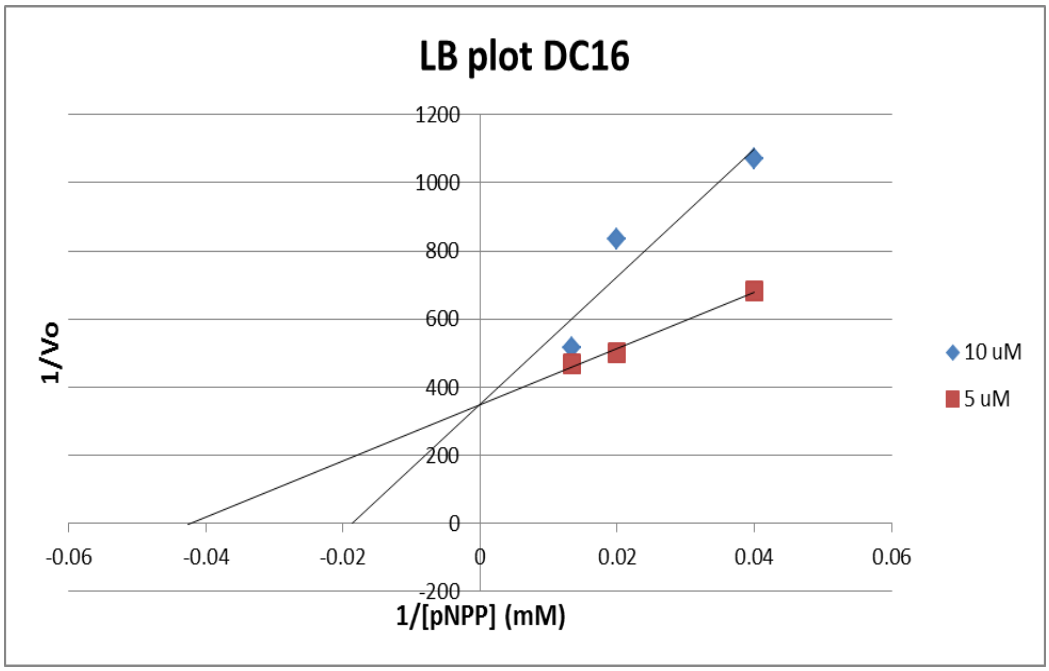

Figure D.5: An LB plot illustrating the competitive mode of inhibition on PTP1*β* by compound DC16.

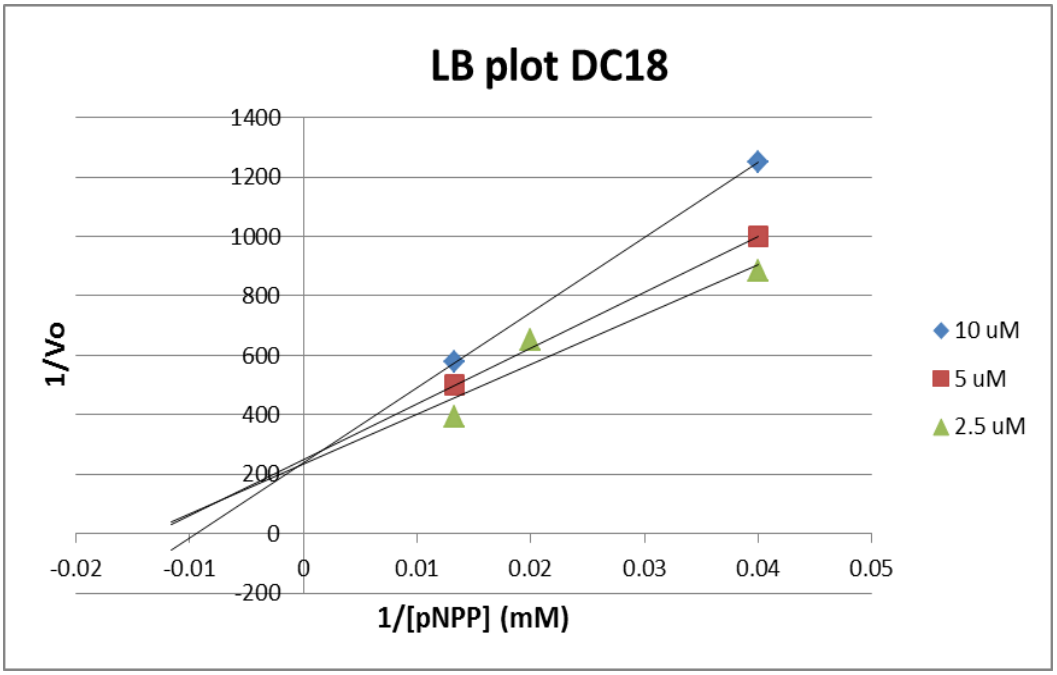

Figure D.6: An LB plot illustrating the competitive mode of inhibition on PTP1β by compound DC18.

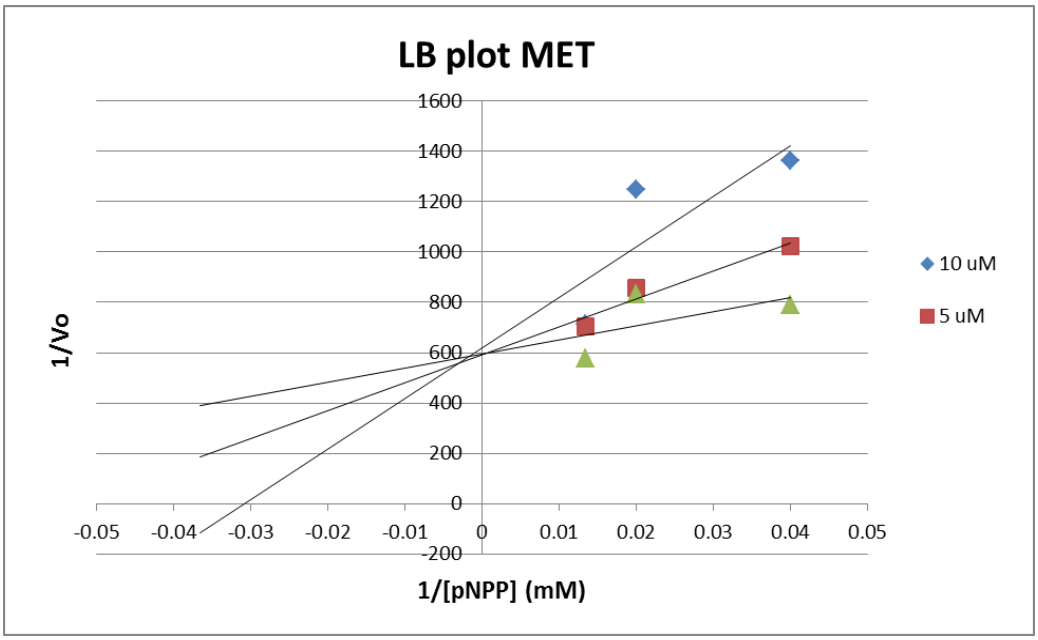

Figure D.7: An LB plot illustrating the competitive mode of inhibition on PTP1β by MET.

E Figures: Double Dixon plots were used in the determination of K_i values. Double Dixon plots are shown here for every inhibitor tested against ALP.

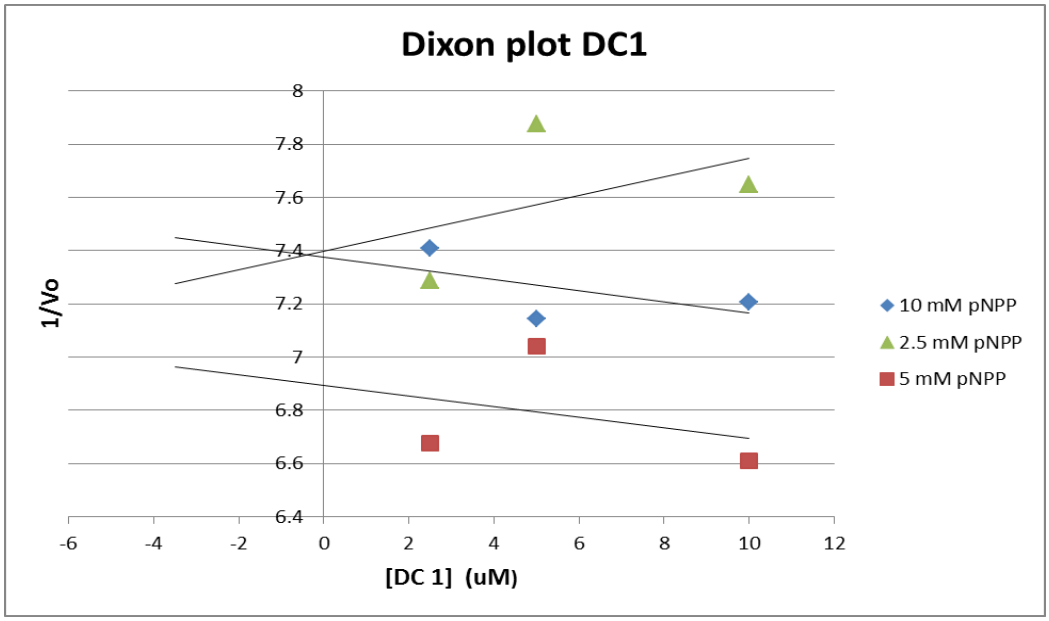

Figure E.1: A double Dixon plot for compound DC1 on ALP.

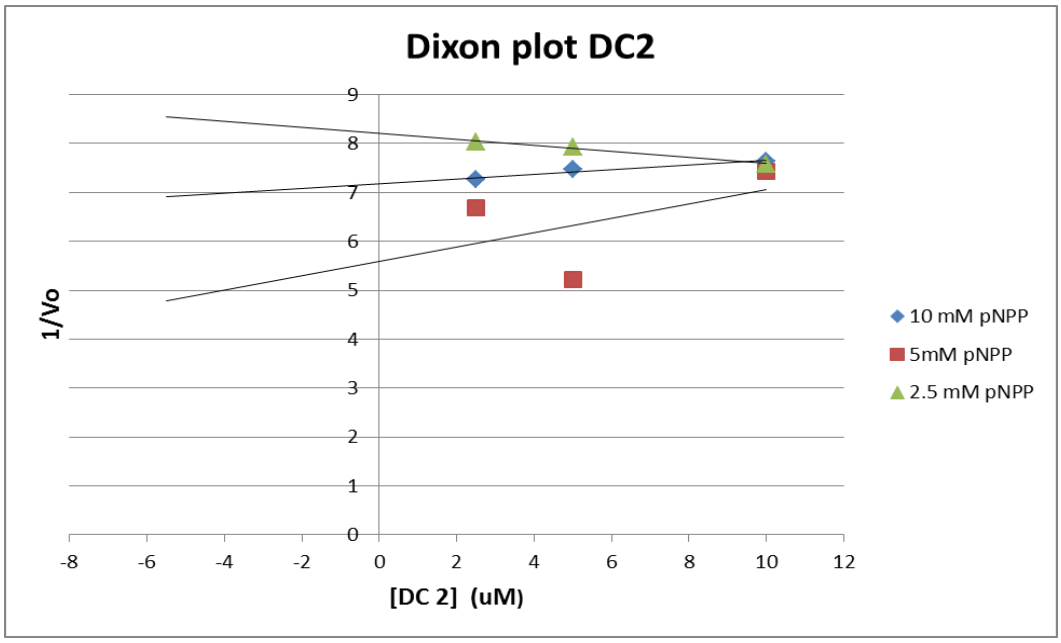

Figure E.2: A double Dixon plot for compound DC2 on ALP.

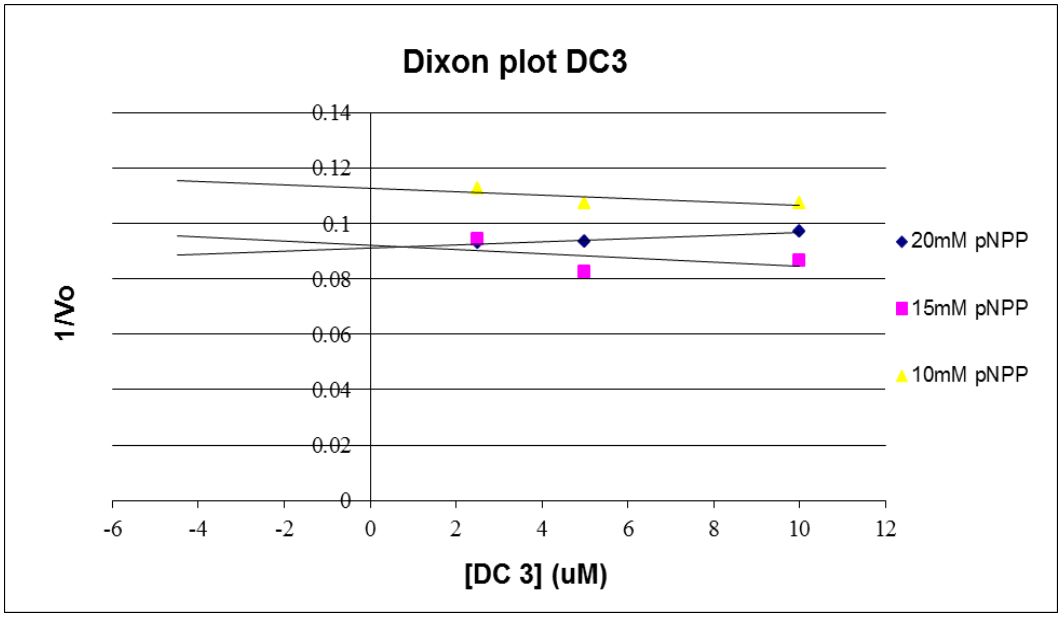

Figure E.3: A double Dixon plot for compound DC3 and on ALP.

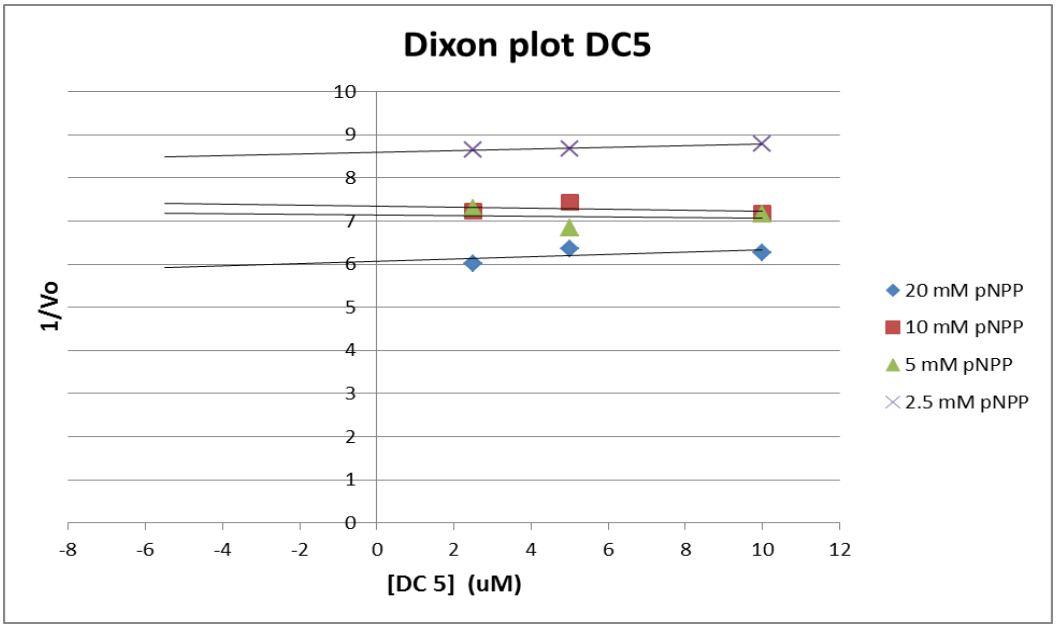

Figure E.4: A double Dixon plot for compound DC5 and on ALP.

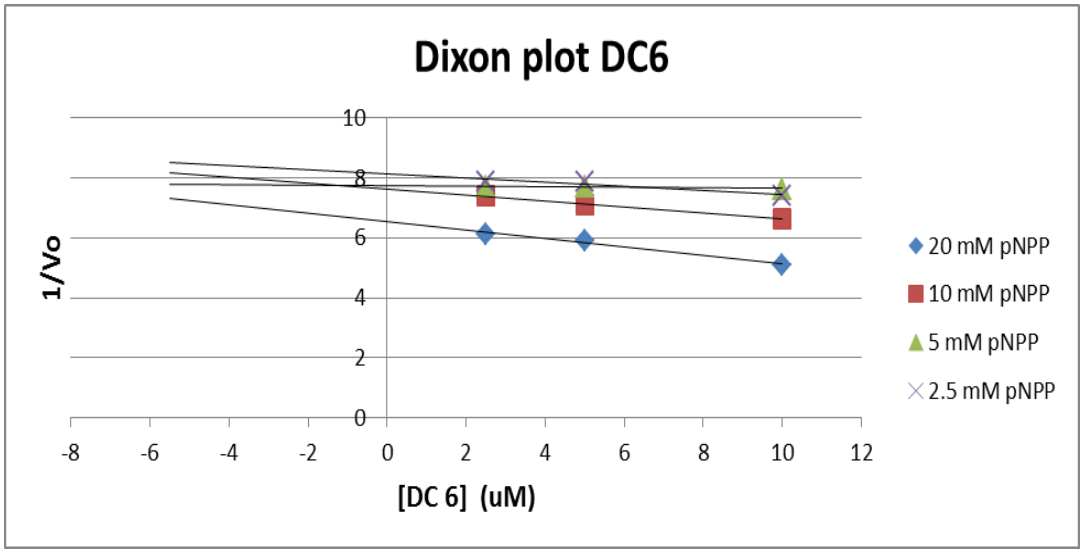

Figure E.5: A double Dixon plot for compound DC6 and its on ALP.

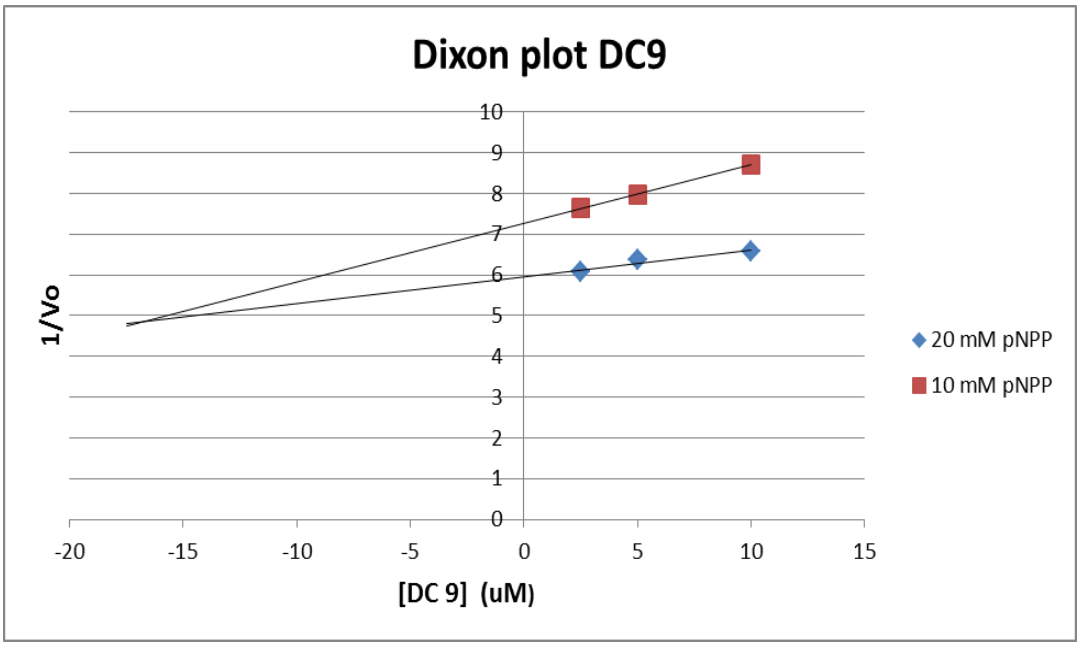

Figure E.6: A double Dixon plot for compound DC9 illustrating its inhibitory effect on ALP (K_i = 17 µM).

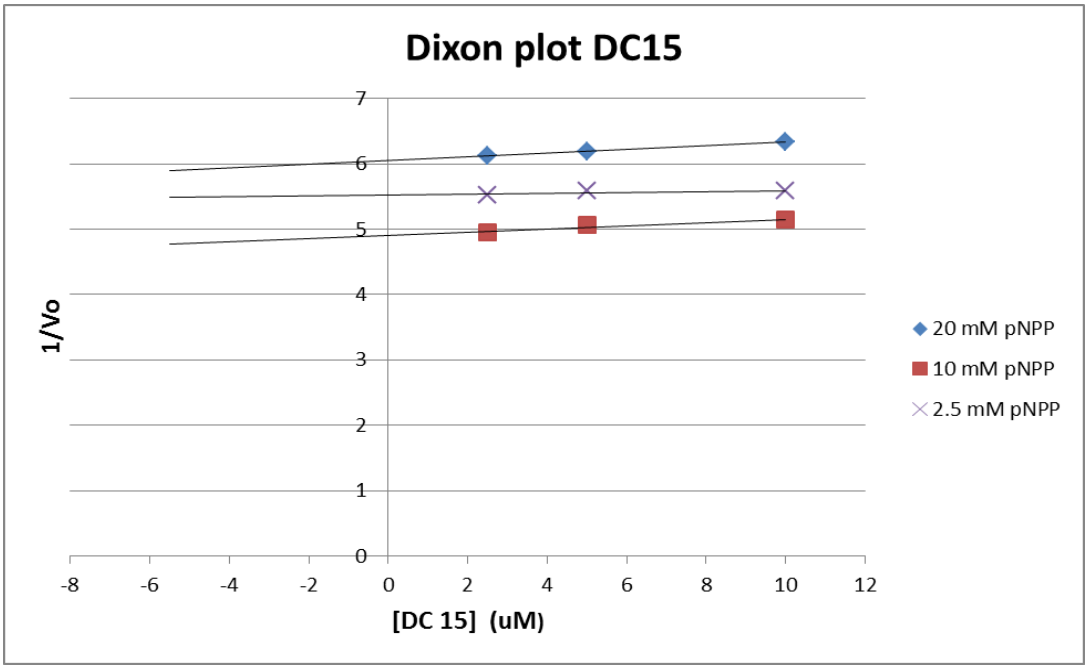

Figure E.7: A double Dixon plot for compound DC15 (MAR) on ALP.

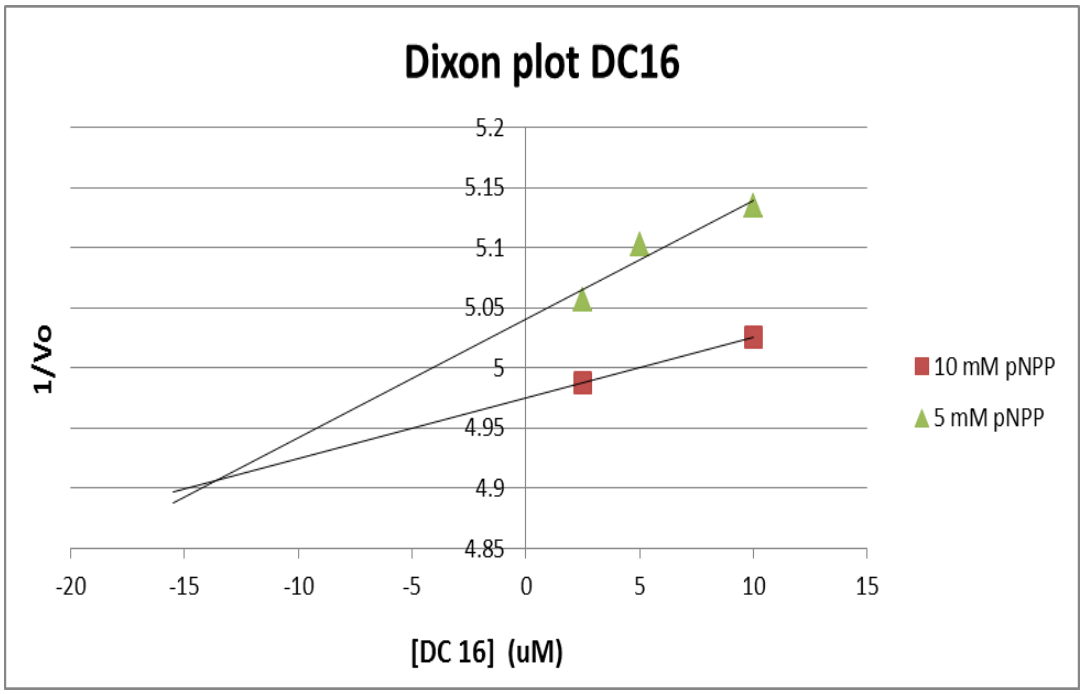

Figure E.8: A double Dixon plot for compound DC16 illustrating an inhibitory effect on ALP (K_i = 14 µM).

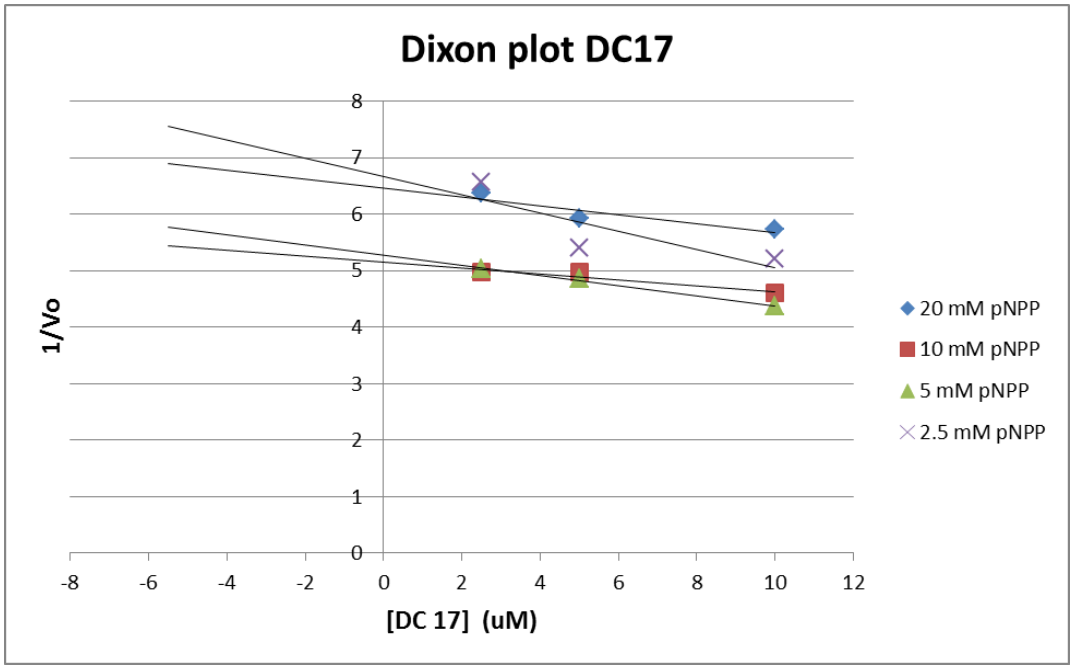

Figure E.9: A double Dixon plot for compound DC17 on ALP.

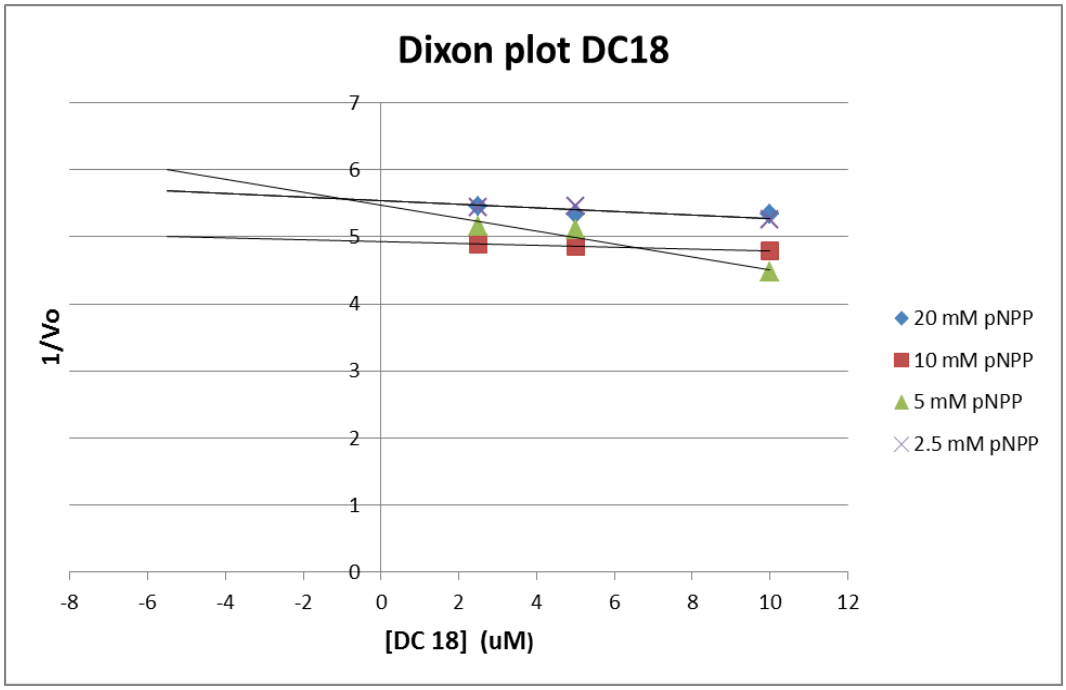

Figure E.10: A double Dixon plot for compound DC18 on ALP.

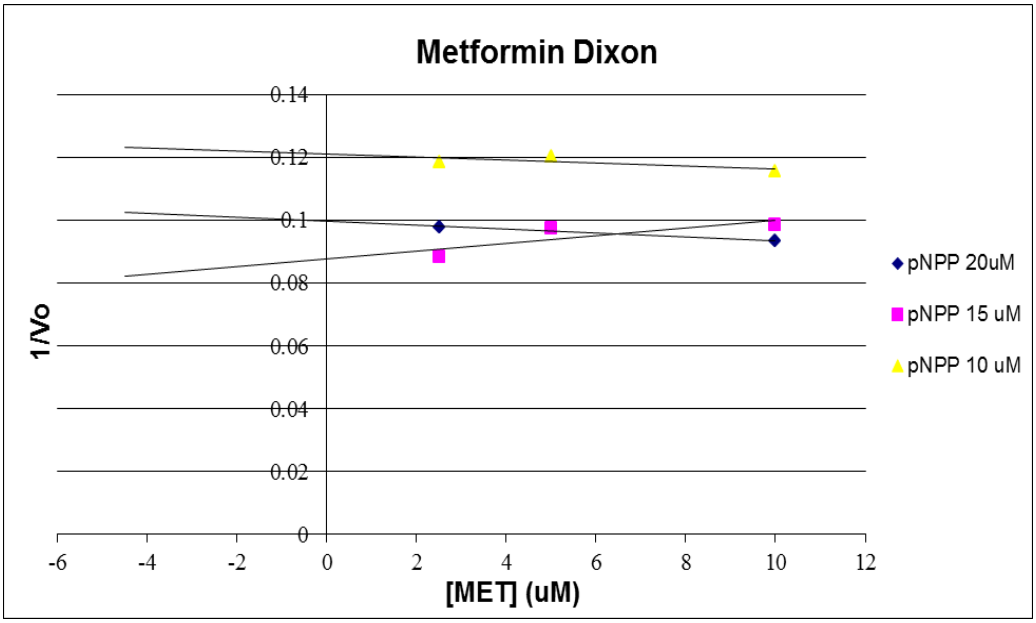

Figure E.11: A double Dixon plot for compound MET on ALP.

F Figures: MTT standard curves.

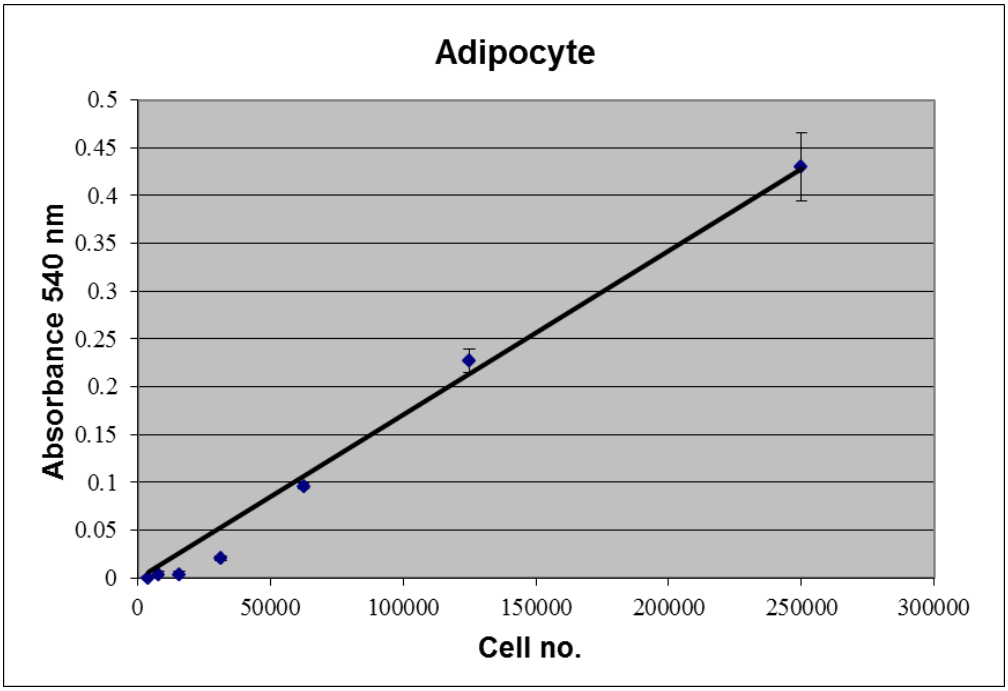

Figure F.1: MTT standard curve constructed using 3T3-L1 adipocytes (R^2 = 0.9871; n = 3).

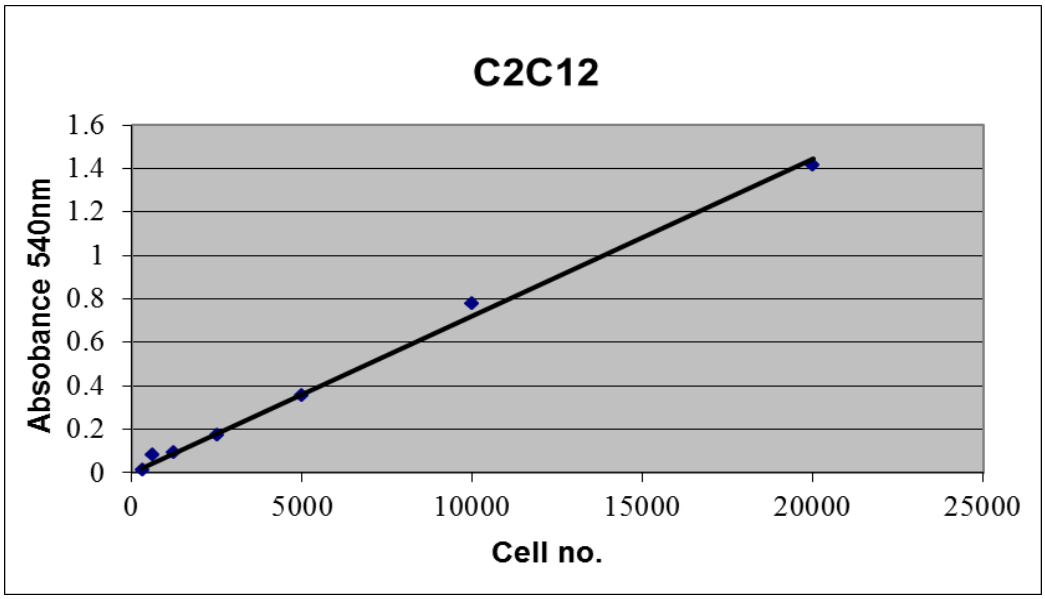

Figure F.2: MTT standard curve constructed using C2C12 myocytes (R^2 = 0.9963; n = 3).

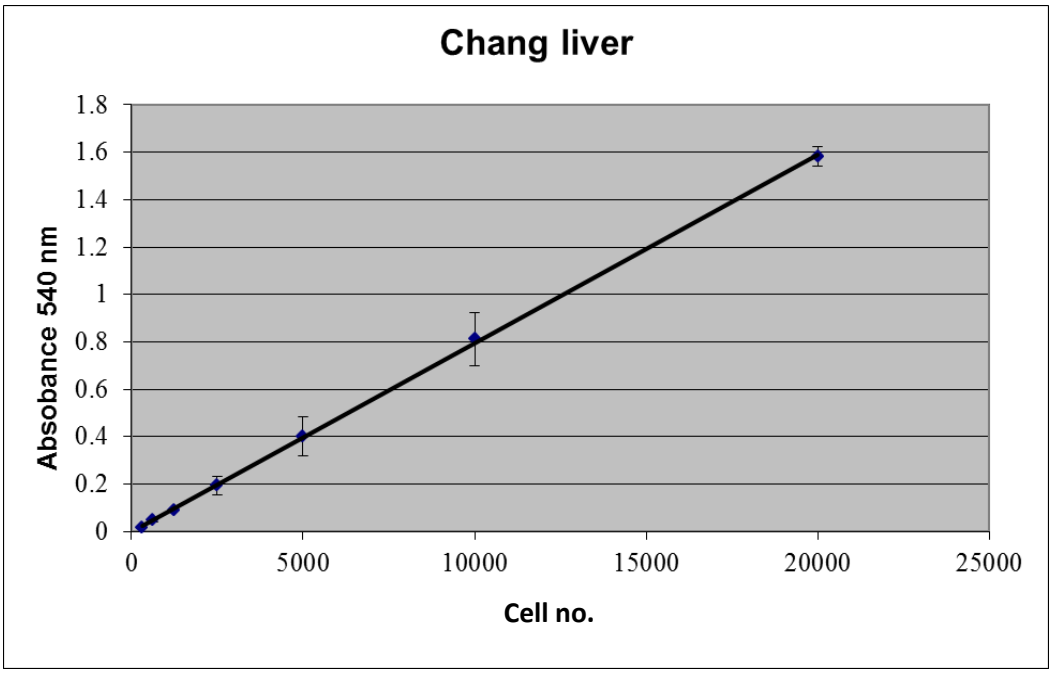

Figure F.3: MTT standard curve constructed using Chang liver cells (R^2 = 0.9997; n = 3).

APPENDIX 2: TABLES NOT SHOWN IN TEXT

Table A.1: A summary of the protein quantification achieved showing the process of converting data from absorbance values to the volume loaded per well. The experiment was done in triplicate and therefore symbols ('-', '*' and 'o') have been given to the groups which correspond to the RNA and cDNA groups.

Replicates	Treatment	Average Absorbance (562 nm)	[Protein] (µg/µL)	Loaded to gel (µL)
-	Untreated control	1.131	2.282	10.95
	DC18	0.710	1.432	17.45
	DC17	1.269	2.561	9.76
	DC6	1.096	2.211	11.30
	Marrubiin	1.162	2.343	10.67
	Metformin	0.870	1.755	14.24
*	Untreated control	1.047	2.112	11.83
	DC18	0.666	1.345	18.59
	DC17	1.148	2.316	10.79
	DC6	1.164	2.348	10.64
	Marrubiin	1.095	2.208	11.32
	Metformin	1.058	2.135	11.71
O	Untreated control	0.905	1.825	13.69
	DC18	0.781	1.576	15.86
	DC17	1.167	2.355	10.61
	DC6	1.088	2.195	11.39
	Marrubiin	1.132	2.284	10.95
	Metformin	0.847	1.709	14.62